DELIVERY OF PROTEINS IN LIVE CELLS WITH VIRAL PEPTIDES: PRINCIPLE AND MECHANISMS

A Dissertation

by

YA-JUNG LEE

Submitted to the Office of Graduate Studies of
Texas A&M University
in partial fulfillment of the requirement for the degree of

DOCTOR OF PHILOSOPHY

May 2011

Major Subject: Biochemistry

Delivery of Proteins in Live Cells with Viral

Peptides: Principle and Mechanisms

DELIVERY OF PROTEINS IN LIVE CELLS WITH VIRAL PEPTIDES: PRINCIPLE AND MECHANISMS

A Dissertation

by

YA-JUNG LEE

Submitted to the Office of Graduate Studies of
Texas A&M University
in partial fulfillment of the requirement for the degree of

DOCTOR OF PHILOSOPHY

Approved by:

Chair of Committee,	Jean-Philippe Pellois
Committee Members,	James C. Hu
	Gregory D. Reinhart
	David H. Russell
Head of Department,	Gregory D. Reinhart

May 2011

Major Subject: Biochemistry

ABSTRACT

Delivery of Proteins in Live Cells with Viral Peptides: Principle and Mechanisms.

(May 2011)

Ya-Jung Lee, B.A., National Chung Hsing University;

M.S., National Yang-Ming University

Chair of Advisory Committee: Dr. Jean-Philippe Pellois

Cell-penetrating peptides (CPPs) mediate the delivery of macromolecules across the plasma membrane of live cells. These peptides are therefore important due to the potential of making the delivery of protein probes or therapeutics a routine procedure. However, CPP-mediated delivery is currently an inefficient process. CPP-protein conjugates are internalized into cells by endocytosis and the macromolecules remain trapped inside endosomes instead of reaching the target cellular localization. To solve this problem, we report a delivery methodology which relies on the use of a chimera of the TAT (transcription transactivator) and of the Influenza haemagglutinin protein, HA2. TAT is a prototypical CPP that can promote macropinocytosis in live cells and HA2 is a pH-sensitive peptide that destabilizes lipid membranes upon acidification. I demonstrate that HA2-TAT can deliver a variety of macromolecular cargos into live mammalian cells by a simple co-incubation protocol. A model is described where TAT causes the endocytic uptake of cargos present in the media and that HA2 disrupts the endosomal membrane upon endosomal acidification. In addition, using red blood cells as a model

system, HA2-TAT binds to membranes in a pH-dependent manner and causes the formation of pores through which macromolecules can diffuse. Additionally, the pro-apoptotic domain (PAD) peptide is also successfully delivered by HA2-TAT and shows significant apoptosis in cells through macropinocytosis.

HA2-TAT is a peptide-based delivery agent that combines the pH-sensitive HA2 fusion peptide from influenza and the cell-penetrating peptide TAT from HIV. This chimeric peptide is engineered to induce the cellular uptake of macromolecules into endosomes via the TAT moiety and to respond to the acidifying lumen of endosomes to cause membrane leakage and release of macromolecules into cells via the HA2 moiety. Using fluorescence microscopy with live cells and hemolysis assays with red blood cells, the fundamental understanding of HA2-TAT-mediated protein delivery are revealed.

DEDICATION

This work is dedicated to my parents, sister, brother, and beloved husband for their continuous support that kept me grounded and focused and made this possible.

ACKNOWLEDGEMENTS

I would like to express my sincere gratitude to Dr. Pellois for his guidance and support with regards to my graduate studies. His patience and consideration have made everything smoother, and his sharing of all his experiences in these years really encouraged my growth. I would also like to acknowledge Dr. Jim Hu, Dr. David Russell, and Dr. Gregory Reinhart for serving as my committee members and for their helpful comments. Dr. Michael Polymenis served as a substitute for Dr. Reinhart during my defense. My appreciation is also extended to all current and former laboratory members. In particular, I would like to thank Dr. Alfredo Angeles and Dr. Daphne Jarrique for all their advice and support. Finally, I am truly grateful for my family. This work would not have been completed without them and I would like to dedicate this work to them.

NOMENCLATURE

Antp	antennapedia homeodomain
Bcl-XL	B-cell lymphoma-extra large
BSA	bovine serum albumin
CBD	chitin binding domain
Cdc42	Cell division control protein 42 homolog
CPP	cell penetrating peptides
DIEA	N,N-Diisopropylethylamine
DMEM	dulbecco's modified eagle medium
DMF	dimethylformamide
(E)GFP	(enhanced) green fluorescent protein
FBS	fetal bovine serum
FGF-2	Fibroblast growth factor
FITC	fluorescein isothiocyanate
FRET	Förster resonance energy transfer
GTPase	guanosine triphosphate hydrolase
GUV	giant unilammilar vesicles
HA	haemagglutinin protein
HBTU	2-(1H-Benzotriazole-1-yl)-1,1,3,3-tetramethyluronium hexafluorophosphate
HEPES	4-(2-hydroxyethyl)-1-piperazineethanesulfonic acid
HPLC	high-performance liquid chromatography

HSPG	heparin sulfate proteoglycan
IMPACT	Intein Mediated Purification with an Affinity Chitin-binding Tag
IPTG	isopropyl β-D-1-thiogalactopyranoside
kDa	kilo dalton
LUV	large unilammilar vesicles
MALDI	matrix-assisted laser desorption/ionization
MAP	model amphipathic peptide
MTT	3-(4,5-Dimethylthiazol-2-yl)-2,5-diphenyltetrazolium bromide
MVB	multivesicular bodies
NMR	nuclear magnetic resonance
p53	protein 53
PAD	pro-apoptotic domain
PBS	phosphate buffer saline
PCR	polymerase chain reaction
PTD	protein transduction domains
RBC	red blood cell
SDS-PAGE	sodium dodecyl sulfate polyacrylamide gel electrophoresis
SPPS	solid phase peptide synthesis
SUMO	small ubiquitin-like modifier
TAT	Transcription activaTor
TCEP	tris(2-carboxyethyl)phosphine
TFA	Trifluoroacetic acid

TMR	tetramethylrhodamine

TABLE OF CONTENTS

Page

ABSTRACT iii

DEDICATION v

ACKNOWLEDGEMENTS vi

NOMENCLATURE vii

TABLE OF CONTENTS x

LIST OF FIGURES xiii

LIST OF TABLES xv

1. INTRODUCTION 1

1.1 History of protein delivery 1
1.2 Development of CPPs as general delivery tools 2
1.2.1 Potential problem of CPP-mediated protein delivery 4
1.3 Proposed mechanism of protein delivery by CPP 4
1.3.1 Cell surface binding 5
1.3.2 Endocytic uptake and endosomal maturation 6
1.3.3 Endosomal escape: The limiting step 7
1.3.4 Endosomal escape model 7
1.4 The possible solution for low CPP delivery efficiency: HA2-TAT, enhances the limiting step, endosomal escape 8
1.4.1 The pH-dependent conformational change of HA2 peptide leads to its membrane destabilizing activity 9
1.4.2 Protonation of negatively charged residues of HA2 peptide contributes to the lipid membrane disruption in acidic environment 11
1.4.3 HA2E5, higher membrane disruption activity 13
1.5 The goal of my study 15

2. HA2-TAT PEPTIDE TAGS FOR THE DELIVERY OF PROTEINS 16

2.1 Introduction 16
2.2 Results 16
2.2.1 Protein solubility and aggregation propensity analysis 17

Page

2.2.2 Cytotoxicity of the protein constructs 21
2.2.3 Hemolytic activity of HA2-TAT-mCherry and E5-TAT-mCherry as a function of pH 23
2.2.4 Characterization of the cellular distribution of HA2-TAT-mCherry and E5-TAT-mCherry 23
2.2.5 Characterization of the endosomolytic and cytosolic release activities of HA2-TAT-mCherry and E5-TAT-mCherry 25
2.2.6 Effect of TAT on the intracellular distribution of the model protein mCherry 33
2.3 Discussion 35
2.4 Materials & Methods 38
2.4.1 Cloning and protein expression of HA2-TAT-mCherry and E5-TAT-mCherry 38
2.4.2 Electron microscopy 40
2.4.3 Analytical ultracentrifugation 41
2.4.4 Microinjection of mCherry and TAT-mCherry into live cells 41
2.4.5 Binding assay 42
2.4.6 Hemolysis assays 42
2.4.7 Microscopy assays 43

3. DELIVERY OF MACROMOLECULES INTO LIVE CELLS BY SIMPLE CO-INCUBATION WITH HA2- TAT 46

3.1 Introduction 46
3.2 Results 47
3.2.1 HA2-TAT cytotoxicity 47
3.2.2 HA2-TAT promote cellular uptake and endosomal escape of co-incubated fluorescent cargos 48
3.2.3 HA2-TATs promote cellular uptake through endocytic pathway 55
3.2.4 PAD delivered by HA2-TAT and induces apoptosis through endocytic pathway 58
3.3 Discussion 61
3.4 Materials & Methods 65
3.4.1 Peptide synthesis 65
3.4.2 Cytotoxicity assay 67
3.4.3 Live cell assay 68
3.4.4 Live cell assay for the delivery of PAD 69
3.4.5 Characterization of the binding interactions between the delivery peptides and proteins 70

4. MODELING OF ENDOSOMOLYTIC ACTIVITY OF HA2-TAT PEPTIDES WITH RED BLOOD CELLS AND GHOSTS 75

Page

4.1 Introduction 75
4.2 Results 76
4.2.1 Peptide design 76
4.2.2 HA2-TAT peptides lyse erythrocytes in a pH-dependent manner 79
4.2.3 Fl-E5-TAT interacts with RBC in a pH-dependent manner 82
4.2.4 Fl-E5-TAT permeabilizes membranes in a manner not reversed under different pH values 87
4.2.5 Peptide binding to RBC is dependent on membrane composition 89
4.2.6 Heparin inhibits membrane binding of E5-TAT and hemolysis 92
4.3 Discussion 93
4.4 Materials & Methods 104
4.4.1 Peptide synthesis and purification 104
4.4.2 Hemolysis assays 105
4.4.3 Microscopy assays 107

5. CONCLUSION 109

REFERENCES 111

VITA 121

LIST OF FIGURES

FIGURE		Page
1-1	The helical structure model of HA2 peptide	10
1-2	A cartoon representation of the secondary conformational change of HA2 peptide in the presence of lipid membrane at neutral pH (pH 7) and pH5	12
1-3	A cartoon representation of the structure of the E5 analog at fusogenic pH, with a helix-hinge-helix structural motif in the interface of water and lipid membrane	14
2-1	Biochemical analysis of E5-TAT-mCherry.	20
2-2	Viability of HeLa cells incubated with TAT-mCherry, HA2-TAT-mCherry, and E5-TAT-mCherry	22
2-3	Hemolytic activities of TAT-mCherry and E5-TAT-mCherry as a function of pH	24
2-4	Microscopy images of HeLa cells incubated with TAT-mCherry or E5-TAT-mCherry	26
2-5	Fluorescence microscopy of HeLa cells incubated with E5-TAT-mCherry (5 μM) and 70 kDa Dextran-fluorescein (Dx-Fl)	29
2-6	Fluorescence microscopy of HeLa cells incubated with E5-TAT-mCherry, TAT-mCherry and mCherry	30
2-7	Fluorescence microscopy of HeLa cells incubated with E5-TAT-mCherry	31
2-8	Fluorescence microscopy of HeLa cells microinjected 70 kDa Dextran-fluorescein (Dx-Fl) and mCherry, TAT-mCherry, or E5-TAT-mCherry	34
3-1	Viability of HeLa cells incubated with TAT, E3-TAT, or E5-TAT	49
3-2	Non-covalent binding interaction between the delivery peptides and serum proteins	52

FIGURE Page

3-3 Non-covalent binding interactions between the delivery peptides and serum proteins 53

3-4 Effects of E5-TAT and mCherry co-incubation on cell viability 54

3-5 Live-cell imaging of cells incubated with E5-TAT, and green and red fluorescent macromolecules 56

3-6 Effects of co-incubation conditions and inhibitors on the delivery of the protein mCherry to HeLa cells 57

3-7 Effects of co-incubation conditions and inhibitors on the delivery of 70k Da Dextran-Texas Red to HeLa cells 57

3-8 Delivery of the proapoptotic peptide domain PAD into live cells by co-incubation with E5-TAT 60

3-9 Proposed model for the delivery of macromolecules mediated by co-incubation with E5-TAT 63

4-1 Hemolysis activities ofHA2 and HA2-TAT analogues as a function of pH 81

4-2 Binding of Fl-E5-TAT to RBCs and ghosts as a function of pH 84

4-3 Binding of Fl-E5-TAT (1.0 μM) to intact RBCs as a function of pH as observed by fluorescence microscopy 86

4-4 Time course of lysis and ghost formation from single RBCs determined by fluorescence and bright field microscopy 88

4-5 Ghosts remain permeable after lysis and Fl-E5-TAT remains tightly bound to their membranes 90

4-6 Binding of Fl-TAT to RBCs and ghosts 91

4-7 Heparin inhibits the hemolytic activity of E5-TAT but not that of E5 94

LIST OF TABLES

TABLE Page

1-1 Representative CPPs for protein delivery: Sequences and major related references 3

2-1 Sequences of the HA2-TAT peptides investigated..... 18

4-1 Sequences of the HA2-TAT peptides investigated..... 77

1. INTRODUCTION

1.1 History of protein delivery

The plasma membrane separates extracellular macromolecules from materials within the cell. Because the plasma membrane is hydrophobic, most protein molecules, which are hydrophilic, cannot pass this barrier (1-4). Nevertheless, manipulations such as microinjection, electroporation and bead loading have been used to introduce proteins into live cells (5,6). However, these methods still need improvement in practicality, cytotoxicity and efficiency (7-10). In another approach, a class of short peptides has been shown to facilitate protein delivery (7-10).

In 1988, Loewenstein and Pabo's groups independently discovered that a transcription transactivator, TAT from HIV-1 virus, was taken up by tissue-cultured cells after protein incubation in the culture medium. After TAT translocated into cells, it rapidly executed its biological function to transactivate viral genes (11,12). Since proteins and large molecules are poorly internalized by cells, Green and Loewenstein suggested that TAT may bind to an unknown cellular receptor and subsequently undergo translocation into cells (12). However, Frankel and Pabo demonstrated that internalization of TAT into cells is independent of any receptors (13). These findings established that protein transduction into cells by simple incubation was possible. This also raised the possibility that proteins could be delivered into cells without any complicated manipulations. In 1998 Lebleu and coworkers showed that the minimal region corresponding to ^{47}YGRKKRRQRR^{57} is required for TAT transduction (14). This

---

This dissertation follows the style of *Journal of Biological Chemistry.*

indicates that only a small portion within a particular protein can promote the delivery of the entire protein.

Following the discovery of the TAT peptide, other peptides that transport proteins into cells have been found (14). Such peptides are called protein transduction domains (PTDs) or cell-penetrating peptides (CPPs) (15). Most of these peptides are less than 30 amino acids long and derived from proteins or chemically synthesized (16-18). Like TAT, many CPPs are rich in positively charged residues or are amphipathic (17,19) (TABLE 1-1). Because of the possible therapeutic value of the ability to deliver proteins across the cell membrane, there is interest in 1) the identification of novel CPPs, 2) the biological applications of CPP-cargo conjugates in vitro/vivo and 3) the molecular mechanism of CPP-cargo delivery (17).

1.2 Development of CPPs as general delivery tools

CPPs have been shown to deliver different therapeutic proteins and peptides (7,20,21). The tumor supressor p53 (protein 53) was delivered by Antp (antennapedia homeodomain) and this restored p53 functions in cancer cells. Bcl-XL (B-cell lymphoma-extra large) delivered by TAT can regulate apoptosis and induce cytoprotection with retinal ganglion cells (9,19). An important breakthrough in the CPP field also came from the first proof-of-concept of their in vivo application. Dowdy's group showed that 120-kDa (kilo dalton) beta-galactosidase protein could be delivered by TAT peptide into many different organ tissues and even cross the blood-brain barrier the context of protein therapy (15). In addition to delivering proteins, CPPs also carrying

Table 1-1 Representative CPPs for protein delivery: Sequences and major related references

Peptides	***Origin***	***Sequences***	***References***
Tat	HIV-Tat protein	PGRKKRRQRRPPQ	Snyder and Dowdy (2005); Schwarze *et al. (1999)*
Penetratin (Antp)	Homeodomain	RQIKIWFQNRRMKWKK	Joliot and Prochiantz (2004)
Transportan	Galanin-mastoparan	GWTLNSAGYLLGKINLKALAALA KKIL	Pooga *et al. (1998)*
VP-22	HSV-1 structural protein	DAATATRGRSAASRPTERPRAPAR -SASRPRRPVD	Elliott and O'Hare (1997)
Pep-1	Trp-rich motif-SV40 NLS	KETWWETWWTEWSQPKKKRKV	Gros *et al. (2006)*
MAP	Chimeric	KALAKALAKALA	
Oligoarginine	Chimeric	Agr8 or Arg9	Wender *et al. (2000); Futaki et al. (2001)*
hCT (9–32)	Human calcitonin	LGTYTQDFNKTFPQTAIGVGAP	Schmidt *et al. (1998)*

nanoparticles and microbeads (2,17,22). In addition, CPPs can deliver cargos into a variety of cell types as well (1,23). These findings suggest that neither the cargo types nor the target cells are restricted in CPP-mediated cargos delivery i (22,24). CPPs appear as general delivery vectors with promising activity.

1.2.1 Potential problem of CPP-mediated protein delivery

Although CPPs can carry different protein molecules into live cells, limited delivery efficiency is still the main bottleneck in this field (17,18,22,25). Only a fraction of incubated proteins can be delivered to the intracellular localization by CPPs. Delivery efficiency is determined by the biological activity of the delivered cargo. This readout confirms that the cargo was not only delivered, but that it also remained in a functional state. The increase in a given biological assay will be considered as a successful CPP-mediated cargo delivery. However, the percentage of cells containing CPP-delivered proteins is still low even though protein delivery is achieved (26,27). Although many studies aim to explore the delivery efficiency of CPPs, the result still remains unclear (26,27). To be able to utilize CPPs as general delivery vector, the low efficiency problem of CPPs needs to be improved. Understanding the cellular mechanism of CPP-mediated protein delivery definitely is necessary in order to enhance the delivery efficiency of CPPs.

1.3 Proposed mechanism of protein delivery by CPP

Different entry routes of CPP-mediated protein delivery have been reported (1,16, 23,

28). Even though some discrepancies remain, a current model of CPPs uptake involves the three following steps: i) binding on the cell surface, followed by ii) stimulation of macropinocytotic uptake into macropinosomal vesicles and finally iii) escape from endosomes into the cytoplasm (10,17). This study will be focused on the most well-studied CPP, TAT.

1.3.1 Cell surface binding

Once TAT is present in the cellular media, binding between TAT and plasma membrane can occur. Since TAT-mediated protein uptake is cell-type independent, it is hypothesized that there is no specific receptor mediating the association between TAT and membrane (13,29-31). In addition, it is proved that positively charged arginine residues in TAT sequence (TAT containing 6 arginines out of 10 residues) are essential to facilitate CPP transduction (31-33). The guanidine group of arginine can form bidentate hydrogen bonds with sulfate, phosphate or carboxylate anions (33-36). Such interactions raise the possibility that TAT may bind to many cell surface molecules (34). Based on findings from studies of TAT-mediated protein transduction, a model regarding the initiation of TAT-mediated protein delivery has been proposed. The positive arginine residues of TAT exhibit high affinity with heparin sulfate proteoglycan (HSPG), the anionic sulfated proteoglycans on extracellular matrix of plasma membrane through electrostatic interaction. This interaction facilitates TAT-mediated protein delivery through endocytosis (7,17). It is also known that most of HSPG on the cell surface are linked to two core protein families, the transmembrane syndecans and the

membrane lipid-anchored glypicans (37-39). Syndecan has been shown to be responsible for uptake of FGF-2 (Fibroblast growth factor) by macropinocytosis. This suggests that syndecan might serve as a binding reservoir for TAT. This binding event might also initiate macropinocytosis (40).

1.3.2 Endocytic uptake and endosomal maturation

Different endocytic routes have been implicated as pathways for internalization of different CPPs with various types of cargos. These routes include caveolin, clathrin-dependent endocytosis and the major route, macropinocytosis (16,23,28). This is also supported by the discovery that TAT fusion cargos can induce the uptake of neutral dextran, a marker of fluid phase endocytosis (36,41). Compared to other endocytosis pathways, macropinocytosis is not well characterized (42,43). Macropinocytosis occurs at regions of actin-induced membrane ruffling and protrusions (43,44). These protrusions create vesicles either by the fusion of two protrusions or of a protrusion and the membrane near the origin of this protrusion (43,44). Macropinocytosis is a form of fluid phase endocytosis performed by all cells, wherein the vesicles take up the surrounding medium (17,45,46). The exact structural changes and proteins involved in macropinocytosis, still need to be elucidated. After macropinocytosis is induced, TAT-conjugated protein internalize into endocytic vesicles (9,17,46,47). These compartments can then undergo multiple steps of maturation. Partition may occur into various endocytic organelles, including sorting endosomes (also called early endosomes), recycling endosomes, multivesicular bodies (MVB), late endosomes and fuse with

lysosomes (25,28,45,48). If TAT-conjugated protein fails to be released from endosomal vesicles before endosome-lysosome fusion, they will be subjected to lysosomal degradation (10,49,50).

1.3.3 Endosomal escape: The limiting step

Both the mechanism and the efficiency of the endocytosis of TAT-mediated protein delivery have been addressed in many studies. After endocytosis, TAT-conjugated protein still needs to be released from the endosome to reach its target cellular locale and begin to function biologically (1). However, it is reported that a large fraction of TAT-conjugated cargos are trapped in endosomes and are not released into cytosolic space (26,27,41). Therefore, endosomal escape seems to be the limiting step during TAT-mediated protein delivery. This is a key factor that leads to low protein delivery efficiency (17,26,27,41). This critical step, endosomal escape, remains obscure, as do later processes in the endocytic pathway (9,17). Some research groups have started making efforts to explore this particular step (26,27,41).

1.3.4 Endosomal escape model

Despite the poor understanding of endosomal escape, TAT is able to disrupt the endosomal membrane without interfering with the plasma membrane and causing cytotoxicity (14,32). As endosomal vesicles are newly formed from the plasma membrane during endosomal maturation, the enrichments in specific membrane lipids and membrane-associated small Rab GTPases (guanosine triphosphate hydrolase) are

altered in all classifications of vesicles (39,51,52). Moreover, the pH in endocytic vesicles from early to late endosomes or lysosomes is found to decline from pH 7.2 to 4.5 (48,53).

The changes in membrane protein and lipid compositions and decreasing in pH within endosomes are suggested leading to TAT-induced endosomal membrane escape (27,38,54). However, the effects of these factors in TAT-related endosomal membrane disruption are not fully defined (27). Furthermore, even though TAT is reported as the most efficient CPP, endosomal entrapment of TAT still results in poor delivery efficiency (41,55). Therefore, in this study, I will explore this critical step, endosomal escape, and attempt to design a more active CPP. Our proposed TAT-mediated protein delivery mechanism is illustrated in Fig 1-1. (TAT associates with HSPG on the cell surface to induce endocytosis. Next, TAT-mediated proteins are internalized into endosomes. The later processes in the endocytic pathways remain unclear. But somehow TAT-mediated proteins need to be released from endosomes and reach the target cellular localizations in order to execute their biological functions).

1.4 The possible solution for low CPP delivery efficiency: HA2-TAT, enhances the limiting step, endosomal escape

Some virus particles infect host cells through an endocytic pathway (56-58). After endocytosis, the viral membrane and endosomal membrane undergo destabilizing then fuse with each other during endosomal acidification (58,59). This fusion event results in releasing viral nucleic acids to the nucleus in host cells for viral propagation (56,60,61).

The Influenza virus belongs to the class of virus that infects through endocytosis. (56,60,61). Haemagglutinin (HA) is the main glycoprotein of the influenza (H3N2) virus that mediates viral fusion with endosomes (5,56,62) . It is a homotrimer of 200 kDa. Each monomer is composed of two disulfide-linked subunits, HA1 and HA2 (5,56,62). HA1 is responsible for initiating the binding of influenza virus to sialic acid-containing receptors on the host membrane. HA2 regulates the fusion event between the viral membrane and the endosomal membrane (61,62). Since endosomal escape of CPP-mediated protein may be correlated with decreasing in pH inside of endosomal lumens, HA2 has been utilized to enhance endosomal escape (21,41,60).

The N-terminal segment of HA2 subunit, composed of twenty nonpolar amino acids (^{1}GLFGAIAGFIENGWEGMIDG^{20}), is required for endosomal fusion (56,63,64). In addition, the membrane fusion activity is profoundly decreased by deletion or mutation of its N-terminal Gly1 (64,65). Since HA2 protein induces membrane fusion during endosomal acidification, the 20 residue HA2 peptide, is considered as a pH-sensitive membrane disruption peptide (60,63).

1.4.1 The pH-dependent conformational change of HA2 peptide leads to its destabilizing activity

Based on circular dichroism studies, the helicity of HA2 increases upon a decrease in pH (62,66,67). This conformational change leads to the association of the peptide with the lipid membrane. This interaction then causes membrane destabilization (62,66,67). Hence, HA2 peptide can disrupt the endosomal membrane during endosomal acidifying

1 GLFGAIAGFIENGWEGLIDG 20

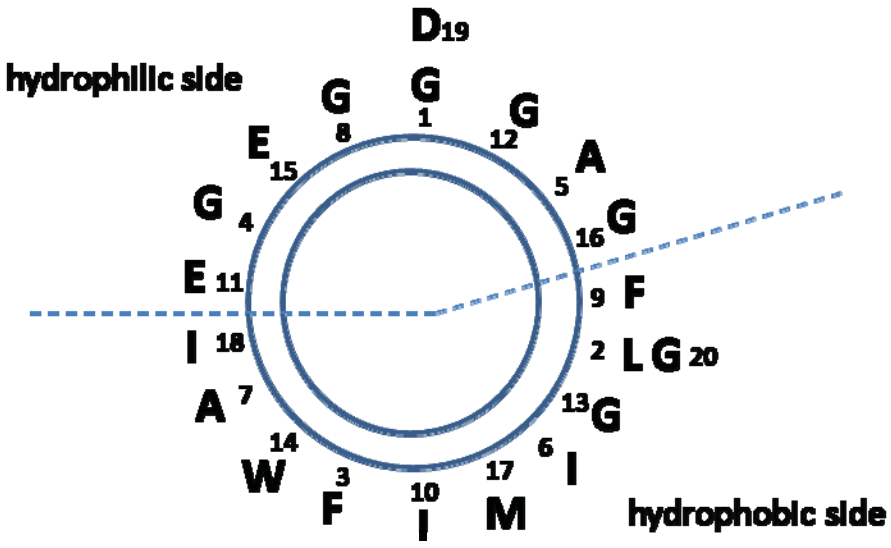

Figure 1-1 The helical structure model of HA2 peptide.

(usually pH 5-7). As a result, lysis of endosomal membrane might be achieved without causing lysis of the plasma membrane or other membraneous organelles. Similarly, HA2 peptide can also enhance endosomal escape during CPP-mediated protein delivery in acid environment. Indeed, HA2 peptide has been fused to the N-terminus of the tumor suppressor p53 modified with the CPP R11. The formed HA2-p53-R11 construct was shown to reduce the proliferation of cancer cells more efficiently than p53-R11 alone (60). In addition, the D-form dTat-HA2 peptide markedly enhanced the release of Tat-Cre from macropinosomes and displayed the cre recombinase activity (then induced EGFP protein expression) in live cells compared to Tat-Cre delivery only. (41).

1.4.2 Protonation of negatively charged residues of HA2 peptide contributes to the lipid membrane disruption in acidic environment

HA2 peptide is an amphipathic sequence. In the α-helical wheel model of this peptide, one face of the proposed helix is rich in hydrophilic residues while the opposite face is rich in hydrophobic residues (66,67). When HA2 peptide is adjacent to the surface of a lipid bilayer, the hydrophobic side of the helix shows higher affinity for the lipid membrane, whereas the hydrophilic side is exposed to the aqueous environment (66,67) (Fig 1-2). Once pH decreases, carboxyl groups on the Glu11, Glu15, and Asp19 side chains will be protonated. The peptide is more hydrophobic due to neutralization of those charged residues. Neutralization can augment the affinity of HA2 peptide for the lipid bilayer (62,66,68). Furthermore, the protonation of acidic residues induces a conformational change of HA2 peptide to a higher helical content of its C-terminal

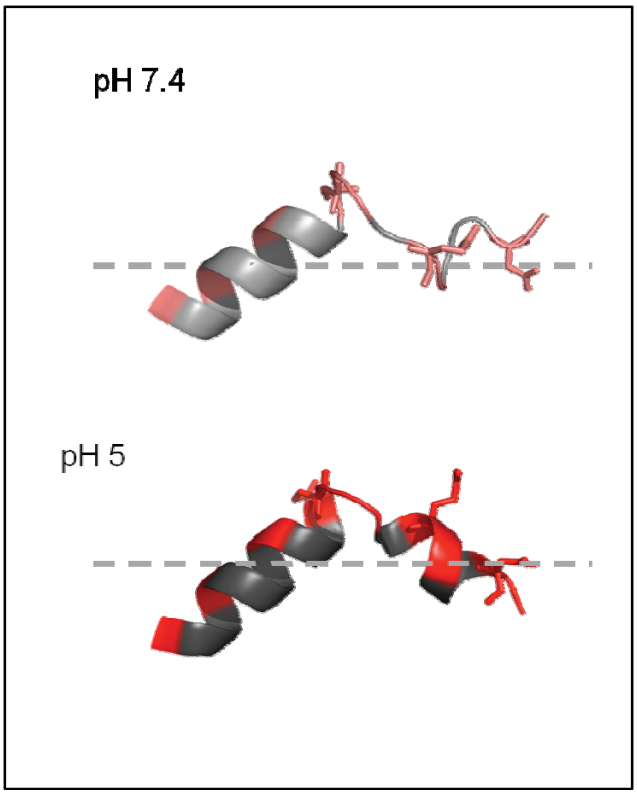

Figure 1-2 A cartoon representation of the secondary conformational change of HA2 peptide in the presence of lipid membrane at neutral pH (pH 7) and pH5. The arrows indicate the positions of Glu11, Glu15, Asp 19. Hydrophilic residues are highlighted in red and hydrophobic residues are highlighted in black.

peptide with a hinge formation between Gly^{12}-Gly^{13} (56,62,69). The neutralized C-terminal α-helical peptide facilitates the insertion into lipid bilayers (Fig 1-2).This results in membrane disruption at acidic environments (56,65,68). (In another words, the electrostatic repulsion among the negatively charged residues, prevents the stable C-terminal α-helix formation at neutral pH (63,65,70). This is believed to be the key factor that contributes to pH-dependent, HA2-mediated membrane disruption).

1.4.3 HA2E5, higher membrane disruption activity

HA2 peptide has been shown to enhance endosomal release for protein delivery and nucleic acid transfection (41,60,70,71). However, this peptide is extremely aggregative, and poorly dissolvable in aqueous media, and therefore was difficult to characterize spectroscopically (62,69). Its solubility behavior limits its usefulness (62,69), so many studies have been focused on enhancing membrane disruption activity and the solubility of HA2 peptide. Due to the proposed mechanism, additional glutamic acid residues have been introduced in HA2 peptide to enhance the pH-dependent membrane disruption activity (and solubility) (63). The hydrophilic side chains of Gly4 and Gly8 along with Glu11, Glu15 and Asp19 on the α-helix structure of HA2 peptide are all located on the exterior of the lipid bilayer (Fig 1-3) (68). Studies of the HA2 peptide mutant, HA2E5, which includes G4E, G8E, and D19E, (GLFEAIAEFIENGWEGMIEG, five glutamic acids) showed that these mutated residues play a pivotal role not only in enhancing pH-dependent membrane disruption activity, but also peptide solubility (57,66). In liposomal assays, HA2E5 exhibited a higher extent of liposomal fusion and leakage than wild type

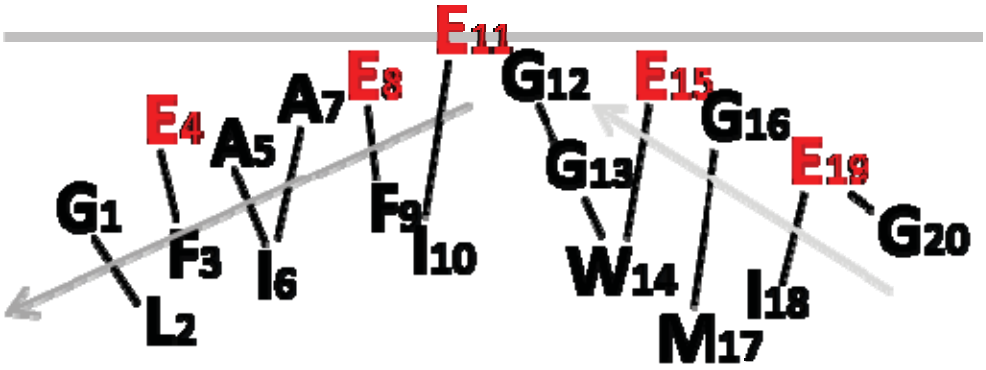

Figure 1-3 A cartoon representation of the possible structure of the E5 analog at fusogenic pH, with a helix-hinge-helix structural motif in the interface of water and lipid membrane.

HA2 peptide at pH5, but not at pH7 (66,69). The NMR (nuclear magnetic resonance) study resolved that the C-terminal helix of HA2E5 sequence is inserted deeper into the lipid bilayer. The deeper insertion and the hinge formation between Gly^{12}-Gly^{13} both contribute to destabilize the membrane (65). These findings provide insights into the molecular mechanism of increased membrane disruption by HA2E5.

1.5 The goal of my study

Although previous studies demonstrated that HA2 peptide appeared to enhance endosomal release for CPP-mediated protein delivery (2,41,60), little is known about how HA2 peptide mediates this particular step. This is partly because it is difficult to investigate endosomal escape in a complex, cellular environment where many other processes take place. In addition, simpler but more controllable lipid bilayer models such as liposomes often fail to reproduce the peptide activities observed in cells (4). To study the effects of HA2 on endosomal escape comprehensively, I will utilize *in vitro* systems. The HA2 peptide and HA2 peptide mutant, HA2E5, fused to TAT will be used as the main chimeric CPPs in my study. HA2-TAT possesses both the delivery properties of TAT and the endosomal escape activity from HA2. My work will focus on investigating theendosomalytic activity of HA2-based peptides *in cellulo* and *in vitro*. The The knowledge acquired in this study will lay the foundation for the design of more efficient CPPs.

2. HA2-TAT PEPTIDE TAGS FOR THE DELIVERY OF PROTEINS

2.1 Introduction

In this section, I highlight the usefulness of HA2 peptide and the HA2 analog, E5 (HA2E5), as endosomolytic reagents that can improve the delivery of macromolecules into live cells. HA2 and E5 fused with TAT-mCherry protein will be the constructs to test the hypothesis that fusion of these peptide tags increases the delivery of macromolecules into the cytosolic space of live cells. The hydrophobicity of HA2 peptide is often problematic, and it is therefore unclear how this peptide might affect the biophysical and cellular properties of a protein fused to it. To answer these questions, the effects of additional HA2 tags on TAT-mCherry will also be also investigated.

2.2 Results

Two different HA2 sequences were fused to the N-terminus of the protein TAT-mCherry. These sequences consist of the wild-type HA2 peptide and of E5. HA2 and E5 typically are N-terminal because the peptides typically need to have a free N-terminal glycine to display a lytic activity and TAT is present to promote endocytosis of mCherry into live cells. mCherry was chosen as the model cargo because this protein is monomeric, soluble, non-cytotoxic and without a cellular activity. The rationale is therefore that the effects of HA2 and E5 would be easy to identify since the protein cargo itself should not interfere with the assays. mCherry is also fluorescent and the trafficking of this protein inside live cells can be monitored by fluorescence microscopy.

Finally, mCherry remains folded at pH as low as 4.0. The lytic activity of HA2 or E5 at acidic pH can therefore be assayed without causing denaturation and precipitation of the protein.

To study the property of the HA2 and E5 peptide tags, mCherry, TAT-mCherry, HA2-TAT-mCherry and E5-TAT-mCherry were cloned, over-expressed and purified using the IMPACT (Intein mediated purification with an affinity chitin-binding tag) system (Table 2-1). To note, the extended WYG residues on the C-terminal of HA2 have been shown to enhance the deliver efficiency (70). HA2-TAT-mCherry, and E5-TAT-mCherry were cloned with an N-terminal SUMO (small ubiquitin-like modifier) tag and the SUMO protease was used to generate the desired N-terminal sequences (confirmed by Edman sequencing).

2.2.1 Protein solubility and aggregation propensity analysis

HA2 peptides are known to have a high propensity to aggregate and precipitate in aqueous media (62). To investigate whether HA2 and E5 would affect the behavior of TAT-mCherry in water, the solubility of each of the protein constructs was first assessed using a HPLC (high-performance liquid chromatography) -based assay. HA2-TAT-mCherry and E5-TAT-mCherry were incubated at 37°C in PBS (phosphate buffer saline) with the pH adjusted to 7.0 or 4.5. These pH values correspond approximately to the pH extremes the proteins might encounter while transiting within endocytic organelles. Immediately after mixing the reagents or after an overnight incubation, the samples were centrifuged to pellet insoluble aggregates. The amount of soluble protein remaining in

Table 2-1 Sequences of the HA2-TAT peptides investigated

Name	Amino Acid Sequence	Mw (Da)
HIV TAT (48-57)	GRKKR RQRRR	
Influenza HA2 (1-23)	GLFGA IAGFI ENGWE GMIDG WYG	
TAT-*mCherry*[a]	GR KKRRQ RRR	29585
HA2-TAT-*mCherry*[a,b]	GLFGA IAGFI ENGWE GMIDG WYGGR KKRRQ RRR	31896
E5-TAT-*mCherry*[a,b]	GLFEA IAEFI ENGWE GLIEG WYGGR KKRRQ RRR	32036

[a] the sequence represented is at the N-terminus of mCherry

[b] the underlined sequence represents the sequence analyzed by Edman sequencing.

of mCherry, TAT-Cherry, and E5-TAT-mCherry was not affected by incubation time or pH. In contrast, HA2-TAT-mCherry showed an approximately 40% decrease in soluble content when exposed to pH 4.5 after an overnight incubation. Importantly, the protein mCherry does not unfold under these conditions and precipitation can therefore be attributed to the HA2-TAT tag.

In addition to being poorly soluble, HA2 peptides have been shown to self-associate in solution (57). The oligomerization propensity of the protein constructs was investigated by Size Exclusion Chromatography (SEC). mCherry and TAT-Cherry eluted as monomers with the expected molecular weight of approximately 29 kDa. In contrast, HA2-TAT-mCherry eluted in the column's dead volume, indicating that soluble aggregates with molecular weights superior to 200 kDa were present in the sample. Only a small fraction of the sample (<5% based on the integrated peak area) eluted as a monomer. In the case of E5-TAT-mCherry, two elution peaks indicating the formation of possible trimers and dimers were present (Fig. 2-1A). Sedimentation velocity analytical ultracentrifugation was performed on E5-TAT-mCherry to confirm these results. However, the sedimentation coefficient obtained from this sample was 2.6 ± 0.1, a value similar to that obtained for TAT-mCherry (2.5 ± 0.1) and corresponding to a molecular weight of approximately 27.5 ± 0.5 kDa. The protein therefore appears to be monomeric in this experiment. A possible explanation for the discrepancy between the size exclusion and sedimentation results is that E5-TAT-mCherry might form weakly bound oligomers that remain associated during SEC but not during analytical ultracentrifugation. Finally, the difference in aggregation propensity between HA2-TAT-

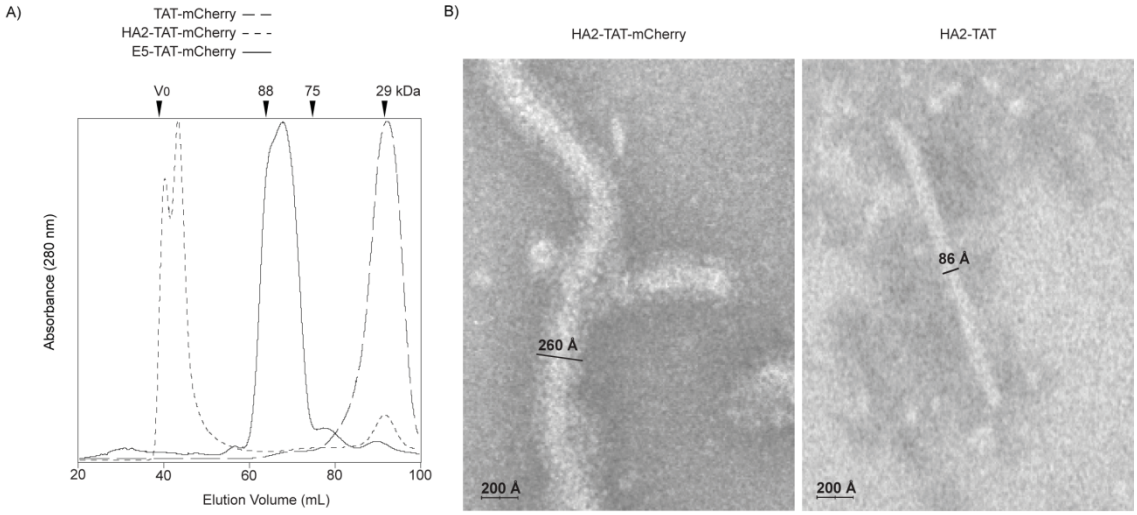

Figure 2-1 Biochemical analysis of E5-TAT-mCherry. A) Size exclusion chromatography of TAT-mCherry, HA2-TAT-mCherry, and E5-TAT-mCherry. The void volume and elution volume of standards with known molecular weights are indicated with black arrows. B) Electron microscopy images of aggregated HA2-TAT-mCherry and HA2-TAT. No aggregates were detected when E5-TAT-mCherry or E5-TAT were analyzed under similar conditions.

mCherry and E5-TAT-mCherry was further revealed by electron microscopy. Consistent with the SEC analysis, no large aggregate could be observed for E5-TAT-mCherry. In contrast, fibrils with a diameter of 260-290 Å were readily observed with HA2-TAT-mCherry, (HA2-TAT alone showed fibrils of 86Å in diameter) (Fig. 2-1B). Overall, these results suggest that HA2 has a strong propensity to aggregate and that its addition to the N-terminus of a protein causes the formation of large yet soluble protein aggregates. In contrast, aggregation is much reduced when the protein is labeled with E5.

2.2.2 Cytotoxicity of the protein constructs

The cytotoxicity of mCherry, TAT-mCherry, HA2-TAT-mCherry and E5-TAT-mCherry toward HeLa cells was assessed using the MTT (3-(4,5-Dimethylthiazol-2-yl)-2,5-diphenyltetrazolium bromide) assay. As expected, the innocuous mCherry did not display significant cytotoxicity in the concentration range tested (2.5 -10 μM). Addition of TAT caused a modest increase in the cytotoxicity of the protein. In contrast, HA2-TAT-mCherry was significantly more cytotoxic, indicating that the addition of HA2 affects the interaction between the protein and cells. Interestingly, HA2-TAT-mCherry was less toxic than HA2-TAT alone at 5 or 10 μM, indicating that the protein moiety reduces the toxicity of the peptide. Finally, E5-TAT-mCherry had a cytotoxicity which was comparable to that of TAT-mCherry. The mutations present in E5 as compared to HA2 therefore appear to be sufficient to reduce the cytotoxicity of the peptide (Fig. 2-2).

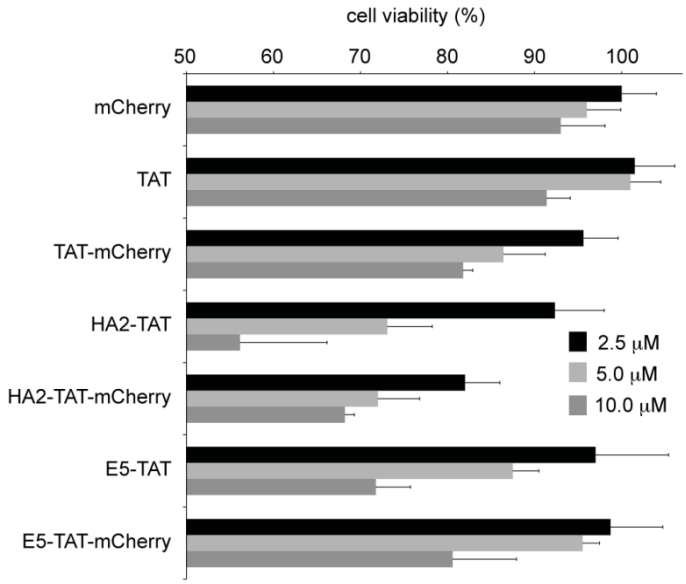

Figure 2-2 Viability of HeLa cells incubated with TAT-mCherry, HA2-TAT-mCherry, and E5-TAT-mCherry. The cytotoxicity of the delivery peptides alone was also tested for comparison. Cells were treated with the molecules at the concentrations displayed for 1 hour, washed, and incubated in fresh media for an additional 3 hours. Viability was then measured using the MTT assay.

2.2.3 Hemolytic activity of HA2-TAT-mCherry and E5-TAT-mCherry as a function of pH

The hemolysis activities of HA2-TAT-mCherry and E5-TAT-mCherry were characterized by an *in vitro* erythrocyte lysis assay (Fig. 2-3). HA2-TAT-mCherry and E5-TAT-mCherry were incubated with human RBCs (red blood cells) in PBS with a pH adjusted to different values. The release of hemoglobin from lysed red blood cells was then measured spectrophotometrically at 450 nm (at the concentrations used, the absorbance of mCherry does not contribute to the signal). The control proteins mCherry and TAT-mCherry did not cause any hemolysis at any of the conditions tested (up to 20 μM, pH 4.0-7.5). Unexpectedly, HA2-TAT-mCherry did not cause lysis either (up to 20 μM, pH 4.0-7.5). In contrast, E5-TAT-mCherry caused hemolysis at pH values below 6.0 (Fig. 2-3A). However, the hemolytic activity of E5-TAT-mCherry was quite reduced in comparison to E5-TAT. The pK50, or pH at which 50% hemolysis is achieved, was reported to be 6.7 for E5-TAT but appears to be approximately 5.7 for E5-TAT-mCherry. E5-TAT-mCherry also needs to be approximately 10-fold more concentrated than E5-TAT to achieve a similar hemolytic yield (Fig. 2-3B).

2.2.4 Characterization of the cellular distribution of HA2-TAT-mCherry and E5-TAT-mCherry

The transduction activities of HA2-TAT-mCherry and E5-TAT-mCherry were tested by incubating the proteins with HeLa cells. The proteins mCherry and TAT-mCherry were used for comparison. A 70 kDa dextran-fluorescein was also added

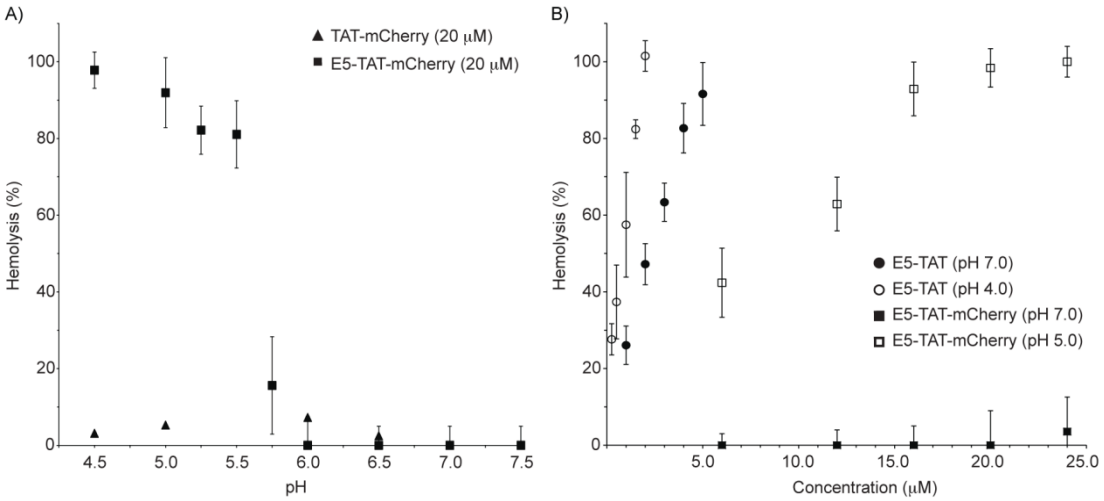

Figure 2-3 A) Hemolytic activities of TAT-mCherry and E5-TAT-mCherry as a function of pH. Hemolysis is reported as a percentage of the maximal release of hemoglobin obtained by treatment of the red blood cells with the detergent Triton X. B) Hemolytic activities of E5-TAT and E5-TAT-mCherry at pH 7.0, 5.0 and 4.0 as a function of peptide or protein concentration for 1.25% RBC suspensions.

as a marker of pinocytosis. After 1 hour incubation with HeLa cells, TAT-mCherry and dextran-fluorescein colocalized and displayed a punctate distribution consistent with these molecules being localized within endocytic organelles. Similar observations were made with HA2-TAT-mCherry and E5-TAT-mCherry. However, in contrast to TAT-mCherry, both HA2-TAT-mCherry and E5-TAT-mCherry were associated with the plasma membrane of cells. The proteins initially appeared homogeneously distributed on the cell surface. However, large fluorescent clusters seemed to form within 20 min of examination, suggesting that the proteins might aggregate on the cell surface over time. The protein residing at the plasma membrane could be washed by treatment with heparin, a negatively charged and soluble glycosaminoglycan known to inhibit the binding of TAT to membrane bound heparan sulfate proteoglycans (72-74). Addition of heparin to HA2-TAT-mCherry and E5-TAT-mCherry during incubation with cells also prevented the binding of the proteins to the membrane of cells and endocytic uptake (Fig. 2-4). These results indicate that the binding of HA2-TAT-mCherry and E5-TAT-mCherry to the plasma membrane is in part mediated by TAT. Yet, since the membrane staining of HA2-TAT-mCherry and E5-TAT-mCherry but not TAT-mCherry showed large fluorescent clusters, it appears that both HA2 and E5 increase the retention of the protein aggregate at the plasma membrane.

2.2.5 Characterization of the endosomolytic and cytosolic release activities of HA2-TAT-mCherry and E5-TAT-mCherry

HA2-TAT-mCherry and E5-TAT-mCherry co-localized with 70 kDa dextran-

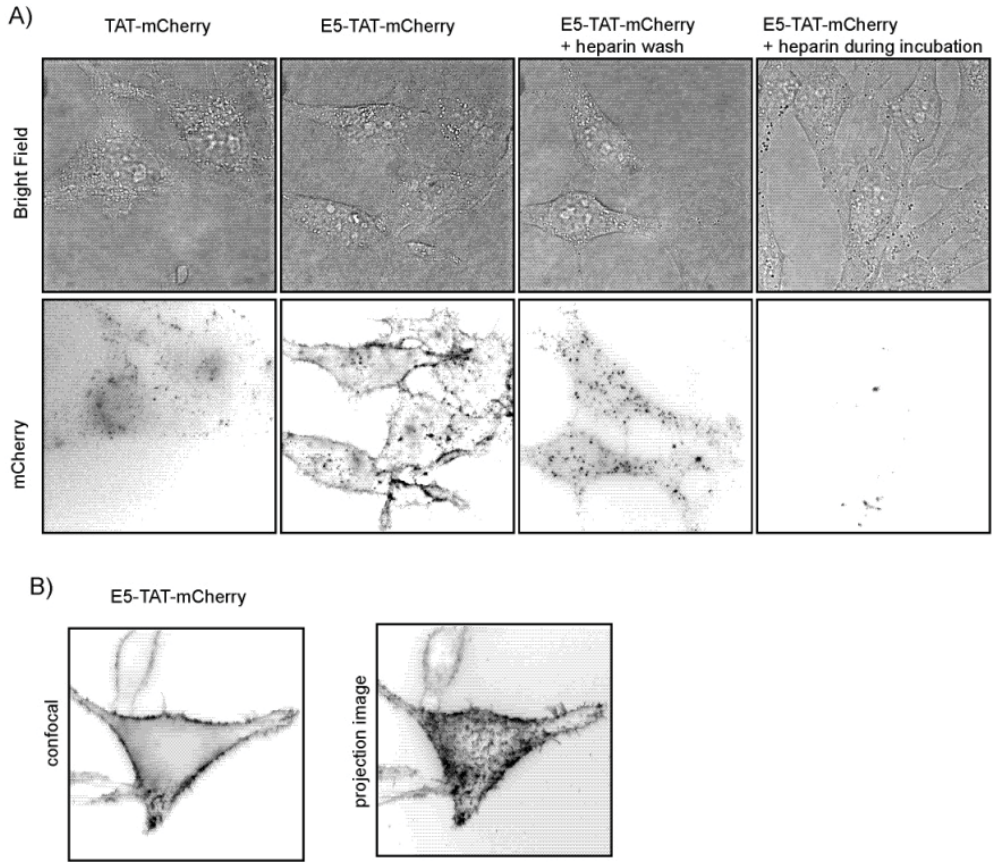

Figure 2-4 Microscopy images of HeLa cells incubated with TAT-mCherry or E5-TAT-mCherry (5 μM, 1 hour incubation). Both TAT-mCherry and E5-TAT-mCherry have a punctate distribution that is consistent with accumulation of these proteins within endocytic organelles. However, E5-TAT-mCherry also remains associated with the plasma membrane even after extensive washing with fresh media (as shown in confocal and 3D projection images). Addition of heparin to the washing media reduces the amount of protein bound to the plasma membrane and the protein accumulated within endocytic organelles appears more clearly. Addition of heparin during incubation suppresses both plasma membrane binding and accumulation within endocytic organelles.

fluorescein within endocytic organelles but the proteins did not appear to diffuse into the cytosolic space of the cells examined. However, in approximately 5% of the cells incubated with E5-TAT-mCherry, the fluorescent dextran had a cytosolic distribution as well as a punctate distribution (Figs. 2-5 and 2-6, the punctate distribution of the fluorescent signal observed in the cytosol is less than that of the dextran left inside endocytic organelles). These cells were not stained by SYTOX Blue, indicating that the permeability of the plasma membrane of these cells was not compromised post-incubation. The cytosolic distribution of dextran was not observed when E5-TAT-mCherry was not added to the incubation media or when TAT-mCherry was used. These results therefore indicate that the E5 moiety in E5-TAT-mCherry might be involved in mediating the transport of the dextran into the cell cytosol. However, the mechanism by which E5-TAT-mCherry might mediate the endosomal release of dextran-fluorescein could not be investigated precisely because of the low efficiency of this process. Nonetheless, the observation that E5-TAT-mCherry was not distributed in the cytosol of cells that showed endosomal release of dextran-fluorescein is intriguing. Instead, the distribution of E5-TAT-mCherry remained punctate. These results therefore suggest that the protein might still be associated with endosomes (co-localization of E5-TAT-mCherry and dextran-fluorescein in these fluorescent spots confirm that the punctate distribution corresponds to endocytic organelles loaded with both species rather than protein aggregates that might have form protein aggregates that might have formed once the protein escapes into the cytosolic space, Fig. 2-7). The gyration radius of 70 kDa dextran-fluorescein is approximately 18 nm while the radius of the 32 kDa E5-TAT-

Figure 2-5 Fluorescence microscopy of HeLa cells incubated with E5-TAT-mCherry (5 μM) and 70 kDa Dextran-fluorescein (Dx-Fl). Images were obtained with a 10 X objective. The fluorescence signals are represented in inverted monochrome images or in an overlay image (mCherry is pseudo-colored red and fluorescein is pseudo-colored green). The fluorescence signal of E5-TAT-mCherry associated with cells corresponds to a punctate endocytic distribution not discernable at 10 X but discernable at 100 X (see Fig. 2-6). The fluorescence signal of Dx-Fl observed is that of molecules delivered into the cytosolic space of cells (the fluorescence signal of fluorescein is quenched inside acidic endocytic organelles and, at 10 X, this signal is not detectable under the imaging conditions used). Only 5% of the cells examined have an observable fluorescein signal. This is increased to 60% when the endosomolytic peptide E5-TAT was added to the incubation media. Addition of bafilomycin, an inhibitor of endosomal acidification, however reduced the release of Dextran-fluorescein into the cytosolic space of cells to non-detectable levels (Dextran-fluorescein is still present within endocytic organelles, see Fig. 2-6). The distribution of E5-TAT-mCherry remains unchanged in these experiments, indicating that the protein is associated with endocytic organelles regardless of whether endosomal lysis is achieved or not. The cells represented were not stained by SYTOX Blue, indicating that the plasma membrane of these cells is not compromised.

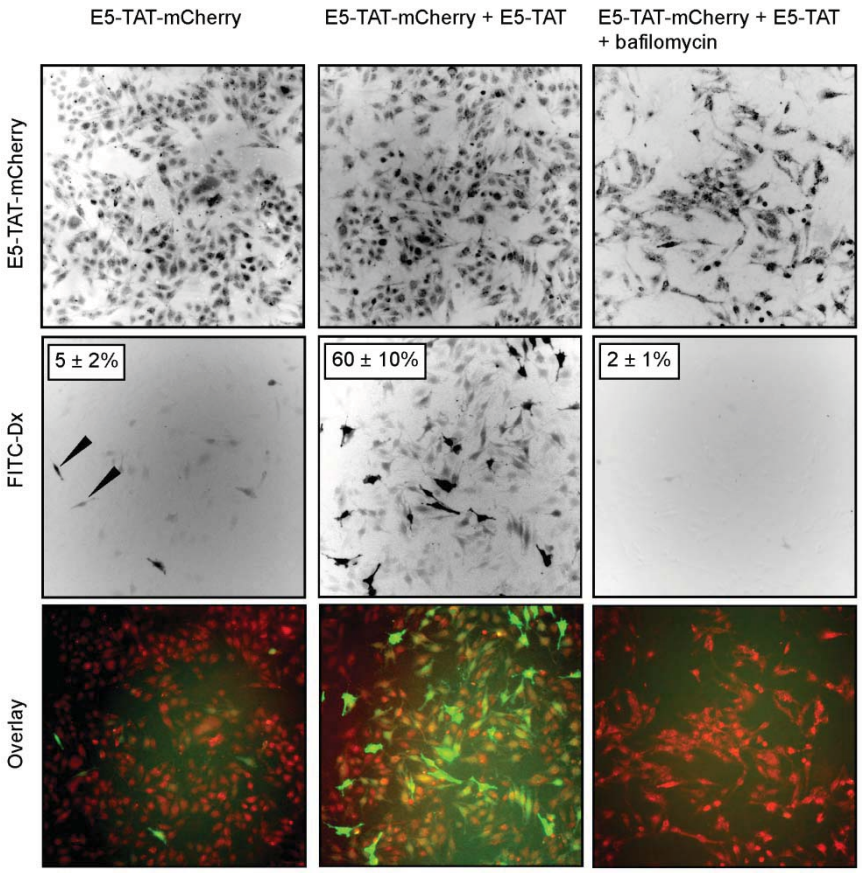
E5-TAT-mCherry
E5-TAT-mCherry + E5-TAT
E5-TAT-mCherry + E5-TAT + bafilomycin
E5-TAT-mCherry
FITC-Dx
Overlay
5 ± 2%
60 ± 10%
2 ± 1%

.

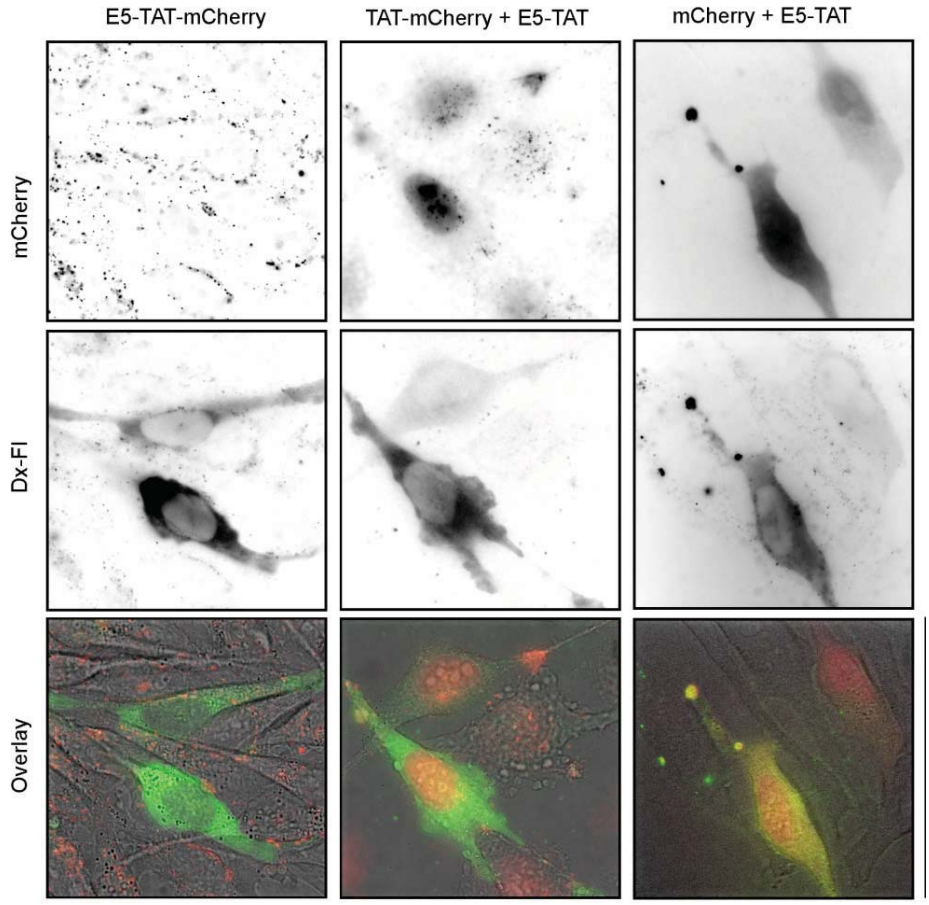

Figure 2-6 Fluorescence microscopy of HeLa cells incubated with E5-TAT-mCherry, TAT-mCherry and mCherry. Images were obtained with a 100 X objective. A 70 kDa Dextran-fluorescein (Dx-Fl) was used during incubation to detect the endosomal release of endocytosed molecules (as detected by its diffuse cytoplasmic distribution accompanied by nuclear exclusion). In the case of TAT-mCherry and mCherry, endosomal release was induced by addition of the endosomolytic peptide E5-TAT in the incubation media. For TAT-mCherry and mCherry cells with a cytosolic distribution of Dx-Fl also show a protein distribution in the cytosolic and nuclear spaces. However, in the case of E5-TAT-mCherry, cells containing a cytosolic distribution of Dx-Fl do not show a cytosolic distribution of the protein but instead a punctate distribution. In all cases, the cytosolic distribution of Dx-Fl and proteins was abolished by addition of bafilomycin during incubation and imaging. The cells represented were not stained by SYTOX Blue, indicating that the plasma membrane of these cells is not compromised.

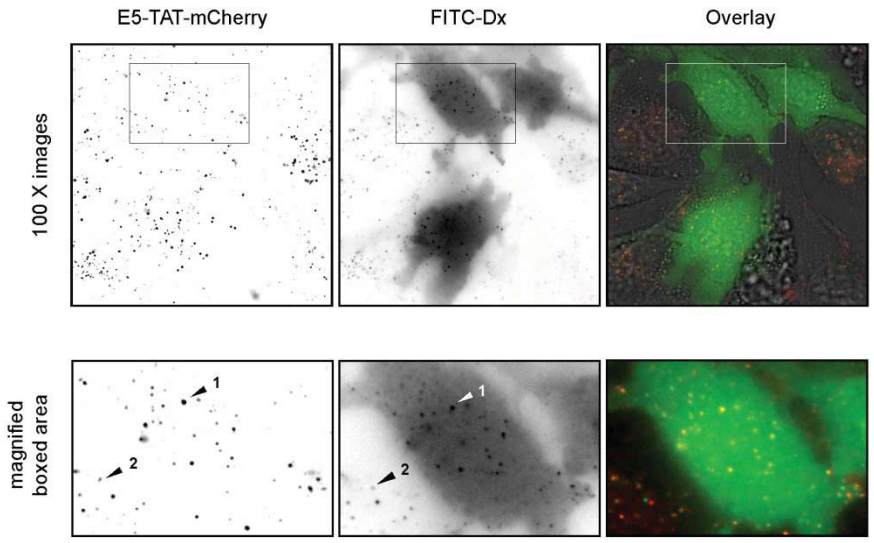

Figure 2-7 Fluorescence microscopy of HeLa cells incubated with E5-TAT-mCherry. Images were obtained with a 100 X objective. A 10 kDa Dextran-fluorescein (Dx-Fl) was used during incubation to detect the endosomal release of endocytosed molecules (as detected by its diffuse cytoplasmic distribution). Dx-Fl showed a protein distribution in the cytosolic. However, in the case of E5-TAT-mCherry, cells containing a cytosolic distribution of Dx-Fl do not show a cytosolic distribution of the protein but instead a punctate distribution. The arrow labeld with 1 indicates Dx-Fl colocalizing with E5-TAT-mCherry in endosomal vesicles of a cell containing a cytosolic distribution. The arrow labeld with 2 indicates Dx-Fl colocalizing with E5-TAT-mCherry in endosomal vesicles of a cell containing only punctate distribution of both molecules.

mCherry is expected to be less than 10 nm (75). If the larger dextran-fluorescein can escape while E5-TAT-mCherry cannot, it is therefore not the size of the protein that limits its ability to reach the cytosolic space.

To address the issue of why E5-TAT-mCherry fails to reach the cytosolic space when dextran-fluorescein does, E5-TAT was added to the incubation mixture. The principle of this approach is that E5-TAT and macromolecules are endocytosed together and that, upon acidification of the lumen of endosomes, E5-TAT causes the release of the macromolecules contained inside the endosomes into the cytosolic space of cells through formation of pores. The goal was therefore, to determine whether E5-TAT-mCherry could be released into the cytosol of cells if endosomes were rendered leaky. Addition of E5-TAT to the E5-TAT-mCherry and dextran-fluorescein incubation mixture greatly increased the population of cells containing dextran-fluorescein (approximately 60% of cells, Fig. 2-5). Addition of the vacuolar H^+-ATPase inhibitor bafilomycin inhibited the endosomal release of dextran-fluorescein. This indicates that acidification of the lumen of endosomes is required for the cytosolic delivery of the dextran and that E5-TAT mediates this process by causing endosomal release (as opposed to plasma membrane permeabilization). Despite this observed increase in the number of cells containing dextran-fluorescein in their cytosolic space, addition of E5-TAT did not increase the delivery of the protein into the cytosol of cells. In contrast, addition of E5-TAT led to the cytosolic delivery of mCherry and TAT-mCherry, as shown in Fig. 2-6 (accumulation of TAT-mCherry in the nucleus can be observed while mCherry has a diffuse distribution throughout the cell, as expected from the

microinjection results). Together these results indicate that E5-TAT-mCherry fails to reach the cytosolic space because of the E5 moiety. These results also suggest that E5-TAT-mCherry does not reach the cytosol because it remains associated with endosomes. This happens even when endosomal lysis and release of dextran-fluorescein takes place and regardless of whether endosomal lysis is mediated by E5-TAT-mCherry itself or by the addition of E5-TAT.

2.2.6 Effect of TAT on the intracellular distribution of the model protein mCherry

To determine the effect that the delivery tags might have on the cellular distribution of their mCherry cargos, the proteins TAT-mCherry, HA2-TAT-mCherry, and E5-TAT-mCherry were microinjected into the cytosol of live HeLa cells. The goal of most delivery applications is to deliver a macromolecule into the cytosolic space. The distribution of the microinjected macromolecules therefore serves as a model for what might be expected after successful delivery with a CPP tag. The proteins were microinjected along with a 70 kDa dextran-fluorescein and the distribution of the fluorescent molecules were observed by wide-field and confocal fluorescence live cell microscopy. The microinjected protein control mCherry was homogenously distributed throughout the cell, including the nucleus (Fig. 2-8). This is expected because the molecular weight of the protein, 28 kDa, is below the nuclear diffusion threshold (~50 kDa) (76). The soluble protein can therefore diffuse across the nuclear pore complex. In contrast, the 70 kDa dextran-fluorescein is excluded from the nucleus and its signal confirm that the material was microinjected in the cytoplasm as opposed to the nucleus.

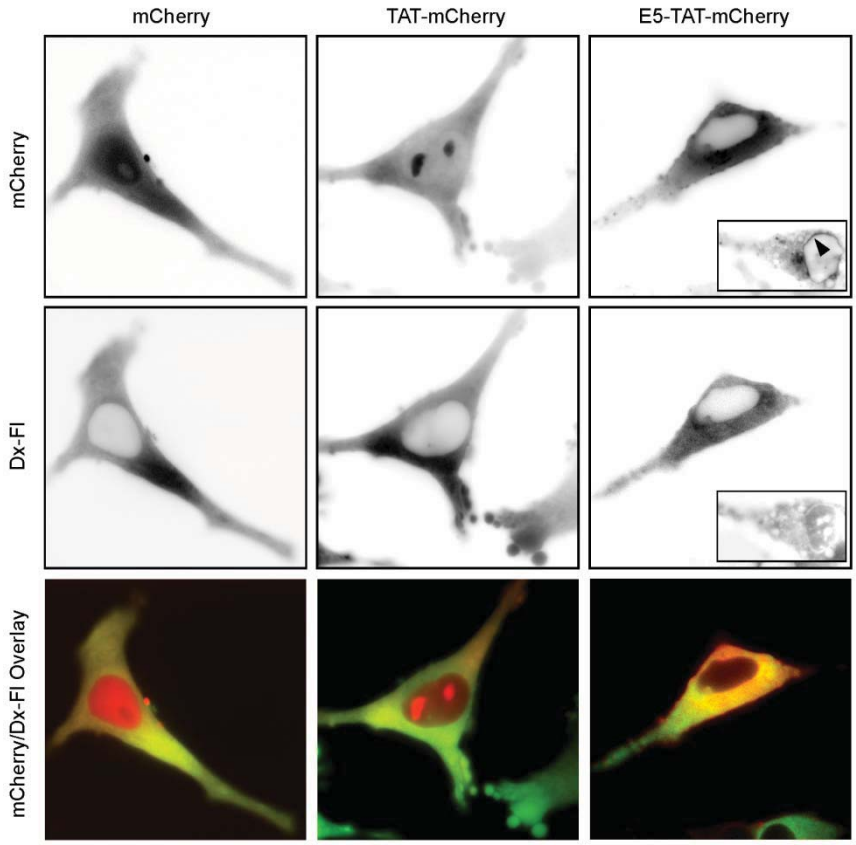

Figure 2-8 Fluorescence microscopy of HeLa cells microinjected 70 kDa Dextran-fluorescein (Dx-Fl) and mCherry, TAT-mCherry, or E5-TAT-mCherry. Nuclear exclusion of the 70 kDa Dextran-fluorescein (Dx-Fl) was used to determine that the site of microinjection was the cytoplasm. Microinjected mCherry diffuses into the nucleus and the protein is distributed homogeneously throughout the cell. TAT-mCherry also diffuses into the nucleus and accumulates at nucleoli. In contrast, E5-TAT-mCherry does not accumulate in the nucleus and appears retained in the cytoplasm instead. When a larger amount of E5-TAT-mCherry is microinjected, the protein appears to accumulate at membraneous organelles (insert, accumulation at the nuclear membrane is highlighted with a black arrow).

TAT-mCherry also diffused throughout the cell. However, in contrast to mCherry, TAT led to the accumulation of the protein at the nucleoli (Fig. 2-8). This is a well-known effect of TAT and is consistent with reports that have suggested that the sequence GRKKR (the TAT sequence is GRKKRRQRRR) acts as a nucleolar localization signal (77). Despite containing the TAT moiety, the microinjected HA2-TAT-mCherry and E5-TAT-mCherry did not accumulate at the nucleoli. Instead, the fluorescence signal of these proteins within the nucleus was greatly reduced in comparison to that of the cytoplasm**.** HA2-TAT-mCherry and E5-TAT-mCherry also appeared to have a non-uniform cytosolic distribution indicative of a possible association with cytoplasmic organelles. Direct microinjection of the proteins into the nucleus of cells led to a similar cytoplasmic distribution, indicating that the proteins were able to traffic out of the nucleus. Together, these observations suggest that HA2-TAT-mCherry and E5-TAT-mCherry are retained in the cytoplasm because the proteins bind to cytosolic components. Overall, covalent attachment of HA2-TAT or E5-TAT to mCherry appears to greatly compromise the localization of the protein inside cells.

2.3 Discussion

Proteins fused to PTDs, while efficiently internalized by endocytic mechanisms, often remain trapped inside endocytic organelles during delivery. Combining the HA2 peptide with a PTD might provide a solution to this problem since HA2 is expected to respond to the acidic environment within endosomes and cause the lysis of the endosomal membrane. However, to be useful as a delivery tool, HA2-PTD fusion tags

should, in principle, have little effect on the biophysical and intracellular properties of their protein cargo. This is based on the notion that a protein delivery tag should not perturb the function of its protein cargo and that it should not disrupt the physiology of cells during or after delivery. HA2, fused to the N-terminus of the model protein TAT-mCherry, did not fulfill these requirements. First, HA2 altered the in vitro behavior of the protein extensively. While TAT-mCherry is monomeric, HA2-TAT-mCherry formed large soluble aggregates. In addition, fusion of HA2 significantly increased the cytotoxicity of the protein. These problems were in part resolved by replacing HA2 to its analog E5. E5 differs from HA2 by including the G4E, G8E, M17L and D19E mutations. Addition of the glutamate residues has been demonstrated to increase the solubility and pH dependent lytic activity of HA2 analogs (*1, 10, 11)*. E5 greatly reduced the propensity of the protein to form large aggregates and to precipitate. The cytotoxicity of E5-TAT-mCherry was also reduced when compared to HA2-TAT-mCherry and was comparable to that of TAT-mCherry. The E5-TAT tag therefore appears to be equivalent to TAT with regard to these properties.

While solving important aggregation and cytotoxicity problems, E5-TAT, like HA2-TAT, did not appear to increase the delivery of its mCherry cargo. First, the lytic activity of E5-TAT-mCherry was significantly lower than that of E5-TAT itself. This is puzzling and understanding how the addition of a protein to the C-terminus of E5-TAT might affect the lytic activity of the peptide remains an important question to answer if one is to use this approach to deliver macromolecules. These observations suggest, however, that enhancing the lytic activity of the fusion tag would not be sufficient to achieve

delivery. For instance, addition of E5-TAT increased the number of cells in which dextran-fluorescein escaped from endosomes but did not increase the cytosolic delivery of E5-TAT-mCherry as the protein still remained localized at endosomes. The results suggest that this might be due to the affinity of E5-TAT for membranes. This membrane affinity was also illustrated by the extensive binding of E5-TAT-mCherry to the plasma membrane of HeLa cells and by the cytoplasmic retention of the microinjected protein.

Overall, these results suggest an important problem in the use of HA2 analogs as delivery tags for protein cargos. HA2 and HA2 analogs are designed to lyse endosomal membranes in a pH-dependent manner. This activity is linked to the amphipathic and helical nature of the peptide and membrane lysis involves a direct binding between the peptide and the endosomal lipid bilayer. However, the hydrophobicity of the peptide and its binding to membranes appears to lead to a failure in the delivery of the protein and a dramatic alteration of the protein's intracellular behavior. This is the case not only for the hydrophobic and poorly behaved HA2 but also for E5, a tag with improved *in vitro* properties. On one hand, it is possible that tuning the properties of HA2 analogs or combining the peptides with other PTDs might solve this problem. On the other hand, data suggest that a solution might be to introduce linkers between the HA2-TAT delivery tag and its protein cargo that could be cleaved inside cells. Because the hemolytic activity of E5-TAT is far greater than that of E5-TAT attached to mCherry, an ideal linker would be one that is cleaved inside endosomes. Linker cleavage would therefore both induce an increase in the endosomolytic activity of E5-TAT but also release an

unperturbed protein that would be able to escape into the cytosol. The design of such systems will be the object of further studies.

2.4 Materials & Methods

2.4.1 Cloning and protein expression of HA2-TAT-mCherry and E5-TAT-mCherry

Cloning was designed to obtain a gene coding for a SUMO-HA2-TAT-mCherry construct in the pTXB1 vector (New England Biolab). The HA2 encoding oligonucleotides 5'-TAT GGG TCT GTT TGG TGC TAT CGC TGG TTT CAT CGA GAA CGG TTG GGA AGG TCA-3' and 5'-TAT GAC CTT CCC AAC CGT TTT CGA TGA AAC CAG CGA TAG CAC CGA ACA GAC C-3' were first annealed and inserted into a Nde-I digested pTXB1. A SUMO-HA2 gene was then constructed by overlap extension by PCR (polymerase chain reaction). The HA2 sequence was amplified by PCR of the pTXB1-HA2 vector with the primers 5'-CAC AGA GAA CAG ATT GGT GGT GGT CTG TTC GGT GCT ATC GCT-3' and 5'-CTC CAG GCG GCC GCC ACC GTA CCA ACC ATC GAT CAT ACC TTC CCA-3'. The SUMO sequence was amplified by PCR of the pET SUMO vector (Invitrogen) with the primers 5'-GAT ATA CAT ATG GGT CAT CAC CAT CAT-3' and 5'-CAG CGA TAG CAC CGA ACA GAC CAC CAC CAA TCT GTT CTC TGT G-3'. The SUMO and HA2 DNA fragments were combined, denatured, annealed, and extended by PCR with the primers 5'-GAT ATA CAT ATG GGT CAT CAC CAT CAT-3' and 5'-CTC CAG GCG GCC GCC ACC GTA CCA ACC ATC GAT CAT ACC TTC CCA-3' to obtain the recombined SUMO-HA2 product. The SUMO-HA2 DNA was inserted into a NdeI and NotI digested pTXB1

to obtain pTXB1-SUMO-HA2. The oligonucleotides 5'-GGC CGC AAA AAA CGT CGT CAG CGT CGT CGT-3' and 5'-GCA ACG ACG ACG CTG ACG ACG TTT TTT GC-3' were annealed and ligated into NotI and SapI digested pTXB1-SUMO-HA2 to yield a pTXB1-SUMO-HA2-TAT product. The SUMO-HA2-TAT sequence was amplified by PCR with the primers 5'-GAT ATA CAT ATG GGT CAT CAC CAT CA-3' and 5'-TGC ATC TCC CGT CAT ATG ACG ACG ACG CTG-3'. The PCR product was digested with NdeI and ligated into a previously described pTXB1-mCherry vector digested with NdeI.(78) The product obtained is pTXB1-SUMO-HA2-TAT-mCherry. It encodes for the protein SUMO-HA2-TAT-mCherry-GyrA-CBD, where GyrA is an intein and CBD a chitin-binding domain. Sequencing of the construct demonstrated the absence of mutations. The product pTXB1-SUMO-E5-TAT-mCherry was obtained by mutagenesis of pTXB1-SUMO-HA2-TAT-mCherry using the QuikChange site-directed mutagenesis kit and the primers.

The plasmids were transformed into BL21-DE3 cells and protein expression was induced with 0.5 mM IPTG (isopropyl β-D-1-thiogalactopyranoside) at 37C for 3 hr. Cells were harvested and resuspended in lysis buffer containing 20 mM Tris-Cl (pH 7.5) and 200 mM NaCl. After cell lysis by sonication and high-speed centrifugation at 15000 rpm for 30 min, the soluble fraction was applied to chitin resin pre-equilibrated with lysis buffer and incubated overnight at 4°C. The resin was washed with 8 column volumes of lysis buffer. The SUMO-HA2-TAT-mCherry and SUMO-E5-TAT-mCherry moieties were cleaved from the resin by incubation of the beads with 1 column volume of buffer supplemented with 100 mM DTT for 24 hr at room temperature. This cleavage step

yields a cleaved protein with a C-terminal carboxylate. The SUMO tag was removed with the SUMO protease with the molar ratio of 1: 25 (SUMO protease: protein). The proteins were purified by cation-exchange chromatography in 50 mM HEPES at pH 7 (HiTrap SP HP, GE Healthcare). The final products are HA2-TAT-mCherry and E5-TAT-mCherry. The protein mass was confirmed by MALDI-TOF (matrix-assisted laser desorption/ionization time of flight) mass spectrometry (AXIMA-CFR, Shimazu, Kyoto). Protein sequence analysis by automated Edman chemistry was performed by the Protein Chemistry Laboratory at Texas A&M University to further confirm that the N-terminus of HA2 and E5 were properly generated. The N-terminal sequence was identified as GLFGAIA and GLFEAIAEFI with 99% confidence for HA2-TAT-mCherry and E5-TAT-mCherry, respectively.

2.4.2 Electron microscopy

Specimens were prepared by adding 5µl of sample (0.04-0.08 mg/ml in 20 mM Tris pH 7.8, 150 mM NaCl) onto freshly glow-discharged formvar-carbon coated grids and left to adhere for 1 minute. Specimens were then stained for 15 seconds in either 2% aqueous uranyl acetate (pH 4.5) or 2% sodium phosphotungstate (pH 7.0) and blotted dry. Specimens were observed on a JEOL 1200EX transmission electron microscope operating at an acceleration voltage of 100kV. Images were recorded at calibrated magnifications on KODAK 4489 film.

2.4.3 Analytical ultracentrifugation

Samples were analyzed by sedimentation velocity ultracentrifugation using a Beckman XLA centrifuge with an An60Ti rotor. Standard double-sector aluminum centerpiece cells with quartz windows and a 1.2 cm optical pathlength were used. Protein loading concentrations were 2–8 μM. Centrifugation was at 28,500 rpm and 25°C with absorbance scans at 280 nm taken at 3.5 min intervals. The absorbance scans were fit to a single sedimentation coefficient by using the computer program Svedberg from John Philo, with the uncertainties given as the 95% confidence intervals (79).

2.4.4 Microinjection of mCherry and TAT-mCherry into live cells

HeLa were cultured on 35 mm plates (P35G-1.5-7-C-grid, MatTek Corp., Ashland, MA) at 100,000 cells/mL in a total volume of 2 mL of Dulbecco's modified Eagle's medium supplemented with 10% FBS in a humidified atmosphere containing 5% CO_2. Cells were washed and incubated with Leibovitz's L-15 Medium and placed on the microscope. mCherry or TAT-mCherry (10 μM) were mixed with 70 kDa Dextran-fluorescein (10 μM) and femtoliter aliquots were directly injected into the cytoplasm of live HeLa cells using an InjectMan NI2 micromanipulator equipped with a FemtoJet microinjector (Eppendorf, Westbury, NY). The microinjected cells were imaged for up to 3 h after microinjection. Microinjection into the cytoplasm rather than nucleus was confirmed by observing nuclear exclusion of the 70 kDa Dextran. The localization of the nucleus within the injected cells was also confirmed by staining with the cell-permeable nuclear stain Hoecht 33342 (Molecular Probes, Carlsbad, CA).

2.4.5 Binding assay

The binding of E5-TAT-mCherry to intact RBCs as a function of pH was determined by incubating peptide (1 μM) with 1.25% RBC suspensions in PBS at different pH values (adjusted with HCl or NaOH, 4.5<pH<7.5). After 5 min incubation, the samples were centrifuged for 5 minutes at 1500g. The amount of peptide present in the supernatants was analyzed by SDS-PAGE (sodium dodecyl sulfate polyacrylamide gel electrophoresis) using 12% SDS-gel (pH 8.8). The gels were stained with coomassie and densitometric analysis of the intensity of the E5-TAT-mCherry bands was performed with the ImageQuant 5.0 software. The data were normalized using a sample containing E5-TAT-mCherry at pH 7.0 but with no RBC present as the one hundred percent soluble control.

2.4.6 Hemolysis assays

A membrane lysis assay was performed with human erythrocytes purchased from the Gulf blood bank (Galveston, TX). Erythrocytes were centrifuged for 5 min at 1500g. The erythrocyte pellet obtained was resuspended in PBS and this procedure was repeated three times to remove the plasma and buffy coat. The erythrocytes (resuspended in PBS to a 50% suspension) were then diluted 20 fold in PBS of different pH values (adjusted with HCl or NaOH, 4.5<pH<7.5). All proteins were diluted with PBS to desired concentrations and added to a 96-well plate. One hundred microliters of the 2.5% RBC suspension was added into each well. The plates were incubated at 37°C for 30 min. After centrifuging the plate for 5 minutes at 1500g, the supernatants were transferred to a

new 96-well plate. The absorbance of hemoglobin present in each well was measured at 450 nm using a plate reader (Bio-RAD, Ultramark Micro plate system, USA). One hundred percent hemolysis was obtained by incubating the RBC with 0.1% Triton X-100. Background hemolysis at various pH was evaluated by incubating the erythrocytes in the corresponding PBS solutions. The background signal from mCherry was also estimated by analyzing the absorbance of samples containing the proteins ate the desired concentration but no RBCs.

2.4.7 Microscopy assays

HeLa cells were seeded on 8-well chamber glass slide at 3.0 x 10^4 cells/well in Dulbecco's modified Eagle's medium supplemented with 10% FBS and incubated for 24 h at 37°C in a humidified atmosphere containing 5% CO_2. Cells were then incubated with L-15 medium (no FBS added) and placed on an inverted epifluorescence microscope (Model IX81, Olympus, Center Valley, PA) equipped with a heating stage maintained at 37°C. The microscope is configured with a spinning disk unit to perform both confocal and wide-field fluorescence microscopy. Images were collected using a Rolera-MGI Plus back-illuminated EMCCD camera (Qimaging, Surrey, BC, Canada). Images were acquired using phase contrast and three standard fluorescence filter sets: CFP (Ex = 436±20 nm / Em= 480±40 nm), Texas Red (Ex = 560±40 nm / Em= 630±75 nm), and FITC (fluorescein isothiocyanate) (Ex = 482±35 nm / Em= 536±40 nm). Cells were co-treated with of HA2-TAT-mCherry or E5-TAT-mCherry (2 μM) in L-15 medium containing 2.5 mg/mL of 70 kDa anionic dextran-fluorescein (78). After incubation at

37°C for 15 or 60 minutes, the cells were washed with PBS 5 times and the medium was replaced with fresh L-15. The integrity of the plasma membrane of the cells was determined by addition of the cell-impermeable DNA stain SYTOX® Blue. Cells with a blue fluorescent nucleus, detected with the CFP filter set, were considered compromised or dead. The cells that were not stained by SYTOX® Blue were further confirmed to be alive by detection of active transport of intracellular endocytic vesicles. To inhibit cell surface binding of the delivery peptides, heparin sodium salt (1 mg/mL) was added during the co-incubation step. For the inhibition of macropinocytosis, cells were first pretreated with 50 μM of amiloride (Sigma*,* MO*)* for 30 minutes, and then with E5-TAT-mCherry and 70 kDa dextran-fluorescein while keeping amiloride present. To inhibit acidification of the endolysosomal organelles, bafilomycin (200 nM) was used in a similar protocol. Cells were then co-incubated with E5-TAT-mCherry and 70 kDa dextran-fluorescein in L-15 supplemented with bafilomycin (200 nM). The fluorescence intensities within cells were measured using the SlideBook 4.2 software (Olympus, Center Valley, PA).

HA2-TAT-mCherry and E5-TAT-mCherry were added to the 1.25% RBC suspension in PBS at pH 4.5 or 7 by dilution from their PBS stock to the desired final concentration. After incubation at 37°C for 20 minutes, two hundred microliters of these suspensions were added to the wells of an 8-well chamber glass slide (Nunc). Cells were placed on an inverted epifluorescence microscope (Model IX81, Olympus, Center Valley, PA) equipped with a heating stage maintained at 37°C. Cells were typically allowed to settle to the bottom of the dish for 5 minutes prior to imaging so as to obtain a

layer of cells in the focal plane. To wash ghosts, 200 μL of 2.5% RBC suspension with the hemolytic peptides were centrifuged for 5 minutes at 1500g. The supernatant was removed and cells were resuspended in 200 μL fresh PBS at a desired pH. A 20 μL aliquot of the cells was added to an 8-well glass slide and imaged to monitor the morphology and fluorescence of cells. These steps were repeated 3 to 5 times, or until spherical ghosts could not be recovered.

3. DELIVERY OF MACROMOLECULES INTO LIVE CELLS BY SIMPLE CO-INCUBATION WITH HA2- TAT*

3.1 Introduction

In Section 2, it has been shown by hemolysis assay that covalently linked E5TAT-mCherry exhibits pH-dependent lipid membrane disruption activity. This result indicates that E5TAT-mCherry could enhance endosomal release compared to TAT-mCherry alone. However, the hydrophobic property of HA2 sequence causes the whole protein tag to associate with the endosomal vesicle instead of escaping from endosomes. In addition, even when TAT-mCherry was released from endosomes, TAT caused the protein to accumulate within nucleoli. In summary, using covalently linked CPP-conjugated cargos for delivery is straightforward; yet CPPs may alter the native cellular localization and bioactivity of conjugated protein. Therefore, co-incubation delivery of CPPs and cargo protein is examined in this study. Dowdy and coworkers have shown that the cytosolic delivery of a TAT-Cre recombinase construct could be increased by co-incubation with a HA2-TAT conjugate. In this example, the increase in cytosolic targeting was demonstrated by measuring the biological activity of the delivered protein inside the cell. However, the delivery efficiency of HA2-TAT is mostly uncharacterized.

In Section 3, I am going to test the hypothesis that optimized CPPs might deliver

---

*Part of this section is reprinted with permission from Delivery of macromolecules into live cells by simple coincubation with a peptide by Lee YJ, Erazo-Oliveras A, Pellois JP *Chembiochem. 2010 Feb 15;11(3):325-30.*, Copyright 2010 by John Wiley & Sons, Inc. http://onlinelibrary.wiley.com/doi/10.1002/cbic.200900527/full

macromolecules to the cytosol of live cells by simple co-incubation without the promotions of increased levels of endocytosis (41,80,81). We therefore reasoned that a CPP might induce a cell to drink-up macromolecules present in its surrounding media and that CPPs and macromolecules might accumulate together inside endocytic organelles. A CPP capable of disrupting these endocytic organelles might then induce the release of the macromolecules into the cytosolic space.

Importantly, macromolecules would not have to be modified with the CPP, and any undesired effect of the CPP on the macromolecule's function or localization after delivery would be avoided. Although this co-incubation protocol might not be suitable for the delivery of molecules in therapeutic applications, it would be simpler and less invasive than other multistep delivery processes (e.g., osmotic lysis of pinocytic vesicles, plasma membrane permeabilization, scrape loading, or microinjection). Therefore this protocol represents a step towards making macromolecule delivery into cultured cells a routine procedure for imaging or cell biology applications.

3.2 Results

3.2.1 HA2-TAT cytotoxicity

To identify an effective concentration of CPP that could be used for the delivery of macromolecules without inducing cell death, the cytotoxicity of these peptides E3-TAT (D19E mutation form wild type HA2 from SPPS, solid phase peptide synthesis purpose), E5-TAT and TAT toward HeLa cells was first examined by using the MTT [3-(4,5-dimethylthiazol-2-yl)-2,5-diphenyl-2H-tetrazolium bromide] assay (Fig. 3-1) and by

observation of the cell morphology by phase-contrast imaging. Cells were exposed to the CPPs at different concentrations for 1 h, washed and incubated in L-15 media from 3 to 24 h before being assayed for viability. The results showed that TAT was essentially noncytotoxic under the conditions tested (1–20 μM) according to the MTT assay. However, above 10 μM, the peptide appeared to affect the morphology of a large population of cells. E3-TAT and E5-TAT did not induce a significant decrease in cell viability at concentrations below 2.5 μM. In contrast to TAT, the cytotoxicity of the peptides were, however, more acute at 5 mm and above. Overall, to minimize the physiological effects that the peptide might have on cells, concentrations of 10 μM of TAT and 2 μM of E3-TAT and E5-TAT were therefore set as upper limits for testing the delivery of fluorescent cargos to live cells.

3.2.2 HA2-TAT promote cellular uptake and endosomal escape of co-incubated fluorescent cargos

To characterize the CPP-mediated delivery of macromolecules in live cells, fluorescent dextrans and proteins were chosen as model cargos, including 10 and 70 kDa anionic Dextran-fluorescein, 10 and 70 kDa neutral Dextran-tetramethylrhodamine, 70 kDa neutral Dextran-Texas Red, the green fluorescent protein EGFP (27 kDa, pI=5.7, -7 charges at pH 7.2), and the red fluorescent proteins mCherry (28 kDa, pI=6.0, -4 charges at pH 7.2), MBP-mCherry (71 kDa, pI=5.5, -10 charges at pH 7) and tdTomato (55 kDa, pI=6.3, -6 charges at pH 7.2) (82). These molecules have different sizes and overall within the cells. Genetically encoded fluorescent proteins were tested because these

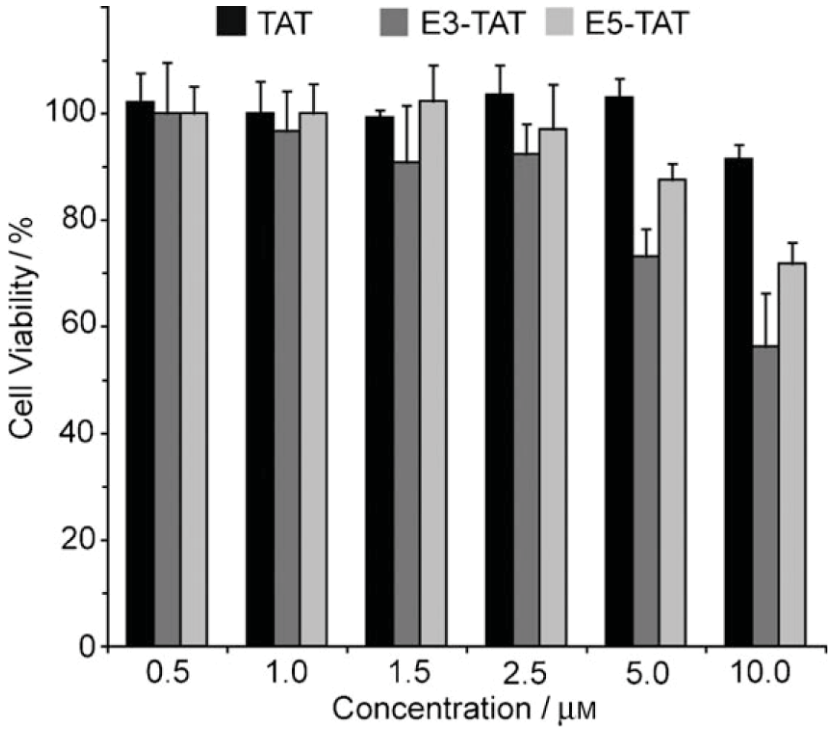

Figure 3-1 Viability of HeLa cells incubated with TAT, E3-TAT, or E5-TAT. Cells were treated with the peptides for 1 h, washed, and incubated in fresh media for an additional 3 h. Viability is measured as a function of peptide concentration by using the MTT assay.

charges as well as different chemical structures that might affect uptake and localization proteins lose their fluorescence if unfolded or proteolytically cleaved (78). Detection of their fluorescent emission inside a cell therefore serves as an indication that the proteins are not degraded. On the other hand, their fluorescent signals might disappear with time if the proteins remain trapped inside degradative organelles such as lysosomes. Dextrans are typically resistant to intracellular degradation, including degradation within the endolysosomal pathway (83). As a result, dextran–tetramethylrhodamine and dextran–Texas Red provide useful markers to measure and compare the endocytic or cytosolic distribution of fluorescent material internalized into a cell. (Fluorescein is pH sensitive and its fluorescence is partially quenched in the acidic lumen of endocytic organelles but tetramethylrhodamine and Texas Red are relatively insensitive to pH) (78). When co-incubated with the different fluorescent cargos, TAT, E3-TAT, and E5-TAT did not affect the fluorescence emission or anisotropy of the various fluorescent molecules tested; this indicates that the peptides do not bind to the cargos at detectable levels. Native-gel-electrophoresis analysis of the peptide/protein mixtures further confirmed that while TAT might bind to negatively-charged proteins to generate low concentrations of peptide/protein complexes, E5-TAT does not appear to interact with the fluorescent proteins tested at detectable levels (Figs. 3-2 and 3-3).

In a typical cell-based delivery assay, the CPPs (2μM) were incubated with two fluorescent cargos, one larger and one smaller than the nuclear diffusion threshold (~50 kDa) (76). Cell viability during these assays was determined by using SYTOX blue staining, and by observation of active transport of intracellular endocytic organelles with

time-lapse imaging **(**Fig. 3-4). HeLa (human cervical adenocarcinoma), COS-7 (SV40 transformed African green monkey kidney fibroblast-like cell line), and COLO 316 (human ovarian carcinoma) cells were incubated with the fluorescent macromolecules (10 μM for the proteins, 2.5 mg/mL for the dextrans, or approximately 250 μM and 36 μM for 10 kDa and 70 kDa dextrans, respectively), in combination with a CPP (2 μM) for 1 h. After washing the cells, internalization of the fluorescent material was imaged by live-cell fluorescence microscopy**.**

Under the conditions tested, cells incubated with just the macromolecules and no CPP displayed an intracellular punctate distribution of fluorescent markers of relative low fluores-cence intensity. This distribution is consistent with internalization of the fluorescent markers by fluid-phase endocytosis at basal level. The markers then remain trapped inside endocytic organelles. In contrast, cells incubated with the CPPs partitioned into two distinct populations: cells with a punctate labeling and cells with diffusely distributed fluorescent cargos. (These two populations are illustrated by the left-side image of Fig. 3-5A on p.56. Please note that 100% of the cells contained the fluorescent macromolecules but that fluorescence is either localized inside endocytic organelles or distributed throughout the cell). Nuclear exclusion of the large cargo served as a demonstration that the fluorescent signal observed was indeed intracellular rather than out-of-focus fluorescence of the cargos bound to the plasma membrane (right-side image in Fig. 3-5A on p.56, the nucleus is labeled with the 10 kDa dextran–fluorescein but not with the larger 70 kDa dextran–Texas Red). When TAT was used as delivery peptide, the population of the cells containing a diffused distribution of the

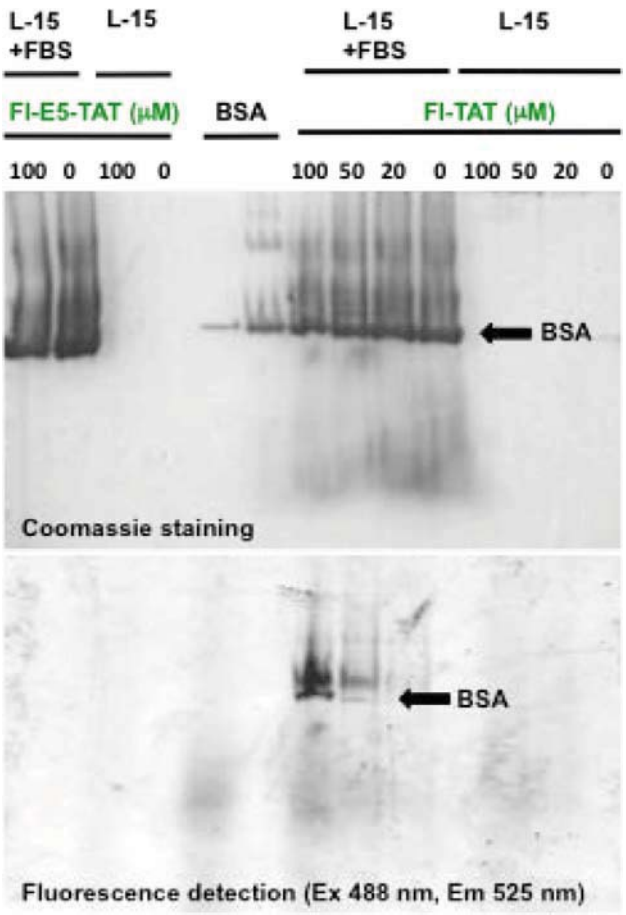

Figure 3-2 Non-covalent binding interaction between the delivery peptides and serum proteins. Fluorescein labeled TAT or E5-TAT was incubated in L-15 with or without 10% FBS and interaction were detected by native gel electrophoresis. The protein bands were detected by coomassie staining while the presence of protein-bound peptides was detected by the fluorescence signal of fluorescein. Fl-TAT binds to serum proteins (including BSA, bovine serum albumin) at 50 μM or more while no binding is observed for Fl-E5-TAT.

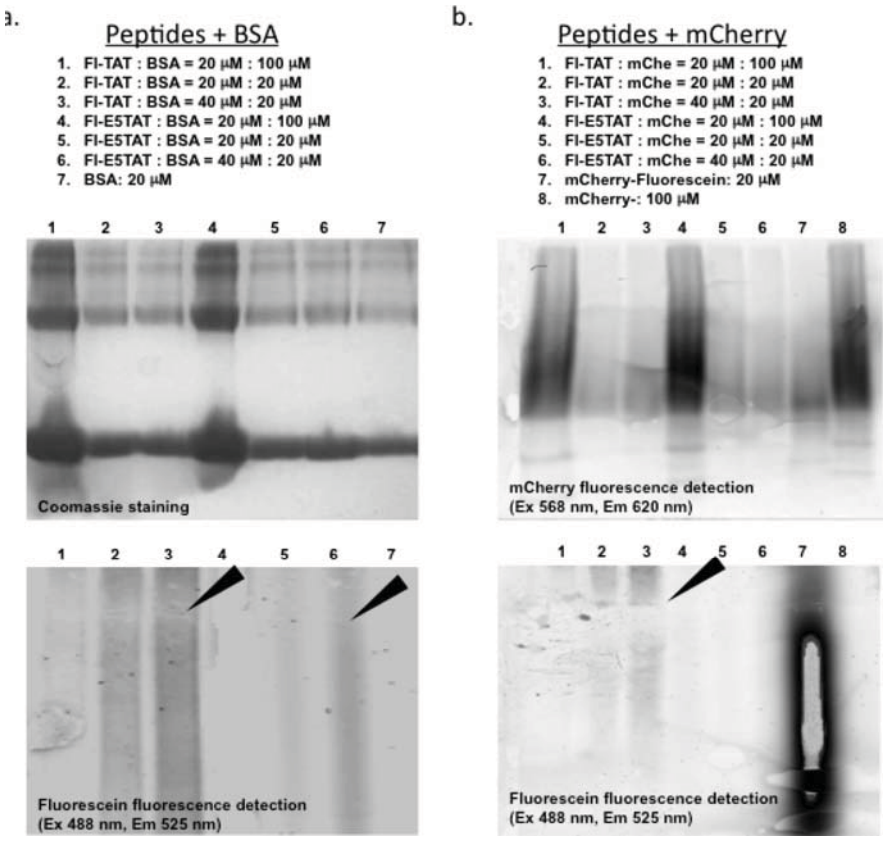

Figure 3-3 Non-covalent binding interactions between the delivery peptides and the proteins BSA (a) or mCherry (b). Fluorescein labeled TAT or E5-TAT was incubated in L-15 with the proteins at different ratio and interactions between peptides and proteins were detected by native gel electrophoresis. a) The protein bands were detected by coomassie staining for BSA (the BSA dimer and larger oligomers can be observed) while the presence of protein-bound peptides was detected by the fluorescence signal of fluorescein. Fl-TAT appears as a smear in lane 2 and 3. A smear is also present in lane 6 for Fl-E5-TAT (the fluorescence intensity is approximately 10% that of Fl-TAT). b) The protein bands were detected by the red fluorescence emission of mCherry while the presence of protein-bound peptides was detected by the green fluorescence signal of fluorescein. mCherry labeled with fluorescein (b, lane 7) was used as a control to validate that both mCherry and fluorescein fluorescence could be detected. Lane 7 is black with a white area in the center because the fluorescence signal is so high in the white area that the detector is saturated.

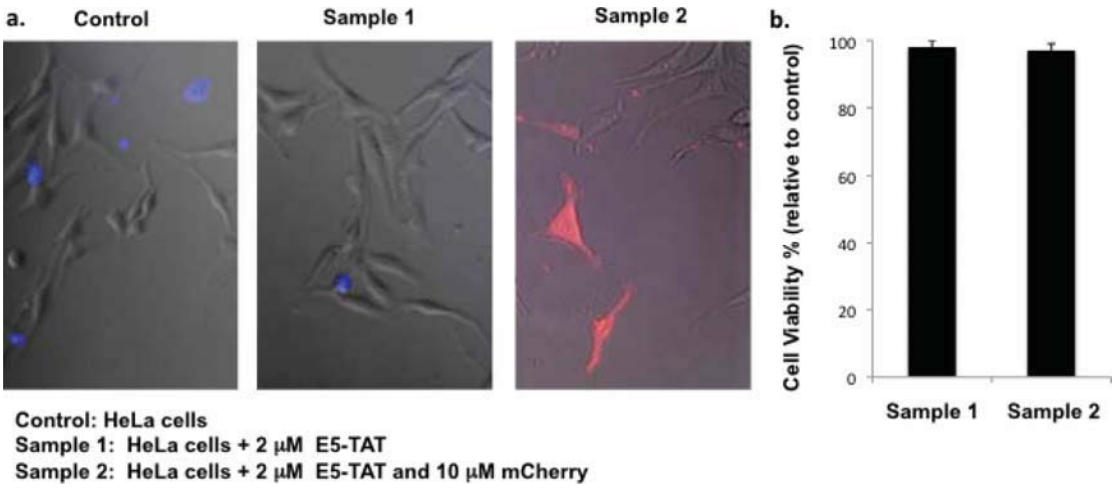

Figure 3-4 Effects of E5-TAT and mCherry co-incubation on cell viability. HeLa cells were treated with E5-TAT or E5-TAT + mCherry for one hour. After washing, the cells were treated with SYTOX Blue so as to detect dead cells or cells with a compromised plasma membrane. Cells were then imaged by phase contrast and fluorescence microscopy for 4 hours. a) Images of different cell samples. Phase contrast (colored grey), SYTOX Blue (pseudocolored blue), and mCherry (pseudocolored red) images were overlayed. Dead cells can be identified by their blue nucleus and cells with mCherry distributed in their cytosolic space are red. Note that the red cells in the "sample 2" image do not have a blue nucleus, thereby confirming that these cells are alive. b) Cell viability was measured by counting the cells containing a blue nucleus (dead cells) and the total cell number from the phase contrast image. Cell viability is reported for each sample as a percentage relative to the control consisting of untreated cells.

than 1% of the total cells observed. (That is, more than 99 % of cells contain the fluorescent macromolecules in endocytic vesicles). No significant differences were observed regardless of the concentration tested (1–10 mm). In contrast, the number of cells with a diffuse cytosolic distribution was 8± 2% and 15%±3% on average in cases in which E3-TAT and E5-TAT were used, respectively (2 μM, Fig. 3-6A , the results represent mCherry and are comparable to the other macromolecules tested, see Fig. 3-7). Based on the measurement of the fluorescence intensities, the cytosolic/nuclear signals of cells with a diffuse distribution were 50-fold above that of cells with a punctate distribution. Similar results were obtained HeLa, COS-7 or COLO 316 cells (Fig. 3-5 B).

3.2.3 HA2-TATs promote cellular uptake through endocytic pathway

The total fluorescence intensity of cells incubated with the macromolecules and TAT, E3-TAT or E5-TAT were three- to fivefold higher than that of cells incubated without delivery peptides; this indicates that increased levels of cellular uptake had been induced by the peptides (Fig.s 3-6B and 3-7, the fluorescence intensities of whole cells are measured to estimate the average amount of fluorescent material internalized inside cells). Internalization of the fluorescent cargos into endocytic organelles was inhibited at 4℃; this indicates that uptake is an energy-dependent process. Internalization was also inhibited by heparin, a molecule known to inhibit the binding of TAT to heparan sulfate proteoglycans or other negatively charged molecules present on the cell surface (Fig. 3-6A) (84). This is consistent with previous mechanistic studies of TAT-mediated uptake and suggests that the TAT moiety in E3-TAT or E5-TAT is in large part responsible for

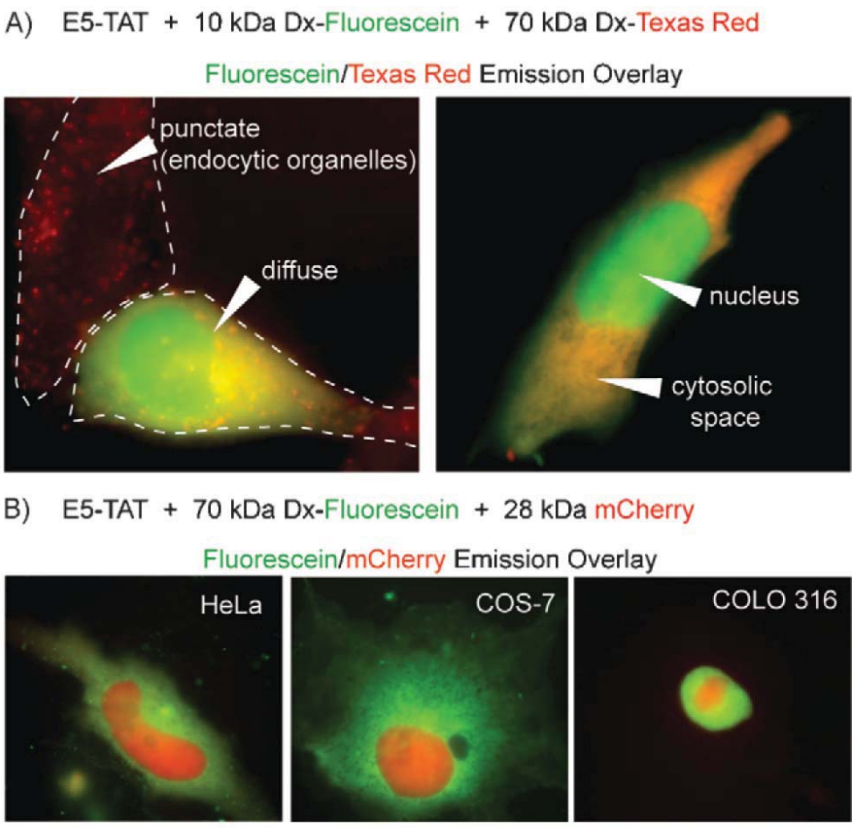

Figure 3-5 Live-cell imaging of cells incubated with E5-TAT, green and red fluorescent macromolecules. A) After a 1 h incubation with E5-TAT, a green and a red fluorescent dextran, HeLa cells display diffuse and punctate distribution of the fluorescent macromolecules. The fluorescence images acquired in the green and red channels are pseudo-colored and overlayed. Colocalization of the green and red fluorescence signals results in a yellow color in the overlay image. The perimeter of the cells is highlighted in the left-hand side image, while the cytosolic and nuclear spaces are indicated by white arrows in the right-hand side image. The 10 kDa green dextran diffuses into the nucleus, while the 70 kDa red dextran does not and the nucleus appears green. B) Delivery of the protein mCherry and of 70 kDa dextran– fluorescein in different cell lines. The protein diffuses into the nucleus, while the 70 kDa green dextran does not and the nucleus appears red.

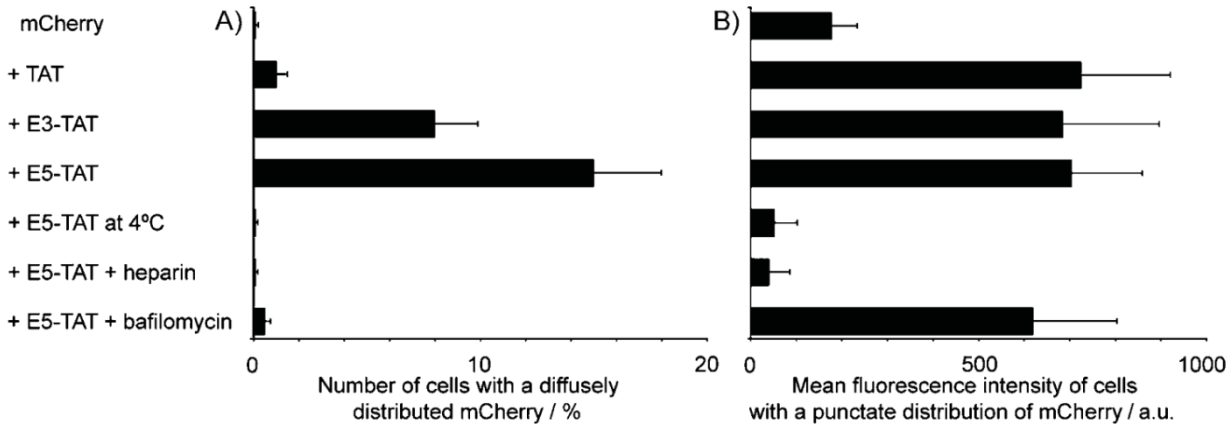

Figure 3-6 Effects of co-incubation conditions and inhibitors on the delivery of the protein mCherry to HeLa cells.

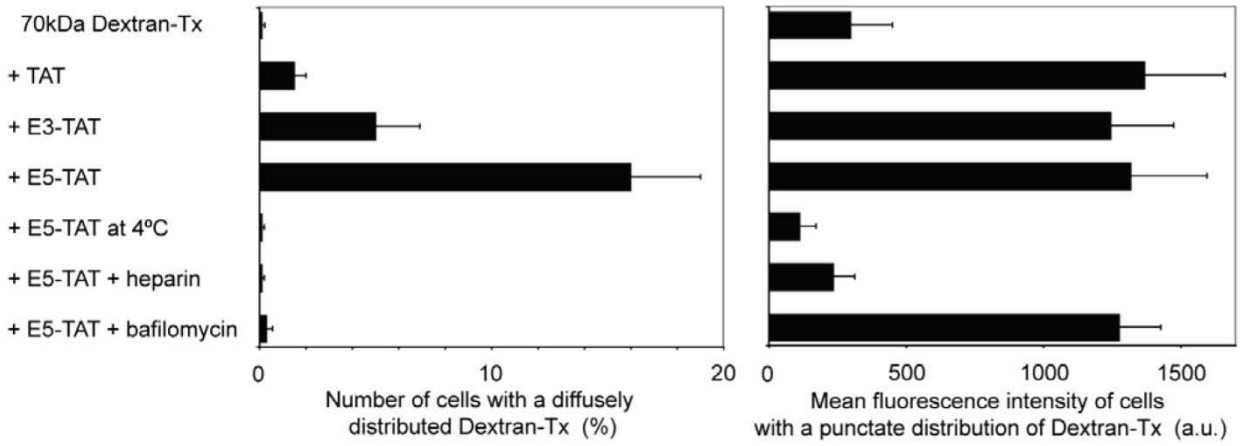

Figure 3-7 Effects of co-incubation conditions and inhibitors on the delivery of 70kDa Dextran-Texas Red to HeLa cells.

the elevated endocytic uptake of the cargos (80). The vacuolar H^+-ATPase inhibitor bafilomycin was used to inhibit endosomal acidification prior to incubation with E3-TAT or E5-TAT and the fluorescent cargos (70). The number of cells containing a diffuse distribution of fluorescent cargos was greatly reduced by this treatment from 8 or 15% to less than 0.5% (Fig. 3-6 A). The amount of material internalized was however unchanged based on the fluorescence intensities of cells containing a punctate distribution of cargos (Fig. 3-6 B). This indicates that the presence of cells with diffusely distributed fluorescent cargos is dependent on the acidification of the lumen of endocytic organelles and that E3-TAT and E5-TAT mediate endosomal release through their pH-dependent membrane-disruption activity.

3.2.4 PAD delivered by HA2-TAT and induces apoptosis through endocytic pathway

To determine whether E5-TAT could mediate the delivery of a biologically active cargo, the delivery of the proapoptotic domain (PAD) peptide KLAKLAKKLAKLAK-NH2 into HeLa cells was evaluated (85,86). If present inside cells, PAD has been shown to induce apoptosis by triggering mitochondrial permeabilization and depolarization (86). However, PAD cannot cross the plasma membrane by itself and shows low cytotoxicity in in vitro assays in cases in which no delivery agent is used (86). In this assay, PAD was therefore co-incubated with TAT or E5-TAT, and cell viability, evaluated with the MTT assay, was used as an indirect measure of the efficiency with which PAD reaches the cytosolic space and the mitochondria. As shown in Fig. 3-8A, co-incubation of TAT

(5 μM) with PAD (20 μM) did not cause more cell death than treatment with PAD (20 μM) alone; this suggests that TAT is not able to deliver PAD efficiently. In contrast, addition of increasing concentrations of E5-TAT to PAD induced an increase in cell death. In order to confirm that the cytotoxicity levels observed were due to an increase in delivery of PAD into cells by E5-TAT as opposed to non delivery-related effects of the combined peptides, this assay was also performed with cells treated with amiloride. Amiloride is an inhibitor of macropinocytosis, a form of endocytosis known to be important for the uptake of TAT-cargo conjugates into cells (80,87,88). I therefore reasoned that macropinocytosis could be involved in the uptake of E5-TAT and that inhibition of macropinocytosis might fully or partially block E5-TAT-mediated delivery of PAD. In agreement with this idea, cell death was significantly reduced upon amiloride treatment. These results therefore suggest that inhibition of macropinocytosis reduces the delivery of PAD into cells and that the cytotoxicity effects observed are in great part due to the E5-TAT-mediated delivery of a bioactive PAD into the cells. (The cytotoxicity observed in the presence of amiloride could be caused by incomplete inhibition of the transport of PAD; it is also consistent with the cytotoxicity observed for E5-TAT alone as shown in Fig. 3-1). These results were further confirmed by using fluorescence microscopy to monitor the delivery of a PAD peptide labeled with the red fluorophore carboxytetramethylrhodamine, TMR-PAD. Cells incubated with both TMR-PAD and E5-TAT displayed a cytoplasmic red fluorescence emission consistent with delivery of PAD into their cytoplasm (Fig. 3-8 B), while cells treated with TMR-PAD alone did not. stain approximately 30 min after incubation with the peptides was completed. The cells

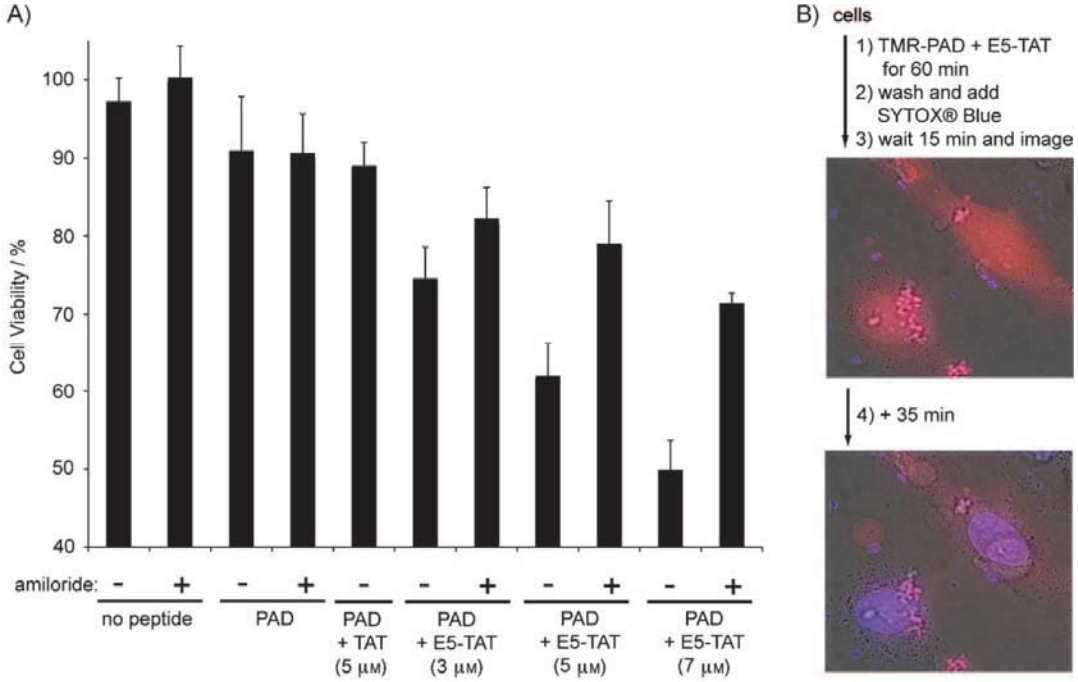

Figure 3-8 Delivery of the proapoptotic peptide domain PAD into live cells by co-incubation with E5-TAT. A) PAD (20 μM) and TAT or E5-TAT (3 to 7 μM) were added to the cell culture media for 1 h. Delivery of the bioactive PAD was assessed by measuring the level of cell death caused by this incubation. Addition of E5-TAT to PAD results in an increase in cell death while addition of TAT does not. Inhibition of macropinocytosis by treatment of the cells with amiloride reduces cell death. These results therefore suggest that inhibition of macropinocytosis reduces the delivery of PAD into cells and that the cytotoxicity effects observed are in great part due to the E5-TAT-mediated delivery of a bioactive PAD into the cells. B) Delivery of the red fluorescent TMR-PAD by E5-TAT detected by microscopy. The phase contrast and fluorescence images acquired in the blue (SYTOX Blue detection) and red channels (TMR-PAD detection) are pseudo-colored and overlayed. Cells showing a cytosolic distribution of TMR-PAD become permeable to SYTOX Blue over time (blue nuclei shown) and apoptotic. This indicates that delivery of PAD precedes cell death and is consistent that the idea that PAD causes apoptosis. Please note that the blue areas in the first image are due to the nuclear debris of cells that have died during the incubation with the peptides and that are stained by SYTOX Blue.

containing the red fluorescent PAD became permeable to the SYTOX blue DNA also displayed marked changes in their morphology consistent with apoptosis, including membrane blebbing, contraction, and nuclear fragmentation. Importantly, cells without red fluorescence were not stained by SYTOX blue. In addition, the control peptide TMR-K9 was also delivered into the cytosol of cells by E5-TAT co-incubation. These cells did not become apoptotic or permeable to SYTOX Blue (see Fig. 3-4 for similar experiments performed with mCherry). These results indicate that delivery alone does not cause cell death but that the cytotoxicity observed is a result of the activity of PAD. Because cells containing TMR-PAD died during the experiment, an exact quantification of the delivery efficiency could not be determined by microscopy. However, based on the MTT assay, it appears that E5-TAT was able to deliver a lethal dose of active PAD to 15– 25% of cells (Fig. 3-8A), as established by the difference in cell viability observed between the cells with or without amiloride.

3.3 Discussion

Overall, these results suggest that TAT performs poorly for the delivery of macromolecules in trans. Addition of endosome disrupting peptides E3 or E5, however, enhances the activity of the peptide and a significant fraction of cells containing macromolecules in the cytosolic and nuclear spaces can then be observed. E3/5-TAT delivery is mediated by endocytosis and endosomal release, rather than by direct translocation across the plasma membrane (Fig. 3-9). First, the TAT moiety binds to the cell surface and induces an increase in endocytic uptake. Macromolecular cargos present

in the media surrounding the cell are then internalized along with the delivery peptide into endosomes. Upon progressive acidification of the lumen of endosomes, the E3/E5 moiety disrupts the endosomal membrane and the cargos escape into the cytosol. E5 is known to induce membrane leakage more actively than E3, and consistent with this observation, E5-TAT appears to deliver fluorescent cargos into cells more efficiently than E3-TAT.

Multiple macromolecules with very different size, charge, hydrophobicity, and chemical structures could be delivered simultaneously to the cell when co-incubated with E5-TAT. This, along with the fact that no binding interactions between E5-TAT and the macromolecules tested could be detected in vitro assays (fluorescence assays and native gel electrophoresis, (Fig. 3-3) suggests that binding of E5-TAT to a macromolecule is not required to achieve delivery. As a result, no chemical or genetic modification of the cargo is required, and this thereby allows for a simple "mix and incubate" protocol to be performed. Moreover, the function of the delivered macromolecule is not altered by the delivery peptide once delivery is achieved. Preliminary delivery experiments with HA2-TAT–mCherry, a macromolecule in which the delivery peptide HA2-TAT is fused to the mCherry cargo, established that the membrane affinity of the HA2-TAT moiety promotes binding of mCherry to intracellular membranes and that, as a result, the protein remains tethered to endosomes and is able to escape into the cytosolic space. This further emphasizes that, at least for in vitro assays, a "nonconjugation" approach might be preferable. It should be noted however the E5-TAT delivery method presented herein could involve the noncovalent

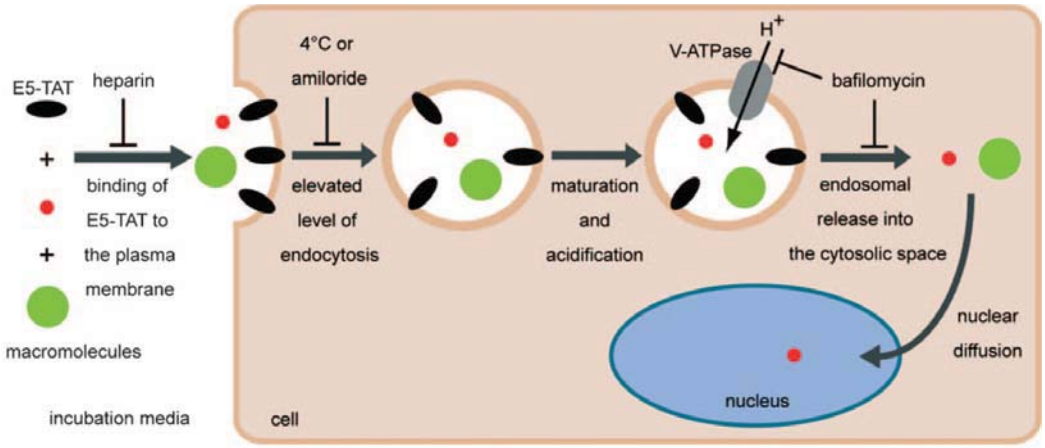

Figure 3-9 Proposed model for the delivery of macromolecules mediated by co-incubation with E5-TAT. Delivery occurs in a two-step process: endocytosis followed by endosomal release. TAT is primarily responsible for the internalization of molecules present in the incubation media by endocytosis while E5 induces escape of the content of endocytic organelles into the cytosolic space. The represented stoichiometry of E5-TAT versus macromolecules is arbitrary.

binding of the peptide to its cargo depending on the nature of themacromolecule used for delivery. Although no binding was detected for the various cargos used in this report (Fig.3-3), it is conceivable that highly negatively charged species (proteins with low isoelectric point, RNA, DNA) might interact with the arginine-rich TAT through multiple electrostatic interactions (Fig.s 3-2 and 3-3). However, it is also possible that such noncovalent interactions might induce a more efficient delivery. Delivery by co-incubation with E5-TAT might therefore serve as a general approach, whether or not noncovalent interactions are involved between peptide and cargo.

In terms of applications, the activity of E5-TAT was sufficient to deliver imaging agents at a level that was well above the detection limit of a standard fluorescence microscopy set-up. A limitation however is the relatively low frequency of cells containing a clear diffuse distribution of the fluorescent agents. Although this might be suitable for certain assays (e.g., 15% of several thousand cells is many more cells than would be obtained by microinjection), it is inconvenient as it renders the imaging of multiple cells in the field of observation unlikely at high magnification. Future improvements should therefore be directed at increasing this aspect of the peptide's activity. Interestingly, the E5-TAT delivery appeared to be an "all or none" process in which cells are distributed between two distinct populations: either the cargo reaches the cytosol with little appearing to be left inside endosomes or it almost completely remains trapped in numerous endocytic organelles. Understanding the phenomena will likely involve further characterization of how the peptide functions. In particular, it is possible that E5-TAT and the internalized macromolecules partition into different endocytic

organelles during or soon after uptake, thereby reducing the overall effectiveness of the delivery. In principle, other TAT-like molecules that could trigger different endocytic mechanisms of uptake combined to HA2-like moieties with greater endosomolytic activites might solve this problem and provide more efficient and general delivery systems.

3.4 Materials & Methods

3.4.1 Peptide synthesis

E3-TAT, E5-TAT, and Fl-E5-TAT were purchased as crude cleavage products from RayBiotech (Norcross, GA). TAT, Fl-TAT, PAD (CKLAKLAKKLAKLAK), and TMR-PAD (TMR-CKLAKLAKKLAKLAK) were synthesized in-house on the Rink amide resin by SPPS using standard Fmoc protocols. Fmoc-Lys(Boc)-OH, Fmoc-Gly-OH, Fmoc-Arg(Pbf)-OH, Fmoc-Gln(Trt)-OH, Fmoc-Gly-OH, Fmoc-Leu-OH, Fmoc-Ala-OH, and Boc-Cys(StBu) were used to assemble the peptides and were purchased from Novabiochem (San Diego, CA). Reactions were carried out in SPPS vessels at room temperature using a stream of dry N2 to provide agitation. Fmoc deprotection was performed by addition of piperidine in DMF (dimethylformamide) (20%, 5 mL) to the Fmoc-peptide resin (0.72 mmol). Deprotection was carried out for 1×3 min and 1×10 min. Coupling 2 reactions were carried out for 2 h with a mixture of Fmoc-amino acid (2.88 mmol), HBTU (2-(1H-Benzotriazole-1-yl)-1,1,3,3-tetramethyluronium hexafluorophosphate) (1.06 g, 2.80 mmol), and DIEA (N,N-Diisopropylethylamine) (1.25 mL, 7.2 mmol) in DMF. Upon completion of the reaction, the resin was washed

with DMF. For Fl-TAT, the Fmoc protecting group at the N-terminus of TAT was cleaved and the resin was washed with DMF. A mixture of 5,6-carboxyfluorescein and HBTU (2 and 1.9 equivalents in respect to the peptide) in DMF was added to the resin and the reaction was carried out overnight with gentle shaking. Following chain assembly, the resins were washed with dichloromethane and dried *in vacuo*. The resin was then treated with TFA (Trifluoroacetic acid) containing 2.5% H2O and 2.5% triisopropylsilane, for 3 hour at room temperature to achieve global deprotection and cleavage from the support. The crude peptide products were precipitated and washed with cold anhydrous Et2O. The precipitates were resuspended in water and lyophilized. The powdery products obtained were then resuspended in 0.1% aqueous TFA/acetonitrile. The peptides were analyzed and purified by reverse phase HPLC. HPLC analysis was performed on a Hewlett-Packard 1200 series instrument and a Vydac C18 column (5 micron, 4 x 150 mm). Flow rate was 1 mL/min and detection was at 214 nm. Semi-preparative HPLC was performed on a Vydac C18 10 × 250 mm column. Flow rate was 4 mL/min and detection was at 214 nm. All runs used linear gradients of 0.1% aqueous TFA (solvent A) and 90% acetonitrile, 10% water and 0.1% TFA (solvent B). To synthesize TMR-PAD, Fmoc-Cys(StBu) was added to the N-terminus of PAD. The StBu group was cleaved by treatment with 3 tributyl phosphine, water, in DMF/DCM (1:1:4:4 volumes). Purified C-PAD (0.3 mg, 0.2 μmol) was then reacted with 5(6)-tetramethylrhodamine-maleimide (0.13 mg, 0.2 μmol, Anaspec, CA) in 500 μL of HEPES (4-(2-hydroxyethyl)-1-piperazineethanesulfonic acid) buffer (25 mM, pH 7.5) containing TCEP (tris(2-carboxyethyl)phosphine) (20 mM) as a reducing agent.

The formed TMR-PAD product was purified by HPLC. The correct identity of the peptides was confirmed by MALDI-TOF mass spectrometry (AXIMA-CFR, Shimazu, Kyoto). All purified and lyophilized peptides were dissolved to 1 mM in DMSO and diluted with PBS to desired concentrations in further experiments. TAT (H-GRKKRRQRRR-NH2) expected mass: 1395.7 Da, observed mass: 1395.5 Da. Fluorescein-TAT (Fl-GRKKRRQRRR-NH2) expected mass: 1754.0 Da, observed mass: 1754.5 Da. E3-TAT (H-GLFGA IAGFI ENGWE GLIEG WYGGR KKRRQ RRR-NH2) expected mass: 3834.4 Da, observed mass: 3835.7 Da. E5-TAT (H-GLFEA IAEFI ENGWE GLIEG WYGGR KKRRQ RRR-NH2) expected mass: 3978.5 Da, observed mass: 3978.8 Da. Fluorescein-E5-TAT (FITC-GLFEA IAEFI ENGWE GLIEG WYGGR KKRRQ RRR-NH2) expected mass: 4596.5 Da, observed mass: 4593.8 Da. PAD (H-KLAKLAKKLAKLAK-NH2) expected mass: 1523.0 Da, observed mass: 1524.6 Da. C-PAD (H-CKLAKLAKKLAKLAK-NH2) expected mass: 1626.15 Da, observed mass: 1625.6 Da. TMR-PAD (H-C(TMR)KLAKLAKKLAKLAK-NH2) expected mass: 2107.6 Da, observed mass: 2108.5 Da.

3.4.2 Cytotoxicity assay

HeLa cells were seeded on 96-well tissue-culture plates at $1.0X10^4$ cells per well. After incubation in a humidified atmosphere containing CO2 (5%) for 24 h at 378C in Dulbecco's modified Eagle's medium supplemented with fetal bovine serum (FBS, 10%), the cells were washed with Leibovitz's L-15 medium and treated with TAT, E3-TAT, and E5-TAT in L-15. After 1 h incubation, the cells were washed with fresh L-15

medium and incubated at 37□ for 3 h. The number of live cells present in each well was then determined by using the Vybrant MTT Cell Proliferation Assay Kit (Molecular Probes). Alternatively, SYTOX Blue, a nucleic acid fluorescent stain that only penetrates cells with compromised plasma membranes, was used to measure cell viability by fluorescence microscopy imaging.

3.4.3 Live cell assay

For the transduction of fluorescent imaging agents: HeLa, COS-7, and COLO 316 cells were seeded on 8-well chamber glass slide at 3.0 $X10^4$ cells per well in Dulbecco's modified Eagle's medium supplemented with FBS (10%) and incubated for 24 h at 37 8C in a humidified atmosphere containing CO2 (5 %). Cells were then incubated with L-15 medium (no FBS added) and placed on an inverted epifluorescence microscope (Model IX81, Olympus, Center Valley, PA) equipped with a heating stage maintained at 378C. The microscope is conFig.d with a spinning disk unit to perform both confocal and wide-field fluorescence microscopy. Images were collected by using a Rolera-MGI Plus back-illuminated EMCCD camera (Qimaging, Surrey, BC, Canada). Images were acquired by using phase contrast and three standard fluorescence filter sets: CFP (lex=436±20 nm/lem=480±40 nm), Texas Red (lex=560±40 nm/lem=630±75 nm), and FITC (lex=482± 35 nm/lem=536±40 nm). Cells were cotreated with TAT or E3/E5-TAT (2 μM) in L-15 medium containing fluorescent imaging agents (10 μM) for the fluorescent proteins EGFP (enhanced green fluorescent protein), mCherry, and tdTomato (obtained as previously described). For the dextrans (10 and 70 kDa anionic dextran–

fluorescein, 10 and 70 kDa neutral dextran– tetramethylrhodamine, and 70 kDa neutral Dextran–Texas Red) 250 μM (for 10 kDa dextrans) or 36 μM (70 kDa dextrans) of fluorescent imaging agent was used.[10] After incubation at 4 or 37℃ for 15 or 60 min, the cells were washed with PBS five times and the medium was replaced with fresh L-15. The integrity of the plasma membrane of the cells was determined by addition of the cell-impermeable DNA stain SYTOX Blue. Cells with a fluorescent blue nucleus, as detected with the CFP filter set, were considered compromised or dead. The cells that were not stained by SYTOX Blue were further confirmed to be alive by detection of active transport of intracellular endocytic vesicles. To inhibit cell surface binding of the delivery peptides, heparin sodium salt (1 $mgmL^{-1}$) was added during the co-incubation step. To inhibit acidification of the endolysosomal organelles, cells were pretreated with bafilomycin (200 μM) for 20 min. Cells were then co-incubated with the fluorescent macromolecules and the delivery peptides in L-15 supplemented with bafilomycin (200 nM). The fluorescence intensities within cells were measured using the SlideBook 4.2 software (Olympus, Center Valley, PA). The mean intensity within cells imaged with the FITC or Texas Red filters was measured as the total intensity of the cell divided by its area. The same protocol was used for cells with either punctate or diffuse distributions. Mean fluorescence intensities were measured over a population of 3000 cells and experiments were reproduced three times.

3.4.4 Live cell assay for the delivery of PAD

Cells grown on 96-well plates were treated with PAD (20 μM) and TAT (5 μM) or

E5-TAT (3, 5, or 7 μM) in L-15. For the inhibition of macropinocytosis, cells were first pretreated with of amiloride (50 nM; Sigma) for 30 min, and then with the peptides while keeping amiloride present. After 1 h incubation, the cells were washed with fresh L-15 medium again and incubated at 37℃ for additional 3 h. The number of live cells present in each well was then determined by using the Vybrant MTT Cell Proliferation Assay Kit (Molecular Probes). After 1 h incubation the cells were washed with L-15. SYTOX Blue (5 μM) was added and cells were incubated for 15 min at 37℃. Cells were then placed on the microscope and images were acquired in the blue fluorescence channel for detection of SYTOX Blue and red fluorescence channel for detection of TMR.

3.4.5 Characterization of the binding interactions between the delivery peptides and proteins

The affinity of the delivery peptides TAT and E5-TAT for proteins was assessed by native gel electrophoresis. Three model protein systems were used in these experiments: mCherry, bovine serum albumin (BSA), fetal bovine serum (FBS). The latter were used because arginine-rich peptides have been shown to interact with FBS proteins. In particular, non-covalent binding of the positively charge peptide R12 (pI = 13, charge of +12 at pH 7) to the negatively charged BSA (pI = 4.7, charge of approximately -18 at pH 7) could be detected.[4] Although BSA was not used in this delivery assays, this protein has a lower pI than mCherry (pI = 6.6) and therefore serves as a control to test whether TAT or E5-TAT might bind to negatively charged proteins.

The peptides TAT and E5-TAT were labeled with fluorescein (Fl) by coupling of this fluorescent molecule to the N-terminus of the peptides during SPPS assembly to generate Fl-TAT and Fl-E5-TAT. Fl-TAT and Fl-E5-TAT were incubated in L-15 supplemented with BSA, mCherry, or with 10% FBS. The delivery peptides and protein samples were incubated for 30 minutes at 37°C to allow for binding and reproduce the conditions used for the cell-based microscopy assays (room temperature were also tested and yielded similar results). In order to have enough material for analysis, the concentrations used were however about 10 to 100-fold higher than those used for the imaging assays. The samples were then analyzed by native gel electrophoresis (15 μL were loaded for each sample). The native 12% gels, and Tris/Glycine running buffers were prepared according to regular SDS-PAGE protocols but with the difference that SDS was replaced by glycerol and that the pH of the running buffer was adjusted to 8 (a pH at which the TAT lysine and arginine residues will remain protonated). Electrophoresis was ran at 150 mV for 2hr and the protein/peptide complexes were detected using a fluorescence scanner (Typhoon, GE healthcare) to obtain images of the fluorescence signals of fluorescein labeled peptides and of the fluorescent mCherry protein. The imaged gels were then stained with coomassie according to standard protocols.

Fig. 3-2 and 3-3 show the results of these experiments. As shown in Fig. 3-7, Fl-TAT was found to bind to serum proteins but this could only be detected when the peptide was incubated at 50 mM or more. In contrast, Fl-E5-TAT could not be detected to bind to the serum proteins under the conditions tested. To confirm that the peptide

was present in the sample loaded on the gel, the sample was centrifuged at 17 k rpm for 10 min and the supernatant was analyzed by HPLC. This analysis confirmed that the peptide was present in the sample at the desired concentration. The binding interactions of the peptides to pure proteins were then characterized with BSA and mCherry as shown in Fig. 3-3. Smears of Fl-TAT, and to a lesser extent Fl-E5-TAT, could be detected when the peptides were incubated at high concentrations and in stoichiometric excess with BSA. These smears were of low intensity and could not be observed in the coomassie stained gel, indicating that the peptide/protein complexes that might generate these smears represent a small population of the total BSA species (e.g. there are no observable differences between the BSA control, Fig. 3-3 (a) lane 7, and the peptide/protein samples, lanes 2, 3, 5, and 6). For the samples incubated with mCherry, a very faint smear was detected for Fl-TAT/mCherry samples (Fig. 3-3 b, lanes 2 and 3) but no signal from Fl-E5-TAT was observable. mCherry labeled with fluorescein (mCherry-Fluorescein, Fig. 3-3 b, lane 7) was used as a control to validate that both mCherry and fluorescein fluorescence could be detected (the protein was prepared as previously reported, the stoichiometry of mCherry:fluorescein is 1:1).[1] The amount of mCherry-Fluorescein loaded (15 μL of 20 μM of protein loaded) on the gel was the same as the amount of mCherry loaded in lanes 2, 3, 5, and 6 from the mCherry/peptide incubation samples. I therefore reasoned that the green fluorescence obtained from lane 7 could be used as an internal calibration to assess the overall amount of peptide bound to mCherry in lanes 2, 3, 5, and 6 (e.g. a 1:1 Fl-peptide/mCherry complex should give a similar signal as mCherry-Fluorescein in the green fluorescence channel). The white

area in the center of Lane 7 represents a fluorescence signal that has saturated (> 100,000 counts) the detector. High sensitivity for the detector was however required to detect the signals of lanes 2 and 3 (signal of < 1000 counts; when lane 7 is not saturated, the signals of lanes 2 and 3 cannot be detected). The total fluorescence intensities of lane 3 and 7 were integrated over the whole lane area using the ImageQuant Software (Molecular Dynamics) and compared (each saturated pixels in lane 7 were counted to have the maximal signal of 100,000 counts even though the "real" signal is probably much greater). I found that the green fluorescence present in lane 3 was less than 0.2 % of the signal of lane 7.

Overall, these results indicate that although TAT or E5-TAT might bind to negatively charged proteins such as BSA, the population of TAT/BSA or E5-TAT/BSA complexes formed appears to be of very low concentration. With mCherry, one of the fluorescent proteins tested in the delivery assays, no E5-TAT/mCherry complexes could be detected at all while a small amount of TAT/mCherry complexes was. It is important to note that the peptide concentrations and peptide to protein ratios used were far greater than those used for the peptide/protein co-incubation microscopy assays (e.g. 2 μM peptide + 10 μM protein for delivery assays versus 40 μM peptide + 20 μM protein for the binding assays). Accordingly, it is expected that absence of binding interactions in the binding assays is likely to indicate that no binding interactions take place in the samples used for the delivery assays. It should be noted that fluorescein might affect the protein binding behavior of the peptides. However, given that it is a hydrophobic molecule, one might expect that fluorescein would enhance the hydrophobic interactions

between the peptides and the tested proteins rather than diminish them. In addition, fluorescein has one negative charge at pH 7 that could interfere with the positively charged TAT. However, E5-TAT should be affected in a similar manner. Overall, I conclude that E5-TAT does not bind to mCherry at detectable levels while TAT exhibits low level of unspecific binding. It is then surprising and interesting to note that E5-TAT, despite containing the TAT sequence and an additional hydrophobic region, appears to have less binding affinity for proteins than TAT itself. My preliminary data suggest that E5 and TAT might interact with one another. This interaction could then reduce the interactions with other binding partners. This model will be the object of future studies.

4. MODELING OF ENDOSOMOLYTIC ACTIVITY OF HA2-TAT PEPTIDES WITH RED BLOOD CELLS AND GHOSTS*

4.1 Introduction

E5-TAT can enhance the endosomal release of endocytosed macromolecules. This process remains, however, obscure. In sections 2 and 3, it has been demonstrated that the inhibitor of endosomal acidification inhibits E5-mediated endosomal escape. After cells were pretreated with bafilomycin, the efficiency of protein delivery by E5-TAT significantly decreased. However, due to the complexity of the cellular environment and the small size of endosomes, it is too difficult to observe how E5-TAT mediates endosomal membrane disruption directly in live cells. In addition, there are many different processes contributing to the observed results that take place simultaneously within live cells and these cannot be eliminated. Therefore, a simpler but similar system compared to cellular environments needs to be applied instead.

Since the plasma membrane of erythrocytes (Red Blood Cells, RBCs) has similar composition to common mammalian lipid membrane and because erythrocytes are relatively stable in acidic environments, they can function as a structural model for endosomal membrane (89,90). To further investigate the membrane disruption mechanism of E5-TAT, the pH-dependent lysis activity of HA2-TAT peptides are first tested *in vitro* with erythrocytes by hemolysis assay.

4.2 Results

4.2.1 Peptide design

Several HA2-TAT analogues were synthesized by solid-phase peptide synthesis (SPPS). HA2 analogues were considered in this study: E3, E5 (Table 4-1). E3 consists of the wild-type HA2 sequence (residues 1-23, strain X31) modified with the mutations M17L and D19E in order to avoid methionine oxidation and aspartyl isomerization during synthesis. E3 contains the residues Trp-21 and Tyr-22 because these residues appear to increase the hemolysis activity of HA2 peptides (70). E5 differs from E3 by including the G4E and G8E mutations. Addition of these two glutamate residues has been demonstrated to increase the lysis activity of HA2 analogues (55,63,66,70). TAT was placed at the C-terminus of the HA2 analogues so as not to affect the insertion of the HA2 peptides into membranes (55,64). For fluorescence labeling, fluorescein isothiocyanate (Fl) was introduced at the N- or C-terminus of E5-TAT during solid phase assembly to generate Fl-E5-TAT or E5-TAT-Fl, respectively. Fl-E5-TATwas synthesized after E5-TAT-Fl was found to be poorly soluble. Modifications at the N-terminus of HA2 have however been found to reduce the fusion and hemolytic activities of HA2 analogues because it is the N-terminus of HA2 that inserts into lipid bilayers (55,64). Therefore, in order to minimize the effect that the fluorophore might have on the peptide's activity, the flexible linker 6-aminohexanoic acid (Ahx) was incorporated during synthesis between Fl and the N-terminal glycine. Fl-E5-TAT was found to closely mimic the hemolytic activity of E5-TAT (Fig. 4-1B, C on page 81). Fl-E5-TAT was therefore preferred as the fluorescent analogue of E5-TAT used to visualize the

Table 4-1 Sequences of the HA2-TAT peptides investigated

Name	Amino Acid Sequence
HIV TAT (48-57)	GRKKR RQRRR
Influenza HA2 (1-23)	GLFGA IAGFI ENGWE GMIDG WYG
E3-TAT[a]	GLFGA IAGFI ENGWE GLIEG WYGGR KKRRQ RRR
E5-TAT[a]	GLFEA IAEFI ENGWE GLIEG WYGGR KKRRQ RRR
Fl-E5-TAT[b]	Fl-Ahx-GLFEA IAEFI ENGWE GLIEG WYGGR KKRRQ RRRK
E5-TAT-Fl	GLFEA IAEFI ENGWE GLIEG WYGGR KKRRQ RRRK(εFl)
E5(3,7)-TAT	GLEGA IEGFI ENGWE GLIEG WYGGR KKRRQ RRR
E5-R9	GLFEA IAEFI ENGWE GLIEG WYGGR RRRRR RRR

[a] the underlined sequence represents the HA2 peptide obtained after trypsin digest.

[b] Ahx is the linker 6-aminohexanoic acid.

peptide interacting with cellular membranes.

Numerous studies with the HA2 fusion peptide have shown that this amphiphilic peptide behaves poorly in water, making the biochemical study of its properties difficult. Han and Tamm have reported the design of host-guest systems where lysine-rich unstructured C-terminal sequences could solubilize N-terminal HA2 guest sequences (5). Therefore it is reasoned that the highly charged TAT peptide could promote the same effect. The solubility of the peptides E3-TAT and E5-TAT in aqueous buffers was first assessed by monitoring the extent to which the peptides remain in solution for extended periods of time. The peptides were dissolved in PBS to 5 μM, and the samples were centrifuged at high speed every hour to separate the soluble peptides from possible precipitate. The concentration of the peptides remaining in solution was then determined by HPLC analysis. Under these conditions, all peptides appeared to remain in solution for at least 24 h. To determine the effect that TAT might have on the solubility of the amphiphilic HA2 sequences, the control peptides TAT, E3, and E5 were also synthesized by SPPS. TAT was obtained in high yield, but this approach did not yield satisfactory results for E3 and E5 as the peptides precipitated and degraded after HPLC purification and storage (65). Instead, E3 and E5 were obtained by trypsin-mediated cleavage of the TAT peptide from E3-TAT and E5-TAT. HPLC and mass spectrometry analysis confirmed that single E3 or E5 products with a C-terminal arginine were produced with less than 3% of the uncleaved peptide remaining. Using this approach, the peptide was found to be soluble and stable in PBS for at least 1 h at room temperature. However, like the synthesized peptides, the E3 and E5 peptides produced by TAT

cleavage also showed a tendency to precipitate and degrade over time as determined by HPLC and mass spectrometry. Overall, these results suggest that the highly charged and hydrophilic TAT sequence has a solubilizing and stabilizing effect on the amphiphilic E3 and E5 sequences.

4.2.2 HA2-TAT peptides lyse erythrocytes in a pH-dependent manner

The pH-dependent hemolysis activities of the HA2-TAT peptides were characterized by an in vitro erythrocyte lysis assay. The peptides were incubated with human RBCs in PBS with the pH adjusted to different values. The release of hemoglobin from lysed cells was then measured spectrophotometrically at 450 nm 30 min after incubation was initiated (hemolysis is complete at this time point in all of the assays). E3-TAT, E5-TAT, E3, and E5 all show a clear pH-dependent lysis activity and display sigmoidal response curves consistent with a single protonation model (Fig. 4-1A). E3-TAT, E3, and E5 displayed an identical apparent pK50 of approximately 5.8 (pH at which 50% of maximum hemolysis is obtained). This pK50 is consistent with values reported for HA2 peptides and the X-31 virus itself (64,91). In contrast, the hemolysis response curve of E5-TAT is significantly shifted toward higher pH and displays an apparent pK50 of 6.7. E5-TAT also appears to have a higher activity than E3-TATat all pHs (Fig. 4-1A).The activities of E3 and E5 were much reduced in comparison to E3-TAT and E5-TAT. E3 and E5 required a concentration of approximately 4 or 3 μM to display a hemolysis activity at pH4.5 similar to that of E3-TAT and E5-TAT at 1.5 μM. A precise comparison of the activity of the E3/5-TAT and E3/5 peptides was however rendered

Figure 4-1 (A) Hemolysis activities ofHA2 and HA2-TAT analogues as a function of pH. Hemolysis is reported as a percentage of the maximal release of hemoglobin obtained by treatment of the red blood cells with the detergent Triton X. TAT shows no lysis activity while E3, E5, E3-TAT, and E5-TAT display sigmoidal response curves. E3, E5, and E3-TAT have a similar pK50 of approximately 5.7. In contrast, E5-TAT displays apK50 of 6.7. E3 and E5 are overall less active than E3-TAT or E5-TAT as they require higher concentrations to achieve similar hemolysis percentages at pH4.5. The plot fitting was performed as described in the Experimental Procedures. The data represent the average of at least three experiments. The standard deviation for each data point, not represented for clarity, was 5%hemolysis or less. Note that the concentration of E3 and E5 reported might be overestimated as the peptides might aggregate and precipitate during the experiment. These data might therefore not accurately reflect the hemolytic activity of the peptide precisely, but, on the other hand, serve to establish the differences in pK50 between the HA2 peptides and their HA2-TAT analogues. (B, C) Comparison of the hemolytic activities of E5-TAT and Fl-E5-TAT.While Fl-E5-TAT has a lower HD50 than E5-TAT, both peptides have an identical pK50. (D) Hemolytic activities of Fl-E5-TAT at pH7.0 (diamonds) and 4.0 (triangles) as a function of peptide concentration and for 1.25% RBC suspensions. The data fit the equations y=27.2x at pH7 and y=4.9x at pH 4.0 with R2 of 0.90 and 0.98, respectively. The HD50 of the peptide are 1.8 and 10.2 μM at pH 4.0 and 7.0, respectively.

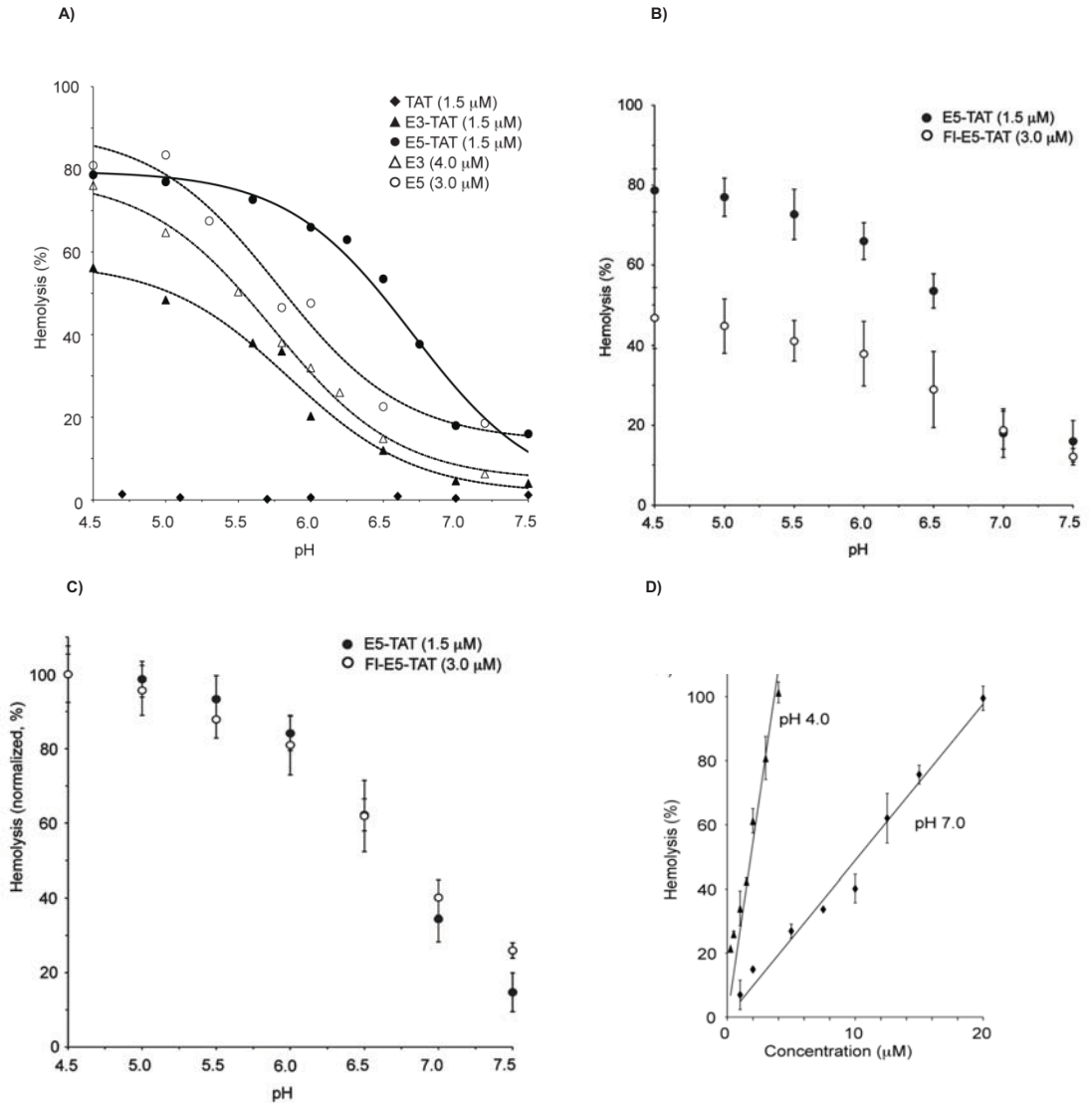
A)
TAT (1.5 μM)
E3-TAT (1.5 μM)
E5-TAT (1.5 μM)
E3 (4.0 μM)
E5 (3.0 μM)
Hemolysis (%)
pH
B)
E5-TAT (1.5 μM)
Fl-E5-TAT (3.0 μM)
Hemolysis (%)
pH
C)
E5-TAT (1.5 μM)
Fl-E5-TAT (3.0 μM)
Hemolysis (normalized, %)
pH
D)
pH 4.0
pH 7.0
Hemolysis (%)
Concentration (μM)

difficult because of the poor solubility of E3/5. Finally, TAT did not induce erythrocyte lysis at any of the concentrations (up to 80 μM) or pH values (4.5-7.5) tested. Together, these results indicate that the increase in activity and the change in pH response observed for E5-TAT appear to be dependent on the presence of both TAT and the G4E and G8E mutations since neither E5 nor E3-TAT displays the same characteristics.

The effect of the concentration of peptide used during the hemolysis was evaluated for E5-TAT and Fl-E5-TAT. The results obtained with the fluorescently labeled peptide are shown in Fig. 4-1D. The HD50 (hemolytic dose for 50% lysis) of E5- TAT and Fl-E5-TAT were approximately 2.6 and 10.2 μM at pH 7.0, respectively, and 0.5 and 1.8 μM at pH4.0, respectively. In both cases, the hemolytic activity of the peptide is increased approximately 5-fold when the pH is decreased from 7.0 to 4.0. Despite an overall decrease in the activity of Fl-E5-TAT as compared to E5-TAT, the pK50 of both peptides were identical at 6.7 (Fig. 4-1C). Overall, these data suggest that Fl-E5-TAT is a fluorescent analogue of E5-TAT that can closely reproduce its properties.

4.2.3 Fl-E5-TAT interacts with RBC in a pH-dependent manner

The hemolytic activity and binding of Fl-E5-TAT to RBCs were investigated by microscopy. The lysis of RBCs after peptide addition was detected by the decrease in the cells' optical contrast observed by bright field microscopy and as reported by Jay and Rowlands (6). The products of the lysis were ghost cells with a visible membrane but with an interior invisible upon bright field imaging. This is consistent with cells losing their content as lysis proceeds and with the lumen of the ghost being filled with the

surrounding media. Lysis was also confirmed by monitoring the loss of red autofluorescence of RBCs upon ghost formation. It is important to note that the red fluorescence present inside the RBCs cannot be accounted by hemoglobin as hemoglobin has been clearly shown to be poorly fluorescent. Instead, porphyrins and other metabolites are more likely to be the fluorescent material observed in these experiments (92). Yet, loss of autofluorescence further confirms that the lysed RBCs are losing their content. In my hands, loss in optical contrast in bright field imaging and loss of red autofluorescence were simultaneous.

Red blood cells were incubated with Fl-E5-TAT at pH 4.5 or 7.0, and the binding of the peptide to membranes was monitored by fluorescence microscopy (Fig. 4-2). Fl-E5-TAT was first incubated with RBCs at pH 7.0 and at a concentration below its HD50 (5 μM, HD50 = 10.2 μM) so as to prevent extensive lysis. The fluorescence of Fl-E5-TAT appeared to be diffused in solution, and no association of the peptide to the membrane of RBCs could be observed. In contrast, when incubated at pH 6.0, 5.0, or 4.5, the peptide was found to increasingly accumulate at the surface of intact RBCs (Fig. 4-2 and Fig. 4-3; a concentration of 1 μM peptide was used to minimize lysis). Together, these results suggest that Fl-E5-TAT remains predominantly soluble at pH 7.0 but associates with the membrane as the pH decreases.

Addition of the E5-TATor Fl-E5-TAT to RBCs incubated at pH 4.5 at concentrations above their HD50 (5 μM) induced rapid lysis. Prior to lysis, RBCs appeared as a mixed population of concave and spherical cells. The presence of spherical cells is consistent with the swelling observed when concave cells are exposed to stress such as low pH (93).

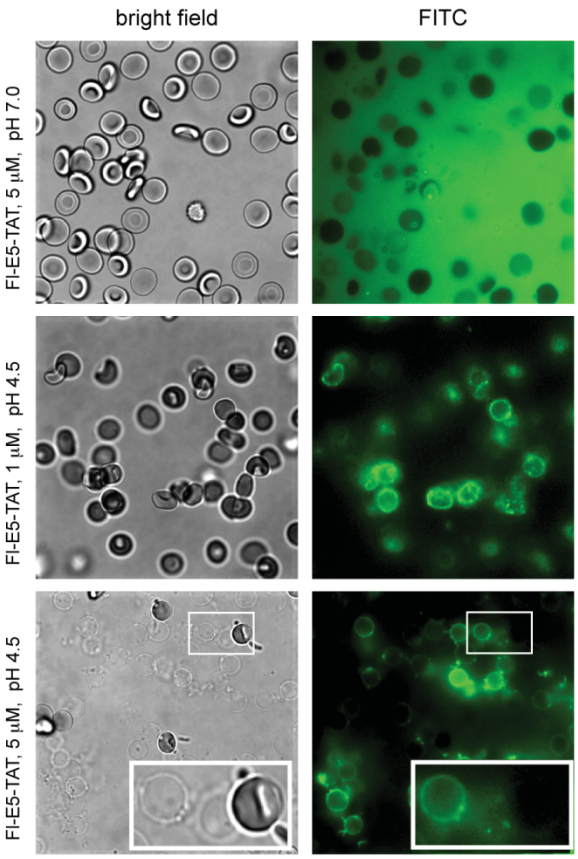

Figure 4-2 Binding of Fl-E5-TAT to RBCs and ghosts as a function of pH. RBCs were incubated with 1 or 5 μM Fl-E5-TAT at pH 7.0 or 4.5, and the samples were observed by fluorescence (Fl-E5-TAT, FITC image, pseudocolored green) and bright field (RBCs/ghosts) microscopy. At pH 7.0 and at a low concentration of peptide (5 μM, below the HD50 at pH 7.0), the RBCs are intact, and the peptide appears to be homogeneously distributed in solution. No binding to the surface of the RBCs is detected under these conditions. At pH 4.5 and at 1 μM peptide (below the HD50 at this pH), the RBCs remain intact, but the peptide appears to preferentially partition at the membrane of the cells. At pH 4.5 and 5 μM peptide (above the HD50 at this pH), the RBCs are lysed, and the peptide binds to the membrane of the ghosts formed.

Figure 4-3 A) Binding of Fl-E5-TAT (1.0 μM) to intact RBCs as a function of pH as observed by fluorescence microscopy. The peptide was added to 1.25% RBC suspensions and the samples were imaged after 5 minutes of incubation. At pH 7.0, the fluorescence signal is detected in solution. As the pH is reduced, the peptide accumulates at the membrane as detected by an increase in the contrast between the signal at the membrane and the signal in solution (the methods used are the same as in Fig. 4-2). Note: The samples also contain 5 to 10% of lysed ghosts but intact RBCs can easily be identified in the bright field image because of their darker contrast. B) The samples described in A) were centrifuged to separate RBC-bound peptides from the fraction of peptide remaining in solution. The amount of soluble peptide was determined by SDS-PAGE and densitometric analysis. Each sample was normalized to a pH 7.0 control containing the fluorescent peptide but no RBCs (= 100% peptide in solution). The data represent the average of three experiments and the error bars correspond to the standard deviation. Binding Assay. The binding of Fl-E5-TAT to intact RBCs as a function of pH was determined by incubating peptide (1 μM, <HD50 to minimize lysis) with 1.25% RBC suspensions in PBS at different pH values (adjusted with HCl or NaOH, 4.5<pH<7.5). After 5 min incubation, the samples were centrifuged for 5 minutes at 1500g. The amount of peptide present in the supernatants was analyzed by SDS-PAGE using 12% SDS-gel (pH 8.8). The gels were imaged with the Typhoon 9410 imager (GE Healthcare) set with an excitation wavelength of 488 nm and a green emission filter at 526 nm to detect the fluorescence of Fl-E5-TAT. Densitometric analysis of the intensity of the Fl- E5-TAT bands was performed with the ImageQuant 5.0 software. The fluorescence of the fluorescein label on E5-TAT is pH dependent. However, because all samples are exposed to the same pH within the gel, the fluorescence intensity of the bands is only proportional to the amount of peptide present in the sample. The data were normalized using a sample containing Fl-E5-TAT at pH 7.0 but with no RBC present as the one hundred percent soluble control.

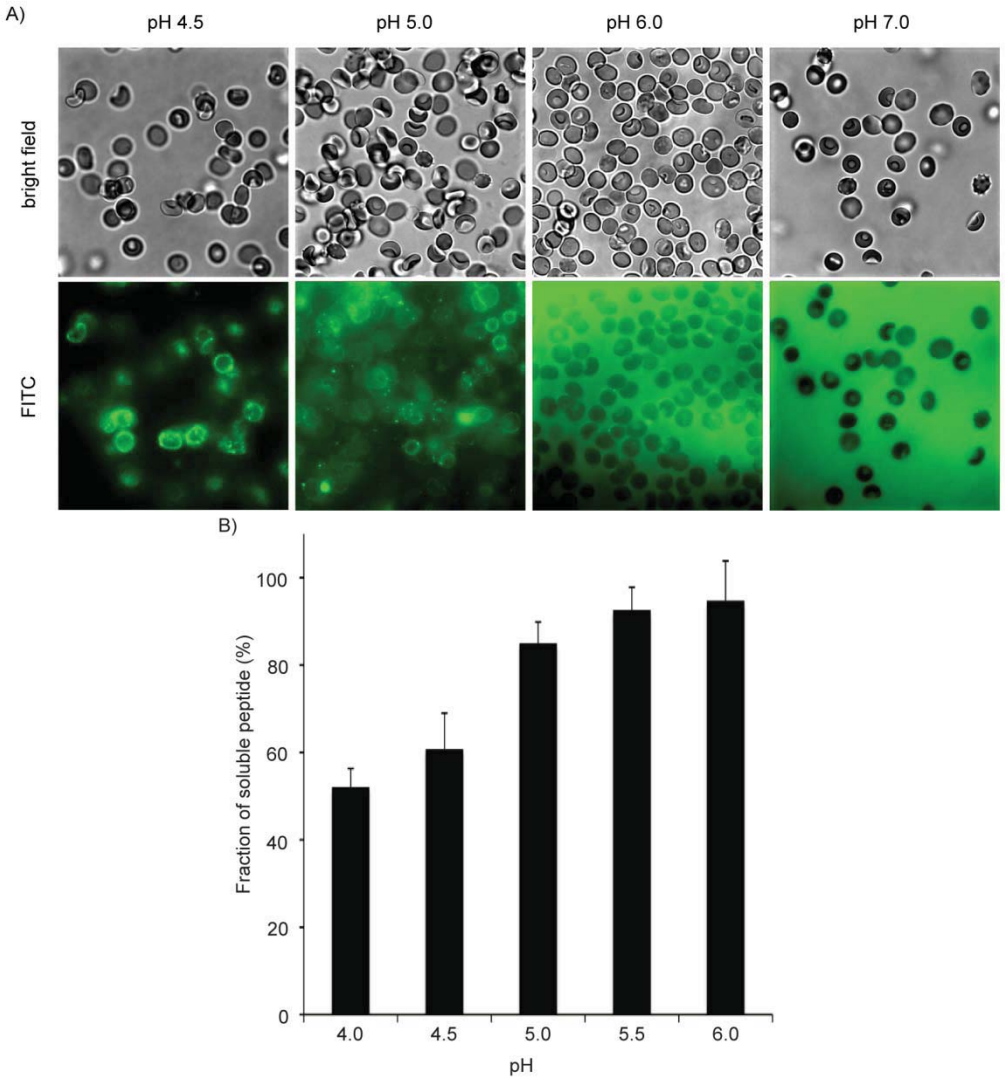
A)
pH 4.5
pH 5.0
pH 6.0
pH 7.0
bright field
FITC
B)
Fraction of soluble peptide (%)
100
80
60
40
20
0
4.0
4.5
5.0
5.5
6.0
pH

Lysis of cells that were initially spherical did not appear to induce an observable change in the diameter or morphology of the cell (Fig. 4-4). Initiation of lysis after E5-TAT addition was different from cell to cell, but once initiated, lysis was complete in 90 (30 s on average to reach completion (average and standard deviation obtained from a population of 50 cells) (Fig. 4-4). Similar results were obtained for E5-TAT and Fl-E5-TAT. In the case of Fl-E5-TAT however, binding of the fluorescent peptide to the surface of ghosts was clearly observable by fluorescence microscopy (Fig. 4-2). RBCs that were not lysed by the end of the experiments typically showed little fluorescence and peptide binding on their surface.

4.2.4 Fl-E5-TAT permeabilizes membranes in a manner not reversed under different pH values

Next, I tested whether the ghost obtained by E5-TAT-mediated hemolysis remained permeable after hemolysis and whether permeability could be reversed. Ghosts were obtained by treatment of RBCs with E5-TAT at pH 4.5. The ghosts were then either kept in the pH4.5 media with the E5-TAT peptide present or washed with fresh pH 4.5 or 7 PBS buffer at 37 C. These latter steps consisted of a repeated dilution protocol as ghosts could not be washed under stringent conditions without loss of membrane integrity and membrane collapse. A 10 kDa dextran-fluorescein was then added to the RBCs and ghosts, and the samples were then observed by fluorescence microscopy. Intact RBCs had internal fluorescence signals much lower than the fluorescence of the surrounding solution (Fig. 4-5). This is consistent with the dextran not being able to penetrate RBCs.

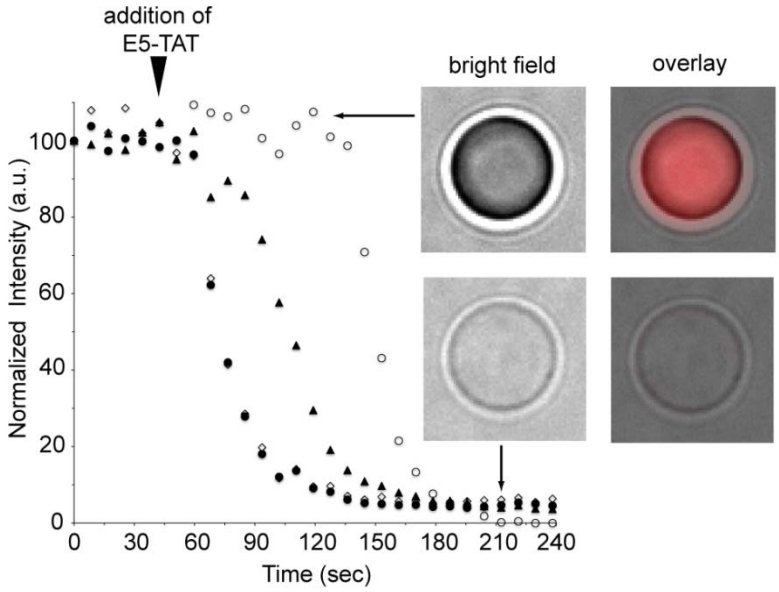

Figure 4-4 Time course of lysis and ghost formation from single RBCs determined by fluorescence and bright field microscopy. RBCs were incubated in PBS at pH 4.5 and imaged every 10 s in a time-lapse experiment. After 50 s, the cells were treated with 1 μM E5-TAT, and imaging was immediately resumed. Lysis was assessed by measuring the decrease in optical contrast of cells in the bright field image (data displayed) or the decrease in their autofluorescence in the red fluorescence image (not represented but identical results were obtained using this method). Cell leakage appears to be initiated at slightly different times. Once initiated, lysis consistently took on average 90 (30 s to reach completion (n=50 cells, four represented in the Fig.). Bright field and fluorescence overlay images (cell autofluorescence, pseudocolored red) show that the morphology of the cells does not change during the experiment and that their diameter remains approximately constant.

In contrast, ghosts showed an internal fluorescence equal to that of the media. This indicates that the 10 kDa dextran-fluorescein had freely penetrated into the ghosts and that the ghosts remained permeable to macromolecules (Fig. 4-5). Fluorescence imaging was also performed immediately after diluting the media of the sample. As seen in Fig. 4-5, fluorescent ghosts were clearly observed over a darker background, further confirming that the fluorescent dextran had penetrated the ghost. Similar experiments were reproduced with Fl-E5-TAT. This time, fluorescence imaging revealed that the Fl-E5-TAT peptide was still bound to the membrane even after repeated dilutions and washing steps at either pH 4.5 or pH 7 (Fig. 4-5). Together, these results suggest that the peptide remains stably anchored to the ghost membrane at either low or neutral pH and that this results in the formation of ghosts that are not resealed.

4.2.5 Peptide binding to RBC is dependent on membrane composition

During the course of the experiments, I observed that the fluorescence at the membrane of ghosts increased during lysis and occasionally after lysis had taken place. This suggested that binding of the peptide might not be dependent on pH only but on changes in membrane composition that might occur during lysis. To address this issue, I first tested whether the TAT sequence might be involved in this effect. TAT labeled with fluorescein, Fl-TAT, was added to RBCs at either pH 4 or pH 7. In both cases, no staining of the RBCs' membranes and no lysis could be observed. However, addition of Triton X and lysis led to an immediate increase in membrane staining at both pHs (Fig. 4-6) . Binding of Fl-TAT to the membrane of the ghosts formed by treatment with

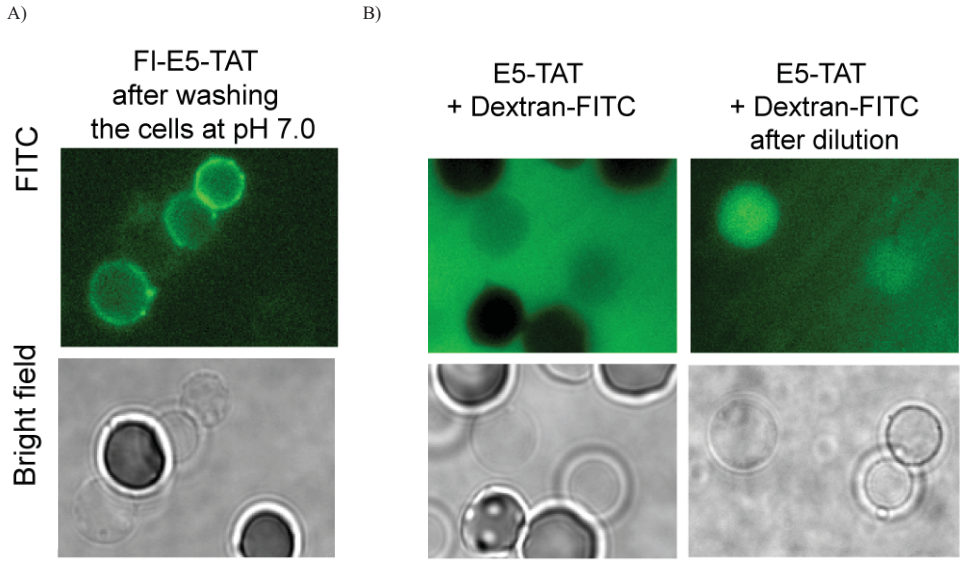

Figure 4-5 Ghosts remain permeable after lysis and Fl-E5-TAT remains tightly bound to their membranes. (A) Binding ofFl-E5-TATto ghosts is maintained after washing at pH 7. Ghosts were formed by treating RBCs with 3 μMFl-E5-TAT at pH 4.5. The ghosts were then washed with PBS at pH7.0 and imaged by fluorescence microscopy. Staining of the ghosts by the peptide was not reduced by repeating the washes or with time. Similar results were obtained when the pH of the PBS was 4.5. (B) The fluorescent marker 10 kDa dextran-FITC was added to cells lysed by treatment with E5-TAT (3 μM) at pH 4.5. A clear fluorescence contrast is observed between the exterior and interior of intact RBCs. Conversely, ghosts display a fluorescence signal similar to that of the media surrounding them, suggesting that the fluorescent dextran is able to penetrate ghosts but not intact RBCs. Rapid dilution of the media generates a higher fluorescence contrast inside ghosts, confirming that the dextran is present in the lumen of ghosts.

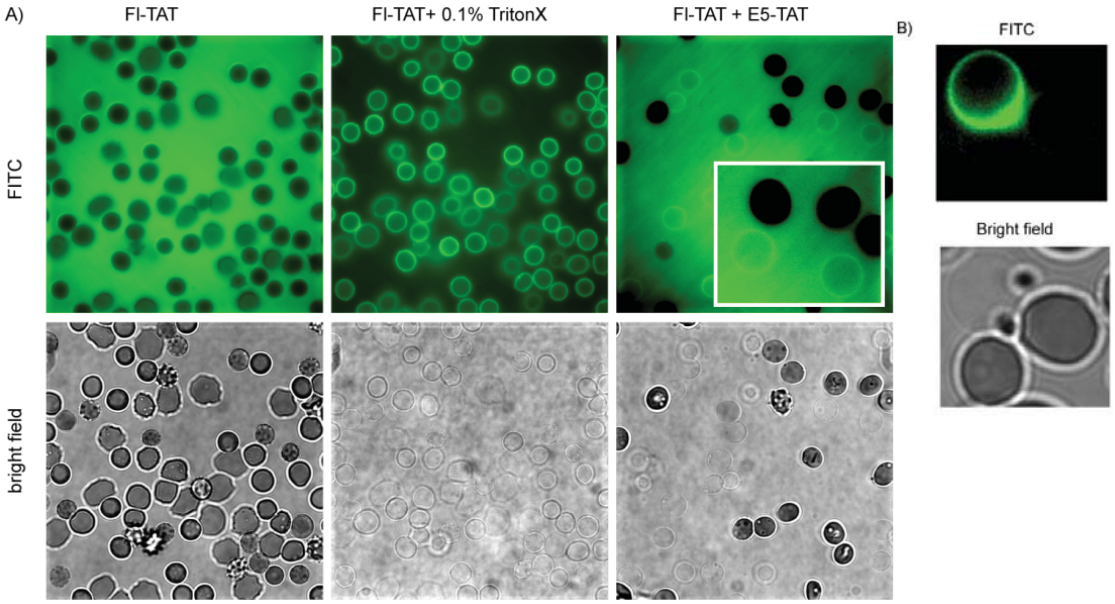

Figure 4-6 (A) Binding of Fl-TAT to RBCs and ghosts. Fl-TAT (5 μM) was added to1%RBCs, and the cells were observed by phase contrast and fluorescence microscopy. Fl-TAT appears to be diffusely distributed in solution and no accumulation of the peptide on the membrane of RBCs can be detected under these conditions. Addition of 0.1% Triton X results in rapid lysis of the RBCs. Fl-TAT is then observed to bind to the membrane of the formed ghosts. The set of images after addition of TritonX represents the same field of cells represented before addition and was acquired less than 10 s after addition of the detergent. Fl-TAT also binds to ghost obtained by E5-TAT-mediated hemolysis. RBCs were treated with 1 μME5-TAT at pH4.5, and Fl-TAT (5 μM) was added to the sample. While binding of Fl-TAT to the membrane of ghosts is clearly visible, the fraction of peptide that remains in solution appears much larger than in the Triton X experiment. The data represented were obtained at pH 4.5, but similar results were obtained at pH7. (B) AnnexinV binds to ghosts but not to intact RBCs. Cells were exposed to 1 mM E5-TAT at pH 6 to generate a mixture of intact RBCs and ghosts. The sample was treated with FITC-annexin V, and binding of annexin V to membranes was detected by fluorescence microscopy (FITC image, pseudocolored green).

E5-TAT at pH 4.5 could also be observed. However, the contrast between the signal in solution and the signal at the membrane was much reduced in this experiment, suggesting that E5-TAT and TAT are competing for binding. Together, this indicates that TAT binds to lysed cells and that TAT has access only after lysis to membrane components that are not accessible before lysis. In particular, I reasoned that these observations could be the result of the binding of TAT to negatively charged phospholipids. Interestingly, phospholipid phosphatidylserine (PS) is known to be predominantly present at the inner leaflet of the membranes of intact erythrocytes (94,95). TAT has also been reported to bind liposomes containing anionic phospholipids (4,96). TAT and E5-TAT could therefore bind to PS after E5-TAT-mediated hemolysis. PS could for instance flop through the aqueous pores formed during lysis and become exposed on the surface of the cells. Alternatively, E5-TAT could have access to luminal PS after lysis and diffusion into the permeable ghost. In order to test whether PS might be involved in the observed E5-TAT and TAT binding to ghost cells, FITC-annexin V, a fluorescently labeled protein with an extremely high affinity for PS, was added to ghosts obtained by E5-TAT-mediated hemolysis (41). As shown in Fig. 4-6B, labeling of the membrane of ghosts by annexin V could be clearly observed while no labeling was observed for intact RBCs.

4.2.6 Heparin inhibits membrane binding of E5-TAT and hemolysis

Other negatively charged molecules that TAT might interact with are the glycosaminoglycans present on the surface of mammalian cells. In particular, TAT binds

to cell-surface heparan sulfate (HS) proteoglycans, and this interaction appears to play a key role in the translocation of the peptide inside cells. Degradation fragments of HS are present within endocytic compartments, and these molecules have been proposed to inhibit the interaction of TAT with endosomal lipid bilayers and thereby reduce the efficiency with which the peptide can escape from endosomes (see Discussion). I was therefore interested in determining whether binding of E5-TAT to HS degradation fragments would inhibit the lytic activity of the peptide. To test this hypothesis, RBCs incubated with the HS analogue heparin were used to model the lumen of endosomes that would contain soluble HS degradation fragments. E5-TAT was added to samples of heparin/RBCs, and the extent of hemolysis was measured spectrophotometrically. E5-TAT-mediated hemolysis at pH4.5 was greatly reduced when RBCs were incubated with heparin (Fig. 4-7A). The extent of this inhibition was dependent on the concentration of heparin used, and hemolysis could be almost completely abolished when a large excess of heparin was used (10 mg/mL). On the other hand, the hemolysis activity of E5 was not affected by addition of heparin at any of the concentrations tested (1-10 mg/mL). In addition, binding of Fl-E5-TAT to the surface of RBCs at pH 4.5 was greatly reduced when heparin was added to the media (Fig. 4-7B). Together, these results suggest that heparin inhibits the binding of the peptide to the membrane of RBCs. As a consequence, the peptide is then unable to cause hemolysis.

4.3 Discussion

The delivery peptides investigated in this study are chimeric peptides derived from

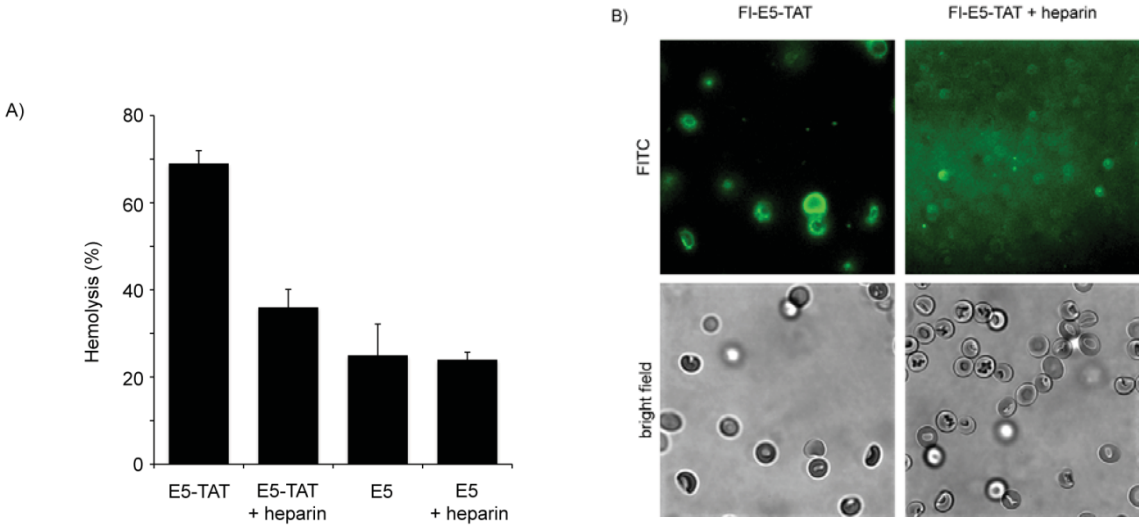

Figure 4-7 (A) Heparin inhibits the hemolytic activity of E5-TAT but not that of E5. RBCs were treated with 3 μME5-TATorE5at pH4.5 in the absence or presence of heparin (1mg/mL). (B) Heparin inhibits the binding of Fl-E5-TAT to the membrane of RBCs. RBCs were treated with 1 μMFl-E5-TAT at pH 4.5 in the absence or presence of heparin (1 mg/mL). No binding of the peptide to the membrane is observable when heparin is present in the sample and hemolysis is inhibited (RBCs in the image are intact).

HA2 fusion peptide of influenza hemagglutinin protein and the TAT peptide derived from the HIV transactivator of transcription protein (residues 47-60). These HA2-TAT peptides are designed to combine the endocytosis-inducing activity of TAT and the pH-dependent endosomal release activity of HA2. The results however highlight a complex interplay between the two peptides and several important parameters that affect their lytic activities. The first evidence of how TAT might affect the activity of HA2 peptides is given by the increase in hemolysis activity measured between E3/E5-TAT and E3/E5. It is well established that HA2 peptides are poorly soluble. Addition of the hydrophilic TAT sequence could therefore reduce the aggregation propensity of the HA2 peptides and be the cause of the increase in activity observed (97). Tamm and coworkers have indeed reported that addition of lysine residues to the C-terminus of HA2 sequences could greatly increase the solubility of the peptides (5). Consistent with this idea is the observation that E3 or E5 would rapidly aggregate and degrade during the experiments while E3/E5-TAT would not. The effect of TAT on the activity of E5 was however more pronounced than on the activity of E3. In particular, a dramatic shift in the hemolysis pK50 could be observed, and this effect appeared dependent on the presence of both TAT and the G4E and G8E mutations. This suggests the presence of electrostatic interactions between the positively charged residues of TAT and the glutamate residues of E5. Tsien and co-workers have indeed reported that the addition of polyglutamate sequences to arginine-rich cell-penetrating peptides results in intramolecular electrostatic interactions that block the cell-penetrating activity of the peptides (98). In section 3, I have reported that E5-TAT, despite containing TAT, binds to a lesser extent than TAT to

a negatively charged protein such as BSA. This suggests that the TAT sequence in E5-TAT has a reduced affinity for negatively charged molecules because it might be involved in intramolecular interactions with E5. Yet, one would expect that these interactions would stabilize E5 in its deprotonated form and lead to a decrease in the pK as of the glutamate residues and in hemolysis pK50. This is however contrary to my observations. Another possibility to explain for the observed increase in pK50 then might be that TAT increases the affinity of E5 for the lipid bilayer. HA2 peptides form amphipathic helices in membrane environments and upon protonation of their glutamate residues (56,99). The helices adopt a boomerang or hairpin-shaped structure at the lipid/water interface with hydrophobic residues facing the lipid environment. Based on these structures, the five Glu residues of E5 are expected to be located in close proximity on the interface exposed to water. Binding of E5-TAT to the membrane could therefore promote helix formation, leading to a clustering of the glutamate residues and to unfavorable like-charge repulsion between these residues. This would in turn facilitate the protonation of the Glu residues to avoid unfavorable Coulombic interactions and lead to an elevation of their pKa and of the pK50 observed (100).

To understand how E5-TAT disrupts membranes, the mechanism by which hemolysis is achieved was further explored. Like other HA2 peptides described, E5-TAT and Fl-E5-TAT exist in equilibrium between soluble and membrane-bound states (62). As observed by microscopy, a decrease in pH, and presumably protonation of the peptide glutamate residues, shifts this equilibrium to the membrane-bound state as the solubility of the peptide is reduced. Similar pH-dependent membrane partitioning has

been observed for AcE4K, an HA2 analogue similar to the E5 and Fl-E5 sequences used in this study (62). The hemolysis data are consistent with a single protonation model where the peptides undergo a transition from a soluble and nonlytic state A^- to a membrane-bound and lytic state HA. The pK50 obtained from the hemolysis plot can then be interpreted as an acid dissociation constant for the A^-/HA pair. In addition, the HD50 obtained at pH 4 and 7 represent the same total concentration of HA if one considers the Henderson-Hasselbach equation of the form pH = pK50 + log $[A^-]/[HA]$. Lysis would therefore appear to only depend on the total amount of HA present in the membrane of RBCs. It is however important to note that the HD50 values correspond to peptide concentrations at which 50% of the RBCs are totally lysed and 50% are intact as opposed to 100% of cells 50% lysed. It therefore appears that the amount of peptide bound to the membrane of single cells has to reach a certain threshold before lysis can be initiated.

When lysis was carried out at concentrations well above the HD50 of the E5-TAT and Fl-E5-TAT, the membrane of ghosts collapsed and fused to one another. In contrast, lysis at concentrations at or below the determined HD50 did not appear to dramatically change the morphology of the membrane, and the diameter of ghosts remained approximately constant under these conditions. Leakage from single cells incubated with E5-TAT was initiated at different times, reflecting the fact that cells are heterogeneous and might have varying degrees of membrane fragilities. Once initiated, lysis was slow since 90 s was required on average to achieve complete hemolysis. Together, these results do not support the formation of dramatic lesions in the membrane as sometimes

observed with the hypotonic lysis of RBCs (101). Instead, they suggest that cell permeability is induced by the formation of aqueous pores large enough for the passage of hemoglobin or dextrans. The relatively slow leakage observed is also indicative of formation of a limited number of pores with a relatively small diameter rather than very large holes. Indeed, hemolysis by osmotic shock in hypotonic media was observed to be complete in 4 s for single RBCs (93,102). Considering that the diffusion constant of hemoglobin is approximately $7x10^{-7}$ cm^2/s, it was then estimated that hemolysis could be achieved at the observed rate if cells contained 100 pores of a diameter of 70 Å (tetrameric hemoglobin has a spheroidal shape 65 x 55 x 50 Å) (102). While such estimates are more qualitative than quantitative since the diameter of pores cannot be accurately determined similar calculations would indicate that E5-TAT mediates the formation of less than three equivalent pores per cell.

Ghosts obtained by hypotonic osmotic shock typically reseal within seconds in isotonic media and at 37□ (102). In contrast, the ghosts obtained by Fl-E5-TAT-mediated lysis remained permeable to dextrans under similar conditions. Interestingly, Fl-E5-TATcould not be washed from the membrane at either pH 4 or pH7.This is very different from what has been observed with AcE4K (62). A possible explanation for this observation is that TAT might play a role in the stable peptide binding to the membrane. Indeed, the data suggest that, while binding of E5- TAT to intact RBCs or liposomes is dependent on the E5 moiety, the binding of the peptide to ghosts is in part due to the affinity of TAT for the lysed membrane. Fl-TAT did not show significant binding to intact RBCs but was bound to the membrane of ghosts lysed with the detergent Triton X

or with E5-TAT. The possible explanation for these observations is that, upon lysis, the peptide is able to access molecules that are not available for binding in intact cells. A possible binding partner is PS, a negatively charged phospholipid which is located on the inner leaflet of the membrane of RBCs (95). My data do not rule out that the peptide binds to other molecules than PS upon lysis but demonstrate that binding to anionic phospholipids such as PS could account for the effects observed.

Overall, the binding of TAT to the lysed membrane of ghosts might contribute to the stable association of the peptide E5-TAT to the lipid bilayer and might explain in part why the peptide could not be washed away and why the permeability could not be reversed. In addition, it raises the possibility that TAT might play an active role in the lysis event. The E5 moiety in E5-TAT is clearly required to trigger lysis since TAT does not cause hemolysis on its own. E5 might be sufficient to initiate the formation of aqueous pores, and TAT might not contribute to this process at first. PS might then diffuse laterally through these pores as outer and inner leaflets are now connected to one another. One can therefore envision how the exposed PS would then lead to more peptide being recruited to this area because of the strong interaction between TAT and PS. This in turn might lead to more membrane disruption and could contribute to the increased activity and pK50 shift observed for E5-TAT when compared to E5.

HA2-TAT analogues can deliver macromolecules into the cytosolic space of mammalian cells. In particular, it has been shown in section 3 that E5-TAT can cause the release of macromolecules trapped inside endocytic organelles, and this activity is dependent on the acidification of these organelles. However, the delivery efficiency

associated with this peptide remains modest. Improving the properties of this delivery agent requires that one understand how this peptide functions. Yet, it is difficult to characterize the lytic activity of E5- TAT inside endocytic organelles because they represent a chemically complex and dynamic environment. After internalization at the plasma membrane, endocytic vesicles loaded with E5-TAT might undergo multiple steps of maturation, and the peptide might partition into various endocytic organelles, including early endosomes, recycling endosomes, late endosomes, and lysosomes (103). These organelles have membranes of different lipid, carbohydrate, and protein composition, and their lumen is acidified to different extents (103). I propose however that the results with RBCs might provide valuable insights into how E5-TAT might behave inside endocytic organelles.

Endocytic organelles have a pH ranging from approximately 6.5 for early endosomes to 5.5 in late endosomes and 4.5 for lysosomes (104-106). The high pK50 observed for E5-TAT would suggest that an increase in the lytic activity of the peptide might occur early in the endocytic pathway. E5-TAT might rapidly bind to the membrane of endosomes as the vacuolar ATPase acidifies the lumen of endocytic organelles and form aqueous pores from which internalized macromolecules could escape (106). In contrast, E3-TAT, with its lower pK50, would be activated later in the endocytic pathway. The data however suggest that parameters other than pH will influence the activity of the peptides, including the presence of heparan sulfate (HS) proteoglycans and the lipid composition of the membrane.

It is now well established that TAT binds to heparan sulfate proteoglycans (HSPGs) on the cell surface and that internalization of TAT is typically reduced in glycosaminoglycan-deficient cell lines (47,81,107,108). Soluble acidic polysaccharides like heparin can also compete with HSPGs for TAT binding and inhibit the translocation of the peptide into cells (72-74). The importance of HSPGs for TAT mediated translocation remains however unclear as TAT might be internalized inside cells by multiple nonexclusive mechanisms that may or may not involve HSPGs (109-111). While association of TAT to HSPGs might contribute to an increase in peptide uptake, it is also possible that HSPGs may sequester TAT away from the lipid bilayer and reduce its ability to translocate across the plasma membrane (41,112,113). It is also known that TAT induces the internalization of cell-surface HSPGs (114). TAT and HSPGs might therefore associate within endocytic compartments, and it is possible that this association inhibits TAT-mediated endosomal release (17,112). In addition, HS proteoglycans are degraded within the endocytic pathway by sequential endoglycolysis and proteolysis (115-118). The polysaccharide chains appear to be degraded in a stepwise manner with a progressive reduction in the size of the degradation fragments that correlates with the maturation of the endocytic compartments from early endosomes to lysosomes. Release of HS chains From the HSPG protein moiety and partial cleavage of the soluble HS chains are initiated early on in the endocytic pathway. Degradation of HS fragments one-half to one-fourth the size of the original HS chain does not appear however to be completed until accumulation into lysosomes occurs. It is therefore possible that HS degradation does not precede TAT degradation and that soluble HS degradation

fragments inhibit the binding of TAT to lipid bilayers throughout the endocytic pathway. I am therefore interested in testing whether similar effects would be observed for E5-TAT. In particular, binding of TAT to soluble HS might prevent E5 from binding to the phospholipid bilayer. On the other hand, the affinity of E5 for the lipid bilayer might promote the binding of E5-TAT to the bilayer regardless of whether TAT is bound to HS or not. To test the effect that TAT binding to HS might have on E5-TAT activity, the soluble HS analogue heparin was used. RBCs were again used as a model because the surface of RBCs has been shown to contain very low levels of HS proteoglycans (89,119). RBCs might therefore be comparable to the membrane of endocytic organelles once cleavage of the HS chains from the HSPGs has taken place. In the experiments, the presence of heparin had a dramatic inhibitory effect on the hemolytic activity of E5-TAT but not of E5. The binding of Fl-E5-TAT to RBCs was also much reduced when heparin was present in solution. Together, these results suggest that binding of TAT to heparin sequesters the E5 moiety away from the membrane of RBCs. By analogy, TAT binding to HS or HS fragments might inhibit the activity of E5-TAT inside endocytic organelles. This effect could offset the gain in lytic activity observed in Fig. 4-1A when TAT is conjugated to E5.

Molecular dynamics simulations suggest that anionic groups present in the inner leaflet of a biological membrane attract TAT present on the outer leaflet of the corresponding bilayer (120). TAT and clustered PS on either side of a bilayer have also been proposed to generate a local capacitor that can induce the electroporation of the membrane (121). It is therefore possible that TAT contributes to the lytic activity of E5-

TAT by acting directly on lipid bilayers according to these proposed mechanisms. In addition, the PS asymmetry present at the plasma membrane of mammalian cells is also thought to be conserved at the membranes of endocytic organelles (122). In analogy to the binding observed between E5-TAT and ghosts, my data would then suggest that E5-TAT could bind to exposed PS after endosomal lysis occurs. A molecular cargo attached to E5-TAT would then remain bound to permeabilized endosomes rather than diffuse freely into the cell. This is consistent with results in section 3 describing how the fluorescent protein HA2-TAT-mCherry, while being able to cause the release of a soluble dextran from endosomes into the cytosol of a cell, remains associated with endocytic organelles. Finally, the composition of the endocytic organelles is also known to change during the transition from early to late endosomes. In particular, late endosomes are enriched in the anionic lipid lysobisphosphatidic acid (LBPA) (123). It is therefore possible that, after trafficking within the endocytic pathway, E5-TAT might encounter a membrane leaflet more negatively charged in a late endosome than in the early endosome. Binding of the TAT moiety to LBPA could bring the E5 to the lipid bilayer. This in turn could contribute to an increase in membrane disruption by E5 in a pH-independent manner.

In conclusion, the results with RBCs provide valuable insights into the behavior of HA2-TAT peptides within endocytic organelles. From the point of view of the design of delivery agents, HA2 is employed as a pH-dependent switch that can disrupt endosomal membranes upon acidification. TAT, on the other hand, is added to the sequence to transport the HA2 moiety into the cell. The results however highlight how the lytic

activity of HA2 is profoundly affected by this addition. For E5-TAT, TAT affects the hemolytic activity, the solubility, and the binding properties of the peptide. The shifted pH response of E5-TAT in particular seems perfectly suited for delivery applications. However, TAT might also contribute to an inhibitory effect by potentially binding to HS and sequestering the peptide away from lipid bilayers. Together, these results provide the basis for the rational design of delivery agents with improved properties.

4.4 Materials & Methods

4.4.1 Peptide synthesis and purification

E3-TAT, E5-TAT, Fl-E5-TAT and E5-TAT-Fl were purchased as crude cleavage products from RayBiotech (Norcross, GA). Peptide sequences are described in Table 4-1. TAT was synthesized in-house on the Rink amide resin by SPPS using standard Fmoc protocols. Fmoc-Lys(Boc)-OH, Fmoc-Gly-OH, Fmoc-Arg(Pbf)-OH, Fmoc-Gln(Trt)-OH, Fmoc-Gly-OH, Fmoc-Leu-OH, Fmoc-Ala-OH, and Boc-Cys(StBu) were used to assemble the peptides and were purchased from Novabiochem (San Diego, CA). Reactions were carried out in SPPS vessels at room temperature using a stream of dry N_2 to provide agitation. Fmoc deprotection was performed by addition of piperidine in DMF (20%, 5 mL) to the Fmoc-peptide resin (0.72 mmol). Deprotection was carried out for 1×3 min and 1×10 min. Coupling reactions were carried out for 2 h with a mixture of Fmoc-amino acid (2.88 mmol), HBTU (1.06 g, 2.80 mmol), and DIEA (1.25 mL, 7.2 mmol) in DMF. Upon completion of the reaction, the resin was washed with DMF. The peptides were analyzed and purified by reverse phase HPLC. HPLC analysis was

performed on a Hewlett-Packard 1200 series instrument and a Vydac C18 column (5 micron, 4 x 150 mm). Flow rate was 1 mL/min and detection was at 214 nm. Semi-preparative HPLC was performed on a Vydac C18 10 × 250 mm column. Flow rate was 4 mL/min and detection was at 214 nm. All runs used linear gradients of 0.1% aqueous TFA (solvent A) and 90% acetonitrile, 10% water and 0.1% TFA (solvent B). All purified and lyophilized peptides were dissolved to 1 mM in DMSO and diluted with PBS to desired concentrations in further experiments. The correct identity of the peptides was confirmed by MALDI-TOF mass spectrometry (AXIMA-CFR, Shimazu, Kyoto). TAT expected mass: 1395.7 Da, observed mass: 1395.5 Da. E3-TAT expected mass: 3834.4 Da, observed mass: 3835.7 Da. E5-TAT expected mass: 3978.5 Da, observed mass: 3978.8 Da. Fl-E5-TAT expected mass: 4609.3 Da, observed mass: 4605.8 Da. E5-TAT-Fl expected mass: 4495.3 Da, observed mass: 4501.5 Da. To obtain the E3 or E5, E3-TAT and E5-TAT were digested with trypsin at a peptide to enzyme ratio of 1:25 for 5h at 37°C. This procedure yielded E3 or E5 with a C-terminal arginine residue and with a yield of 97% (The TAT sequence is digested and the sequence of the product is described in Table 4-1), as demonstrated by HPLC and mass spectrometry. E3 (GLFGAIAGFIENGWEGLIEGWYGGR) expected mass: 2667.3 Da, observed mass: 2659.2 Da. E5 (GLFEA IAEFI ENGWE GLIEG WYGGR) expected mass: 2813.3 Da, observed mass: 2809.9 Da.

4.4.2 Hemolysis assays

A membrane lysis assay was performed with human erythrocytes purchased from the

Gulf blood bank (Galveston, TX). Erythrocytes were centrifuged for 5 min at 1500g; following 20 ml of erythrocyte pellet was resuspended with an equal volume of PBS. This was repeated three times to remove plasma and buffy coat. The erythrocytes (50% volume in PBS) were diluted 20 fold in PBS of different pH values (adjusted with HCl or NaOH, 4.5<pH<7.5). All peptides were diluted with PBS to desired concentrations and added to a 96-well plate. One hundred microliters of the 2.5% RBC suspension was added into each well. One hundred microliters of hemolytic peptides diluted in PBS from a DMSO stock (100 μM) to a 2x concentration were added to the RBCs to generate a 1.25% suspension of cells with peptides at the desired concentration. To test the effects of heparan sulfate, aliquots of heparin sodium salt (sigma) stock in PBS (100 mg/mL) were to obtain a final concentration of 1 to 7 mg/mL Addition of heparin was done prior to the addition of peptide to the RBCs suspension. The plates were incubated at 37°C for 30 min. After centrifuging the plate for 5 minutes at 1500g, the supernatants were transferred to a new 96-well plate. The absorbance of hemoglobin present in each well was measured at 450 nm using a plate reader (Bio-RAD, Ultramark Micro plate system, USA). One hundred percent hemolysis was obtained by incubating the RBC with 0.1% Triton X-100. Background hemolysis at various pH was evaluated by incubating the erythrocytes in the corresponding PBS solutions. The obtained data was plotted using the software KaleidaGraph (Synergy Software, Reading, PA). The data was fitted to an equation of the form $\%=\%min+(\%max-\%min)*[H^+]/([H^+]+K50)$, where %max and %min are the maximum and minimum lysis activities observed, and K50 is the proton concentration at which $\%=(\%max+\%min)/2$, with R^2 between 0.99, 0.97, 0.98 and 0.96

for E3-TAT, E5-TAT, E3 and E5, respectively.

4.4.3 Microscopy assays

Hemolytic peptides were added to the 1% RBC suspension in PBS at pH of 4.5 or 7 by dilution from their DMSO stock to the desired final concentration (final DMSO content was kept below 5% in all experiments). After incubation at 37°C for 20 minutes, the solution was diluted in PBS at pH of 4.5 or 7 to obtain a 1 % suspension. Two hundred microliters of these suspensions were added to the wells of an 8-well chamber glass slide (Nunc). Cells were placed on an inverted epifluorescence microscope (Model IX81, Olympus, Center Valley, PA) equipped with a heating stage maintained at 37°C. Cells were typically allowed to settle to the bottom of the dish for 5 minutes prior to imaging so as to obtain a layer of cells in the focal plane. The microscope is configured with a spinning disk unit to perform both confocal and wide-field fluorescence microscopy. Images were collected using a Rolera-MGI Plus back-illuminated EMCCD camera (Qimaging, Surrey, BC, Canada). Images were acquired using bright field imaging and two standard fluorescence filter sets: Texas Red (Ex = 560±40 nm / Em= 630±75 nm), and FITC (Ex = 482±35 nm / Em= 536±40 nm). For time-lapse experiments, the hemolytic peptides, prepared as 2X solutions in PBS at pH 4.5 or 7, were added directly to the 1% RBC suspension already placed on the microscope. To wash ghosts, 200 μL of 2.5% RBC suspension with the hemolytic peptides were centrifuged for 5 minutes at 1500g. The supernatant was removed and cells were resuspended in 200 μL fresh PBS at a desired pH. A 20 μL aliquot of the cells was

added to an 8-well glass slide and imaged to monitor the morphology and fluorescence of cells. These steps were repeated 3 to 5 times, or until spherical ghosts could not be recovered. An aliquot of 10kDa FITC-Dextran (Invitrogen) was added to the resuspendend ghosts to a final concentration of 250 μM. The bright field and fluorescence intensities of cells and ghosts were measured using the SlideBook 4.2 software (Olympus, Center Valley, PA). Mean intensities within cells imaged was measured as the total intensity of the cell divided by its area. Annexin V-FITC (ApoDETECT KIT, Invitrogen) was incubated with RBCs lysed with E5-TAT (1 μM) at pH 6 according to the vendor's recommended protocol (10 μL of stock solution to 190 μL of cell suspension in PBS supplemented with 2.5 mM $CaCl_2$).

5. CONCLUSION

Due to its unique pH-dependent membrane disruption property, I propose HA2 peptide can enhance endosomal escape upon endosomal acidification during CPP-mediated protein delivery. In section 1, the covalently linked CPP protein constructs, HA2-TAT-mCherry and E5-TAT-mCherry were incubated with cells to test if HA2 and its mutant, E5 can enhance endosomal escape and release more proteins into the cytosol. The results revealed that HA2 and E5 are hydrophobic and tend to associate with all the lipid membrane compartments inside of cells. Therefore, HA2/E5-TAT-mCherry was only able to release the coincubated dextran molecule to the cytosol while it could not itself escape. This further indicates that the covalently linked strategy for HA2/E5-TAT with protein cargo may not be ideal for protein delivery since this CPP tag can alter the protein behavior. For this reason, in section 2, the endosomal escape efficiency of HA2/E5-TAT on mCherry was tested by simple co-incubation. It was revealed that E5-TAT first associates with heparan sulfate proteoglycan (HSPG) on the extracellular matrix, then internalizes into endosomes through macropinocytosis. Next, this tag disrupts the endosomal membrane during endosomal acidification, releasing mCherry into the cytosolic space. In summary, the results showed that the efficiency of E5-TAT-induced endosomal escape to the cytosol is only 16%, this is still an improvement over the 8% efficiency of HA2-TAT. Although there is still an increase for endosomal escape with E5-TAT, 16 % of endosomal escape is still not ideal.

To further explorer the cause for the low efficiency of escape, red blood cells (RBC) were used to served as the model system for endosomes. Through the hemolytic assay, E5-TAT showed the highest pH-dependent lytic activity and pK50 (pH value at 50% hemolysis) of 6.7, while HA2-TAT was at 5.7. Fl-E5-TAT also showed that pH-dependent membrane binding is suggested to be related to the hemolytic event. Furthermore, the peptide disrupted RBCs by forming a certain number of pores to release the cytosolic content into the medium. Most importantly, HSPG fragments showed a significant affinity for E5-TAT so that the peptide-induced hemolytic activity was inhibited. This observation may provide a fundamental understanding for why the efficiency of endosomal escape is still low. Overall, through a combination of assays including microscopic and biochemical with mammalian cells and RBCs, the mechanism of protein delivery and biological application of E5-TAT has been comprehensively studied. The collective results may provide the basis for the molecular design of future delivery agents.

REFERENCES

1. Gump, J. M., and Dowdy, S. F. (2007) *Trends Mol Med* **13**, 443-448
2. Wadia, J. S., and Dowdy, S. F. (2002) *Curr Opin Biotechnol* **13**, 52-56
3. Wadia, J. S., and Dowdy, S. F. (2005) *Adv Drug Deliv Rev* **57**, 579-596
4. Thoren, P. E., Persson, D., Esbjorner, E. K., Goksor, M., Lincoln, P., and Norden, B. (2004) *Biochemistry* **43**, 3471-3489
5. Kreis, T. E., and Birchmeier, W. (1982) *Int Rev Cytol* **75**, 209-214
6. Arnheiter, H., Dubois-Dalcq, M., and Lazzarini, R. A. (1984) *Cell* **39**, 99-109
7. Kabouridis, P. S. (2003) *Trends Biotechnol* **21**, 498-503
8. Morris, M. C., Vidal, P., Chaloin, L., Heitz, F., and Divita, G. (1997) *Nucleic Acids Res* **25**, 2730-2736
9. Dietz, G. P., and Bahr, M. (2004) *Mol Cell Neurosci* **27**, 85-131
10. Patel, L. N., Zaro, J. L., and Shen, W. C. (2007) *Pharm Res* **24**, 1977-1992
11. Frankel, A. D., and Pabo, C. O. (1988) *Cell* **53**, 675
12. Green, M., and Loewenstein, P. M. (1988) *Cell* **55**, 1179-1188
13. Mann, D. A., and Frankel, A. D. (1991) *EMBO J* **10**, 1733-1739
14. Vives, E., Brodin, P., and Lebleu, B. (1997) *J Biol Chem* **272**, 16010-16017
15. Schwarze, S. R., Ho, A., Vocero-Akbani, A., and Dowdy, S. F. (1999) *Science* **285**, 1569-1572
16. Zorko, M., and Langel, U. (2005) *Adv Drug Deliv Rev* **57**, 529-545
17. Fischer, R., Fotin-Mleczek, M., Hufnagel, H., and Brock, R. (2005) *Chembiochem* **6**, 2126-2142

18. El-Andaloussi, S., Jarver, P., Johansson, H. J., and Langel, U. (2007) *Biochem J* **407**, 285-292

19. Gupta, B., Levchenko, T. S., and Torchilin, V. P. (2005) *Adv Drug Deliv Rev* **57**, 637-651

20. Noguchi, H., and Matsumoto, S. (2006) *J Hepatobiliary Pancreat Surg* **13**, 306-313

21. Denicourt, C., and Dowdy, S. F. (2003) *Trends Pharmacol Sci* **24**, 216-218

22. Green, I., Christison, R., Voyce, C. J., Bundell, K. R., and Lindsay, M. A. (2003) *Trends Pharmacol Sci* **24**, 213-215

23. Richard, J. P., Melikov, K., Vives, E., Ramos, C., Verbeure, B., Gait, M. J., Chernomordik, L. V., and Lebleu, B. (2003) *J Biol Chem* **278**, 585-590

24. Schwarze, S. R., Hruska, K. A., and Dowdy, S. F. (2000) *Trends Cell Biol* **10**, 290-295

25. Barka, T., Gresik, E. W., and van Der Noen, H. (2000) *J Histochem Cytochem* **48**, 1453-1460

26. Song, B. H., Lee, G. C., Moon, M. S., Cho, Y. H., and Lee, C. H. (2001) *J Gen Virol* **82**, 2405-2413

27. Fischer, R., Kohler, K., Fotin-Mleczek, M., and Brock, R. (2004) *J Biol Chem* **279**, 12625-12635

28. Caron, N. J., Quenneville, S. P., and Tremblay, J. P. (2004) *Biochem Biophys Res Commun* **319**, 12-20

29. Schwarze, S. R., and Dowdy, S. F. (2000) *Trends Pharmacol Sci* **21**, 45-48

30. Derossi, D., Calvet, S., Trembleau, A., Brunissen, A., Chassaing, G., and Prochiantz, A. (1996) *J Biol Chem* **271**, 18188-18193

31. Wender, K. F., and Rothkegel, R. (2000) *Psychol Res* **64**, 81-92

32. Futaki, S., Suzuki, T., Ohashi, W., Yagami, T., Tanaka, S., Ueda, K., and Sugiura, Y. (2001) *J Biol Chem* **276**, 5836-5840

33. Mitchell, D. J., Kim, D. T., Steinman, L., Fathman, C. G., and Rothbard, J. B. (2000) *J Pept Res* **56**, 318-325

34. Rothbard, J. B., Jessop, T. C., Lewis, R. S., Murray, B. A., and Wender, P. A. (2004) *J Am Chem Soc* **126**, 9506-9507

35. Umezawa, N., Gelman, M. A., Haigis, M. C., Raines, R. T., and Gellman, S. H. (2002) *J Am Chem Soc* **124**, 368-369

36. Futaki, S., Nakase, I., Suzuki, T., Youjun, Z., and Sugiura, Y. (2002) *Biochemistry* **41**, 7925-7930

37. Bernfield, M., Gotte, M., Park, P. W., Reizes, O., Fitzgerald, M. L., Lincecum, J., and Zako, M. (1999) *Annu Rev Biochem* **68**, 729-777

38. Velleman, S. G., Coy, C. S., and McFarland, D. C. (2007) *Poult Sci* **86**, 1406-1413

39. Bai, X. M., Van der Schueren, B., Cassiman, J. J., Van den Berghe, H., and David, G. (1994) *J Histochem Cytochem* **42**, 1043-1054

40. Couchman, J. R. (2003) *Nat Rev Mol Cell Biol* **4**, 926-937

41. Wadia, J. S., Stan, R. V., and Dowdy, S. F. (2004) *Nat Med* **10**, 310-315

42. Overath, P., and Engstler, M. (2004) *Mol Microbiol* **53**, 735-744

43. Mayor, S., and Pagano, R. E. (2007) *Nat Rev Mol Cell Biol* **8**, 603-612

44. Jones, A. T. (2007) *J Cell Mol Med* **11**, 670-684

45. Watson, P., Jones, A. T., and Stephens, D. J. (2005) *Adv Drug Deliv Rev* **57**, 43-61

46. Asundi, V. K., Keister, B. F., Stahl, R. C., and Carey, D. J. (1997) *Exp Cell Res* **230**, 145-153

47. Poon, G. M., and Gariepy, J. (2007) *Biochem Soc Trans* **35**, 788-793

48. Samaj, J., Baluska, F., Voigt, B., Schlicht, M., Volkmann, D., and Menzel, D. (2004) *Plant Physiol* **135**, 1150-1161

49. Terlecky, S. R., and Koepke, J. I. (2007) *Adv Drug Deliv Rev* **59**, 739-747

50. Fischer, R., Bachle, D., Fotin-Mleczek, M., Jung, G., Kalbacher, H., and Brock, R. (2006) *Chembiochem* **7**, 1428-1434

51. Noguchi, H., and Matsumoto, S. (2006) *Acta Med Okayama* **60**, 1-11

52. Lories, V., Cassiman, J. J., Van den Berghe, H., and David, G. (1992) *J Biol Chem* **267**, 1116-1122

53. Maxfield, F. R., and McGraw, T. E. (2004) *Nat Rev Mol Cell Biol* **5**, 121-132

54. Gnoatto, N., Lotufo, R. F., Matsuda, M., Penna, V., and Marquezini, M. V. (2007) *J Periodontal Res* **42**, 553-558

55. Zhang, X., Wan, L., Pooyan, S., Su, Y., Gardner, C. R., Leibowitz, M. J., Stein, S., and Sinko, P. J. (2004) *Mol Pharm* **1**, 145-155

56. Han, X., Bushweller, J. H., Cafiso, D. S., and Tamm, L. K. (2001) *Nat Struct Biol* **8**, 715-720

57. Chang, D. K., Cheng, S. F., Lin, C. H., Kantchev, E. B., and Wu, C. W. (2005) *Biochim Biophys Acta* **1712**, 37-51

58. Tsurudome, M., Gluck, R., Graf, R., Falchetto, R., Schaller, U., and Brunner, J. (1992) *J Biol Chem* **267**, 20225-20232

59. Steinhauer, D. A., Wharton, S. A., Skehel, J. J., and Wiley, D. C. (1995) *J Virol* **69**, 6643-6651

60. Michiue, H., Tomizawa, K., Wei, F. Y., Matsushita, M., Lu, Y. F., Ichikawa, T., Tamiya, T., Date, I., and Matsui, H. (2005) *J Biol Chem* **280**, 8285-8289

61. Wagner, E., Plank, C., Zatloukal, K., Cotten, M., and Birnstiel, M. L. (1992) *Proc Natl Acad Sci U S A* **89**, 7934-7938

62. Zhelev, D. V., Stoicheva, N., Scherrer, P., and Needham, D. (2001) *Biophys J* **81**, 285-304

63. Esbjorner, E. K., Oglecka, K., Lincoln, P., Graslund, A., and Norden, B. (2007) *Biochemistry* **46**, 13490-13504

64. Wharton, S. A., Martin, S. R., Ruigrok, R. W., Skehel, J. J., and Wiley, D. C. (1988) *J Gen Virol* **69 (Pt 8)**, 1847-1857

65. Hsu, C. H., Wu, S. H., Chang, D. K., and Chen, C. (2002) *J Biol Chem* **277**, 22725-22733

66. Murata, M., Takahashi, S., Kagiwada, S., Suzuki, A., and Ohnishi, S. (1992) *Biochemistry* **31**, 1986-1992

67. Matsumoto, T. (1999) *Biophys Chem* **79**, 153-162

68. Dubovskii, P. V., Li, H., Takahashi, S., Arseniev, A. S., and Akasaka, K. (2000) *Protein Sci* **9**, 786-798

69. Takahashi, S. (1990) *Biochemistry* **29**, 6257-6264

70. Plank, C., Oberhauser, B., Mechtler, K., Koch, C., and Wagner, E. (1994) *J Biol Chem* **269**, 12918-12924

71. Midoux, P., Kichler, A., Boutin, V., Maurizot, J. C., and Monsigny, M. (1998) *Bioconjug Chem* **9**, 260-267

72. Hakansson, S., Jacobs, A., and Caffrey, M. (2001) *Protein Sci* **10**, 2138-2139

73. Hakansson, S., and Caffrey, M. (2003) *Biochemistry* **42**, 8999-9006

74. Rusnati, M., Coltrini, D., Oreste, P., Zoppetti, G., Albini, A., Noonan, D., d'Adda di Fagagna, F., Giacca, M., and Presta, M. (1997) *J Biol Chem* **272**, 11313-11320

75. Lenart, P., Rabut, G., Daigle, N., Hand, A. R., Terasaki, M., and Ellenberg, J. (2003) *J Cell Biol* **160**, 1055-1068

76. Gorlich, D., and Kutay, U. (1999) *Annu Rev Cell Dev Biol* **15**, 607-660

77. Ruben, S., Perkins, A., Purcell, R., Joung, K., Sia, R., Burghoff, R., Haseltine, W. A., and Rosen, C. A. (1989) *J Virol* **63**, 1-8

78. Lee, Y. J., Datta, S., and Pellois, J. P. (2008) *J Am Chem Soc* **130**, 2398-2399

79. Philo, J. S. (1997) *Biophys J* **72**, 435-444

80. Nakase, I., Niwa, M., Takeuchi, T., Sonomura, K., Kawabata, N., Koike, Y., Takehashi, M., Tanaka, S., Ueda, K., Simpson, J. C., Jones, A. T., Sugiura, Y., and Futaki, S. (2004) *Mol Ther* **10**, 1011-1022

81. Nakase, I., Tadokoro, A., Kawabata, N., Takeuchi, T., Katoh, H., Hiramoto, K., Negishi, M., Nomizu, M., Sugiura, Y., and Futaki, S. (2007) *Biochemistry* **46**, 492-501

82. Shaner, N. C., Campbell, R. E., Steinbach, P. A., Giepmans, B. N., Palmer, A. E., and Tsien, R. Y. (2004) *Nat Biotechnol* **22**, 1567-1572

83. Ohkuma, S., and Poole, B. (1978) *Proc Natl Acad Sci U S A* **75**, 3327-3331

84. Ziegler, A., and Seelig, J. (2004) *Biophys J* **86**, 254-263

85. Javadpour, M. M., Juban, M. M., Lo, W. C., Bishop, S. M., Alberty, J. B., Cowell, S. M., Becker, C. L., and McLaughlin, M. L. (1996) *J Med Chem* **39**, 3107-3113

86. Ellerby, H. M., Arap, W., Ellerby, L. M., Kain, R., Andrusiak, R., Rio, G. D., Krajewski, S., Lombardo, C. R., Rao, R., Ruoslahti, E., Bredesen, D. E., and Pasqualini, R. (1999) *Nat Med* **5**, 1032-1038

87. West, M. A., Bretscher, M. S., and Watts, C. (1989) *J Cell Biol* **109**, 2731-2739

88. Kerr, M. C., and Teasdale, R. D. (2009) *Traffic* **10**, 364-371

89. Vogt, A. M., Winter, G., Wahlgren, M., and Spillmann, D. (2004) *Biochem J* **381**, 593-597

90. Steck, T. L. (1974) *J Cell Biol* **62**, 1-19

91. Birchmeier, W., Libermann, T. A., Imhof, B. A., and Kreis, T. E. (1982) *Cold Spring Harb Symp Quant Biol* **46 Pt 2**, 755-767

92. Sebban, P., Coppey, M., Alpert, B., Lindqvist, L., and Jameson, D. M. (1980) *Photochem Photobiol* **32**, 727-731

93. Anderson, P. C., and Lovrien, R. E. (1977) *Biophys J* **20**, 181-191

94. Zoon, K. C., and Arnheiter, H. (1984) *Pharmacol Ther* **24**, 259-278

95. Boon, J. M., and Smith, B. D. (2002) *Med Res Rev* **22**, 251-281

96. Zorko, M., and Suselj, M. (2005) *Stud Health Technol Inform* **116**, 59-64

97. Han, X., and Tamm, L. K. (2000) *J Mol Biol* **304**, 953-965

98. Jiang, T., Olson, E. S., Nguyen, Q. T., Roy, M., Jennings, P. A., and Tsien, R. Y. (2004) *Proc Natl Acad Sci U S A* **101**, 17867-17872

99. Lorieau, J. L., Louis, J. M., and Bax, A. (2010) *Proc Natl Acad Sci U S A* **107**, 11341-11346

100. Harris, T. K., and Turner, G. J. (2002) *IUBMB Life* **53**, 85-98

101. Lieber, M. R., and Steck, T. L. (1982) *J Biol Chem* **257**, 11651-11659

102. Hoffman, J. F. (1992) *Adv Exp Med Biol* **326**, 1-15

103. Mellman, I. (1996) *Annu Rev Cell Dev Biol* **12**, 575-625

104. Schmid, S., Fuchs, R., Kielian, M., Helenius, A., and Mellman, I. (1989) *J Cell Biol* **108**, 1291-1300

105. Demaurex, N. (2002) *News Physiol Sci* **17**, 1-5

106. Forgac, M. (2007) *Nat Rev Mol Cell Biol* **8**, 917-929

107. Tyagi, M., Rusnati, M., Presta, M., and Giacca, M. (2001) *J Biol Chem* **276**, 3254-3261

108. Console, S., Marty, C., Garcia-Echeverria, C., Schwendener, R., and Ballmer-Hofer, K. (2003) *J Biol Chem* **278**, 35109-35114

109. Richard, J. P., Melikov, K., Brooks, H., Prevot, P., Lebleu, B., and Chernomordik, L. V. (2005) *J Biol Chem* **280**, 15300-15306

110. Silhol, M., Tyagi, M., Giacca, M., Lebleu, B., and Vives, E. (2002) *Eur J Biochem* **269**, 494-501

111. Violini, S., Sharma, V., Prior, J. L., Dyszlewski, M., and Piwnica-Worms, D. (2002) *Biochemistry* **41**, 12652-12661

112. Fuchs, S. M., and Raines, R. T. (2006) *Cell Mol Life Sci* **63**, 1819-1822

113. Kosuge, M., Takeuchi, T., Nakase, I., Jones, A. T., and Futaki, S. (2008) *Bioconjug Chem* **19**, 656-664

114. Wittrup, A., Zhang, S. H., ten Dam, G. B., van Kuppevelt, T. H., Bengtson, P., Johansson, M., Welch, J., Morgelin, M., and Belting, M. (2009) *J Biol Chem* **284**, 32959-32967

115. Yanagishita, M., and Hascall, V. C. (1984) *J Biol Chem* **259**, 10270-10283

116. Brauker, J. H., and Wang, J. L. (1987) *J Biol Chem* **262**, 13093-13101

117. Bame, K. J. (1993) *J Biol Chem* **268**, 19956-19964

118. Egeberg, M., Kjeken, R., Kolset, S. O., Berg, T., and Prydz, K. (2001) *Biochim Biophys Acta* **1541**, 135-149

119. Drzeniek, Z., Stocker, G., Siebertz, B., Just, U., Schroeder, T., Ostertag, W., and Haubeck, H. D. (1999) *Blood* **93**, 2884-2897

120. Herce, H. D., and Garcia, A. E. (2007) *Proc Natl Acad Sci U S A* **104**, 20805-20810

121. Cahill, K. (2009) *Phys Biol* **7**, 16001

122. Bandyopadhyay, D., Sharma, A., and Shankar, V. (2008) *J Chem Phys* **128**, 154909

123. Kobayashi, T., Beuchat, M. H., Chevallier, J., Makino, A., Mayran, N., Escola, J. M., Lebrand, C., Cosson, P., and Gruenberg, J. (2002) *J Biol Chem* **277**, 32157-32164

VITA

Name: Ya-Jung Lee

Address: Department of Biochemistry & Biophysics
103 Biochemistry/Biophysics Building
Texas A&M University
2128 TAMU
College Station, Texas 77843-2128

Email Address: vot358@gmail.com

Education: B.A., Food Science, National Chung Hsing Medical University, 2001

M.S., Biotechnology in Medicine, National Yang-Ming University, 2003

Ph.D. Biochemistry, Texas A&M University, 2011